TECHNICAL REPORT C-69-3

THE EFFECT OF CONFINING REINFORCEMENT ON THE DUCTILITY OF REINFORCED CONCRETE BEAMS

by

J. E. McDonald

March 1969

Sponsored by

Assistant Secretary of the Army (R&D)
Department of the Army

Conducted by

U. S. Army Engineer Waterways Experiment Station
CORPS OF ENGINEERS
Vicksburg, Mississippi

154

TECHNICAL REPORT C-69-5

THE EFFECT OF CONFINING REINFORCEMENT ON THE DUCTILITY OF REINFORCED CONCRETE BEAMS

by

J. E. McDonald

March 1969

Sponsored by

Assistant Secretary of the Army (R&D)
Department of the Army
Project 4A013001A91D

Conducted by

U. S. Army Engineer Waterways Experiment Station
CORPS OF ENGINEERS
Vicksburg, Mississippi

ARMY-MRC VICKSBURG, MISS.

THE CONTENTS OF THIS REPORT ARE NOT TO BE USED FOR ADVERTISING, PUBLICATION, OR PROMOTIONAL PURPOSES. CITATION OF TRADE NAMES DOES NOT CONSTITUTE AN OFFICIAL ENDORSEMENT OR APPROVAL OF THE USE OF SUCH COMMERCIAL PRODUCTS.

FOREWORD

This report is based on a thesis prepared by Mr. James E. McDonald of the Concrete Division of the U. S. Army Engineer Waterways Experiment Station (WES) in partial fulfillment of the requirements for the degree of Master of Science in the Department of Civil Engineering, Mississippi State University.

The investigation was funded by Department of the Army Project 4A013001A91D, "In-House Laboratory Independent Research Program," Item AP, sponsored by the Assistant Secretary of the Army (R&D). The investigation was conducted at the Concrete Division, WES, from August 1967-December 1968.

Directors of the WES during the conduct of the investigation and the preparation and publication of this report were COL John R. Oswalt, Jr., CE, and COL Levi A. Brown, CE. Technical Director was Mr. J. B. Tiffany.

BLANK PAGE

TABLE OF CONTENTS

TABLE OF CONTENTS--Continued

NOTATION

$\bar{A}$	Area under concrete stress-strain curve for given concrete strain
A_s	Area of tensile reinforcement (A_{s_i} for distinct layer of reinforcement)
A'_s	Area of compressive reinforcement
b	Width of beam
C	Total concrete compressive force
CG	Center of gravity
d	Distance from center of gravity of tensile reinforcement to top fiber (d_i for distinct layer of reinforcement)
d'	Distance from center of gravity of compressive reinforcement to top fiber
E_r	Elastic modulus of elasticity of reinforcement
E_{sh}	Modulus of elasticity of reinforcement in the strain-hardening region
f_c	Concrete stress
f'_c	Ultimate concrete stress
f_y	Reinforcement yield strength
kd	Distance from neutral axis to top fiber
k_1, k_2	Coefficients defining the magnitude and position, respectively, of the internal compressive force in the concrete
L	Length of beam between supports
M	Moment
n_r	Number of layers of tensile reinforcement
p_b	Reinforcement ratio producing balanced conditions at ultimate strength
p,p'	Tensile and compressive reinforcement ratios, respectively
P	Load
T	Total force in tensile reinforcement (T_i for distinct layer of reinforcement)

T' Total force in the compressive reinforcement

W Reinforcement weight

$\bar{X}$ Distance from center of gravity of an area $\bar{A}$ under the stress-strain curve for an assumed ϵ_{co}

Y_m Midspan deflection

ϵ Strain

ϵ_c Concrete strain at any location

ϵ_{co} Concrete compressive strain in top fiber

ϵ_s Strain in tensile reinforcement (ϵ_{s_i} for distinct layer of reinforcement)

ϵ'_s Strain in compressive reinforcement

ϵ_{sh} Strain at which strain hardening starts

θ_A Angle between the tangent to the bending line at point A and the original beam axis

μ Ductility ratio

σ_s Stress in tensile reinforcement (σ_{s_i} for distinct layer of reinforcement)

σ'_s Stress in compressive reinforcement

ϕ Curvature

ABSTRACT

Some means of improving the compressive strain capacity of concrete is necessary to provide the ductile members or connections which will safely allow for formation of the plastic hinges assumed in designs based on collapse and energy-absorption concepts.

The primary objectives of this investigation were to evaluate the effects of various types of confining reinforcement (helices, plane and tubular meshes, and rectangular ties) on the static stress-strain characteristics of rectangular concrete prisms tested in uniaxial compression, and, based on the results of these tests, determine the effectiveness of using selected confining reinforcement in the compressive zone of reinforced concrete flexural members to increase their ultimate strength and ductility.

One hundred and eighteen 4- by 4- by 12-in. concrete prisms (one hundred and twelve with and six without confining reinforcement) were cast and tested. The ability of confining reinforcement to increase the ultimate strain capacity and ductility of rectangular concrete prisms in uniaxial compression was clearly demonstrated by the results of these tests. Concrete properly confined by lateral reinforcement had a considerable load-carrying capacity up to strains in excess of two percent, or more than six times the amount of strain usually considered as ultimate for concrete. The data indicate that the horizontal plane mesh (14-gage wire; 1- by 1-in. openings) was the most efficient confining reinforcement of those investigated. Within the range of spacings, sizes, and mesh openings studied, it appears that the primary

factor affecting ductility is the amount or weight of the confining reinforcement used.

Twenty-four 4- by 9- by 78-in. concrete beams (6-ft span) reinforced with various amounts of high-strength steel, with and without confining compressive reinforcement (plane meshes, helices, and closed stirrups), were cast. The beams were tested to failure under two symmetrical line loads applied 6 in. from the beam center line. Results of these tests clearly demonstrated the ability of confining compressive reinforcement, particularly plane mesh, to significantly increase the ductility of reinforced concrete beams using high-strength steel. Plane mesh confining compressive reinforcement transformed the brittle failure mode normally associated with an overreinforced section into a plastic failure mode which gave ample warning of imminent collapse. This increased ductility can and should be used to advantage in structural designs based on collapse and energy-absorption concepts.

CHAPTER I: INTRODUCTION

Background

Both limit design in reinforced concrete and plastic design in steel are based on the fact that, due to inelastic moment redistribution, statically indeterminate structures do not fail when plastic hinging occurs at points insufficient in number to create a mechanism. However, as pointed out by Winter,[1] there are some basic differences between the behavior of mild steel, a ductile strain-hardening material, and that of concrete, a semibrittle strain-softening material, which affect their inelastic structural behavior. The strain capacity of mild steel is such that plastic hinges may form without causing any visible damage to the steel. In contrast, conventionally reinforced concrete beams cannot sustain strains as great as those which can be sustained by a mild steel beam. In reinforced concrete beams, cracking and spalling occur at concrete compressive strains as low as 0.0025 to 0.0035 in./in. Consequently, some means of improving the compressive strain capacity of concrete is necessary to provide the ductile members or connections which will safely allow for the formation of plastic hinges. Also, in the design of protective structures where energy-absorbing capacity is a primary objective, allowable deformations are so great that improved ductility is of paramount importance.

Under the auspices of the European Concrete Committee, a cooperative program of research on limit design for structural concrete has been carried out at various laboratories. Results of some of these studies, as well as results of other investigations of hinge formation in reinforced concrete, were presented at the ASCE International

Symposium, Flexural Mechanics of Reinforced Concrete, November 10-12, 1964.[2] Based on these results, the primary factors affecting hinge rotation are the depth of the compression zone, the maximum compressive strain in the concrete, and the amount of lateral reinforcement.

Tests on columns and prisms[3-10] have demonstrated that concrete, if properly confined by lateral reinforcement, may develop strains in excess of one percent, or more than three times the amount of strain usually considered ultimate for concrete, and still possess considerable load-carrying capacity. Because circular ties or spiral (helical) reinforcement and rectangular ties are commonly used in columns, their effects on the ductility of reinforced concrete flexural members have received some attention. Investigators[11-15] have found that both helical binding and closely spaced rectangular ties (stirrups) significantly increase the ductility of reinforced and prestressed concrete members and are effective means of assuring ductile-type failure even in overreinforced beams.

Objectives

The primary objectives of this investigation were to (a) evaluate the effects of various types of confining reinforcement (helices, plane and tubular meshes, and rectangular ties) on the static stress-strain characteristics of rectangular concrete prisms tested in uniaxial compression, and (b) determine the effectiveness of using selected confining reinforcement in the compressive zone of reinforced concrete flexural members to increase their ultimate strength and ductility.

Scope

One hundred and twelve 4- by 4- by 12-in. prisms reinforced with

helices, rectangular ties, plane meshes (vertical and horizontal), and tubular meshes (square and circular) of various sizes and weights were cast. In addition, six unreinforced prisms were cast. The prisms were tested to failure under a uniaxial compressive load applied along the long axis. Continuous records of load versus total deformation were obtained for each specimen.

Twenty-four 4- by 9- by 78-in. concrete beams (6-ft span) reinforced with various amounts of high-strength steel, four without and twenty with confining compressive reinforcement, were cast. The beams were tested to failure under two symmetrical line loads applied 6 in. from the beam center line. Continuous records of load versus deflection were obtained.

CHAPTER II: MATERIALS AND CONCRETE MIXTURE

Materials

The materials used in the concrete mixtures were type II Portland cement and crushed limestone aggregate (3/8-in. maximum size). Nine different reinforcing materials were used in the investigation and are described as follows:

a. Galvanized hardware cloth, 23 gage, 1/4- by 1/4-in. mesh.

b. Galvanized hardware cloth, 19 gage, 1/2- by 1/2-in. mesh.

c. Galvanized hardware cloth, 17 gage, 5/8- by 5/8-in. mesh.

d. Galvanized wire mesh, 14 gage, 1- by 1-in. mesh.

e. Galvanized wire mesh, 14 gage, 1- by 2-in. mesh.

f. Galvanized wire mesh, 16 gage, 2- by 2-5/8-in. mesh.

g. Smooth steel annealed wire, 12, 14, and 16 gage.

h. Plain structural-grade steel bars, No. 2.

i. Deformed high-strength steel bars, No. 4.

A stress-strain curve showing the results of standard tensile tests on the high-strength steel bars is presented in plate 1.

Concrete Mixture

A concrete mixture was proportioned with 3/8-in. maximum-size crushed limestone aggregate to have a slump of 2 $\pm$ 1/2 in. and a compressive strength of 3000 psi at 28 days age. Mixture proportions were as follows:

Material	Solid Volume, ft^3	Dry Batch Weight, lb
Type II cement	0.479	94.0
Fine aggregate	2.154	358.3

(Continued)

Material	Solid Volume, ft^3	Dry Batch Weight, lb
Coarse aggregate	2.070	349.5
Water	1.297	80.8
Admixtures	None	None

A typical stress-strain curve for this concrete, as determined from testing a standard 6- by 12-in. cylinder, is shown in plate 2.

CHAPTER III: PRISM TESTS

Specimens

One hundred and eighteen 4- by 4- by 12-in. rectangular prisms (one hundred and twelve with and six without confining reinforcement) were tested to failure under a uniaxial compressive load. The confining reinforcements fabricated from locally available material for use in the reinforced prisms are described in table 1. Also, photographs of the reinforcements are included in the presentation of test results (plates 3-19). Two specimens were cast for each type of reinforcement. The reinforcement types can be grouped into the following general categories.

Tubular meshes

The twenty-four types of circular and square tubular mesh reinforcements fabricated (specimens 1-13, 22-27, and 33-37) were 3 in. in diameter and width, respectively. Wire and mesh sizes ranged from 14 to 23 gage and from 1/4 by 1/4 to 2 by 2-5/8 in., respectively. Both square and rectangular mesh openings were used. Also, the effects of horizontal ring location, i.e., inside or outside the longitudinal wires, and the effects of single and double cross bracing were investigated.

Helices

Twelve types of 3-in.-diam helices (specimens 14-21 and 42-45) were fabricated from 12-, 14-, and 16-gage smooth steel wire. Pitches of the helices were varied from 1/2 to 2 in. in 1/2-in. increments. In addition, four types of 4-in.-diam helices (specimens 57-60), two

each from 12- and 16-gage wire with pitches of 1/2 and 1 in., were fabricated.

Plane meshes

Nine types of horizontal plane meshes (specimens 29 and 30 and 50-56) were fabricated from 3-in. squares of mesh vertically spaced at 1/2, 1, and 1-1/2 in. Wire sizes were 14, 17, and 23 gage with corresponding mesh openings of 1 by 1, 5/8 by 5/8, and 1/4 by 1/4 in. In addition, two types of vertical plane meshes (specimens 31 and 32) were fabricated from 3- by 12-in. rectangles horizontally spaced at 1 in. Corresponding wire sizes and mesh openings were 17 and 23 gage and 5/8 by 5/8 and 1/4 by 1/4 in., respectively.

Lateral ties

Lateral ties, 3 in. square with hooked ends, were fabricated from 12-gage smooth steel wire. These ties, used in conjunction with vertical reinforcement of four 1/4-in.-diam steel rods, were spaced at 1, 2, 3, 4, and 12 in. to comprise specimens 61-65, respectively.

Upon completion of reinforcement fabrication, reinforcement cages were properly positioned in the steel molds, and the specimens were cast in horizontal position. After consolidation on a small vibrating table and finishing of the exposed surface, specimens were stored in a fog room and cured for 28 days. Molds were removed at 3 days age.

Test Procedure

A rectangular prism was centered in a 440,000-lb-capacity hydraulic universal testing machine, and a steel frame on which two linear displacement transducers had been mounted was positioned around the

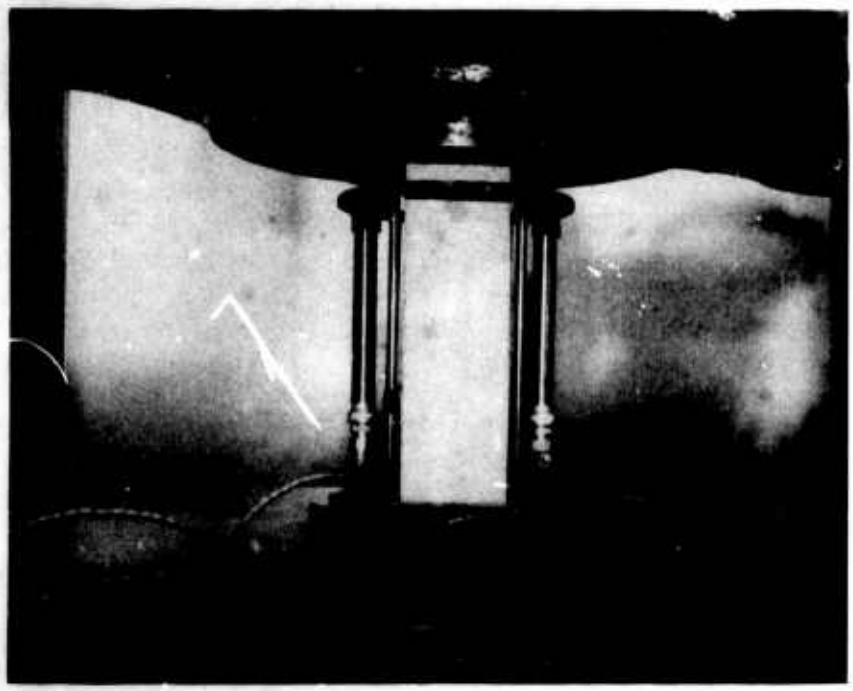

Fig. 1. Prism test arrangement

specimen (fig. 1). The transducers had linear ranges of ±0.50 in., and a linearity of 0.5 percent of range calibrated.

A small load (300 lb) was applied to the specimen to seat the loading platen properly. This load was then reduced to approximately 10 lb, and necessary adjustments to transducer zero were made. Load was applied at a uniform rate of approximately 28,000 lb/min. Output from the two transducers was averaged, and this signal was fed into an x-y recorder to obtain a continuous record of load versus total deformation.

Loading was continued beyond ultimate until either the load-carrying capacity was less than 50 percent of ultimate or a total deformation of 0.25 in. was attained, whichever occurred first. At this point loading was discontinued, and the specimen was removed from the machine and photographed.

Test Results

Load-deformation measurements

Normalized stress-strain curves (average of two specimens) for each type of confining reinforcement are shown in plates 3-19. In addition, a normalized stress-strain curve (average of six specimens) for the unreinforced control specimens is presented in each plate for comparison purposes. These average unit strains were obtained by dividing the total deformation, as determined by two transducers, by the length of the specimen and are probably slightly less than the actual maximum unit strain present at midheight in the test specimen. This somewhat unusual technique for determining strain was predicated by the magnitudes of the strains resulting from continuing the loading beyond ultimate to either 50 percent of ultimate or 0.25-in. total deformation. Conventional electrical resistance gages bonded to the specimen surfaces were impractical due to spalling of the concrete cover at strains approximately one-sixth of the maximum. Also, the magnitude of the maximum strain (greater than 20,000 μin.) exceeded the ranges of most conventional embedded gages.

Concrete ductility

Strain at 60 percent postultimate strength was arbitrarily chosen as a measure of ductility, and reinforcement weight-ductility relations are given in plates 20-24. For each type of reinforcement, the curve of best fit for the given points was calculated, and these curves are compared in plate 25 to indicate the relative efficiency of the reinforcement types investigated. Specimens 50 and 57 were excluded from these calculations for the horizontal plane mesh and helices ,

respectively, because the stress at tests end (0.25-in. total deformation) still exceeded 60 percent postultimate stress. In fact, at an average unit strain of 0.02 in./in., specimen 50 still possessed 88 percent of its ultimate strength, and the trend (see plate 15) was for this postultimate strength to increase. At the same strain (0.02 in./in.), specimen 57 possessed 72 percent of its ultimate strength; however, the trend was downward, and an extension of the curve would indicate an average unit strain of approximately 0.028 in./in. at 60 percent postultimate stress. Because the postultimate strengths of these specimens exceeded 60 percent of ultimate for the strain range investigated, the horizontal plane mesh and helices, particularly the mesh, are somewhat more efficient than indicated in plate 25.

Discussion of Test Results

The ability of confining reinforcement to increase the ultimate strain capacity and ductility of rectangular concrete prisms in uniaxial compression is clearly demonstrated by the results of the tests discussed in the foregoing paragraphs. Concrete properly confined by lateral reinforcement has a considerable load-carrying capacity up to strains in excess of 2 percent, or more than six times the amount of strain usually considered as ultimate for concrete.

The load-deformation curves and visual observations made during testing indicated three stages of loading. In the first stage, the specimen appeared to behave elastically, with the confining reinforcement having little or no influence. The second stage was a spalling stage in which the reduction of concrete compressive area due to spalling of the concrete cover caused a drop in the load. The final

stage was a plastic stage in which the confining reinforcement enabled the confined concrete to continue to resist load. Photographs of prisms exhibiting typical failure patterns are shown in figs. 2 and 3.

The test results indicate that the horizontal plane mesh was the most efficient confining reinforcement of those investigated. Within the range of spacings, sizes, and mesh openings studied, it appears that the primary factor affecting ductility was the amount or weight of the confining reinforcement used.

Helices used as confining reinforcement, though less efficient than horizontal plane mesh, resulted in greater ductility than was obtained when tubular meshes and lateral ties were used. A comparison of the results obtained with 3- and 4-in.-diam helices indicates that an increase in the ratio of the bound concrete area to the total area significantly increases the confining effect of the reinforcement. Specifically, the drop in load due to spalling of the concrete cover is minimized for the larger helicies with the smaller pitches.

Results of tests on prisms containing compressive reinforcement and lateral ties indicated that compressive reinforcement had little effect on ductility unless the spacing of lateral ties was sufficiently small to prevent premature buckling failure.

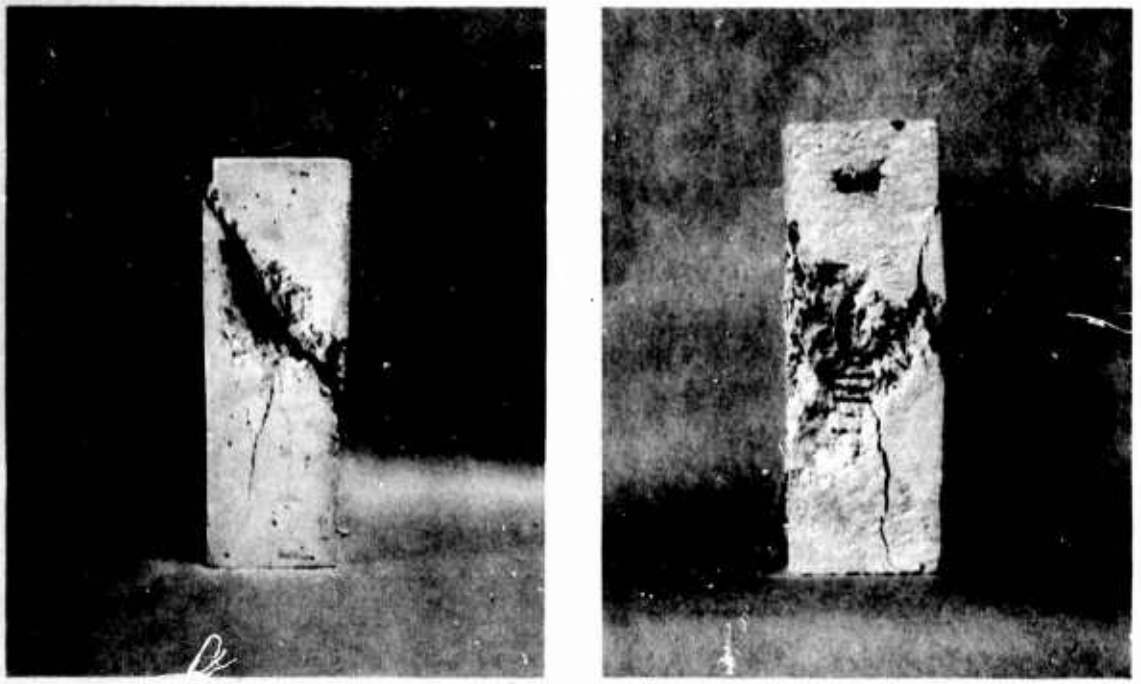

a. Unreinforced prism

b. Helical reinforcement

Fig. 2. Typical failure patterns for unreinforced and helix-reinforced prisms

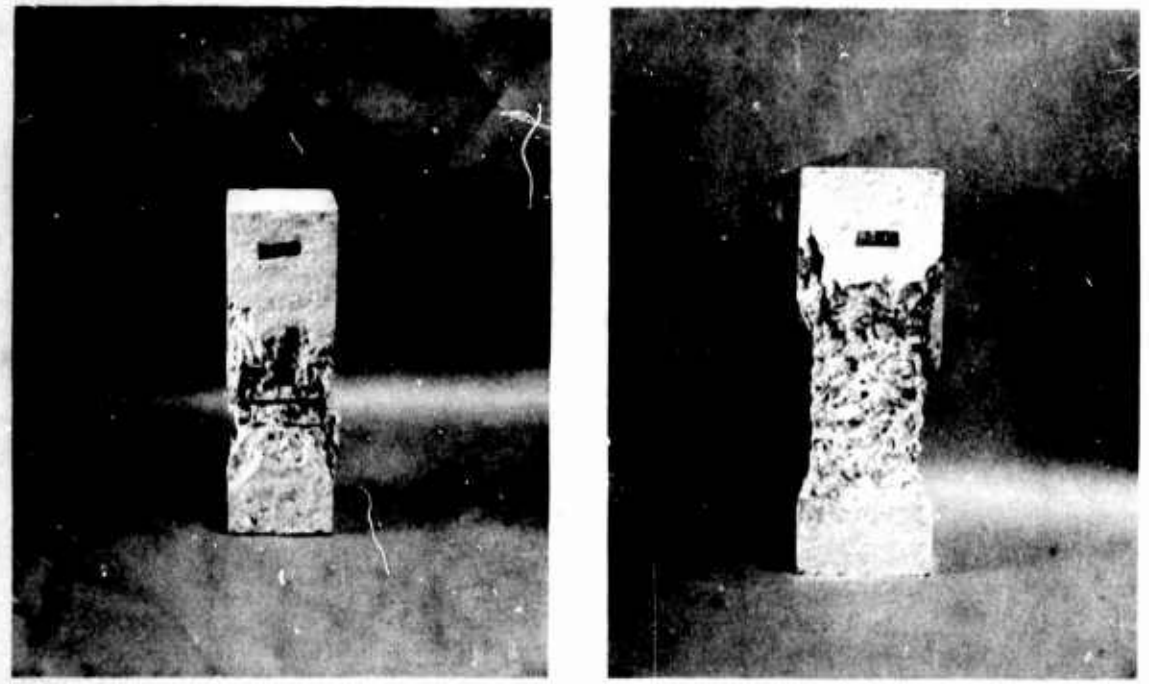

a. Lateral tie reinforcement

b. Horizontal plane mesh reinforcement

Fig. 3. Typical failure patterns for lateral tie- and horizontal plane mesh-reinforced prisms

CHAPTER IV: BEAM TESTS

Specimens

Twenty-four rectangular reinforced concrete beams having a constant width of 4 in., a constant depth of 9 in., and a length of 78 in., were tested on a simply supported span of 72 in., center-to-center of the supports. Two symmetrical line loads were applied 6 in. off the beam center line. Four basic beams were designed based on an average concrete strength of 3000 psi and No. 4 high-strength steel bars with an average yield strength of 60,000 psi. Of the three designs with tensile reinforcement only, design 1 was conventionally reinforced, i.e., underreinforced with $p < 0.75p_b$; design 2 was slightly underreinforced, $0.75p_b < p < p_b$; and design 4 was overreinforced, $p > p_b$. The remaining design (design 3) contained compressive reinforcement and was underreinforced. All designs provided vertical stirrups (No. 2 at 4-in. spacing) except for the 12-in. length between the two loading points. Amount and arrangement of reinforcement are shown in fig. 4.

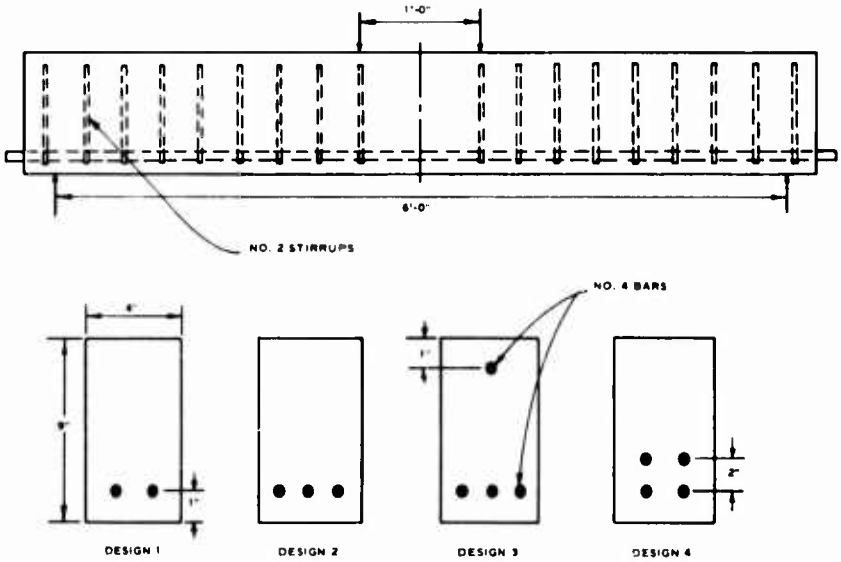

Fig. 4. Arrangement of reinforcement

Six series of test beams, with each series consisting of one beam of each design, were cast. Types of confining reinforcement in the individual test beams are shown in table 2, which presents a summary of beam test results. Each series of beams is described briefly in the following paragraphs.

Series A

These four beams (A-1 - A-4), the control specimens, were cast according to the designs previously discussed.

Series B

The four beams in this series (B-1 - B-4) were similar to those in series A with the exception that the vertical stirrups (No. 2 at 4-in. spacing) were extended throughout the entire length of the beams in this series only.

Series C

These beams (C-1 - C-4) contained helical confining reinforcement in the compression zone. A 3-in.-diam helix with 1/2-in. pitch fabricated from 12-gage smooth annealed wire was positioned in a 16-in. section at the midspan of each beam.

Series D

Beams D-1 - D-4 contained 14-gage, 1- by 1-in. plane mesh confining reinforcement, a sample of which is shown in fig. 5. The horizontal mesh spacing, 0.9 in., was selected to provide the same area of shear reinforcement as provided by the additional stirrups in series B.

Series E

Beams E-1 - E-4 were similar to those of series D with the exception that the horizontal mesh spacing was reduced to 0.5 in.

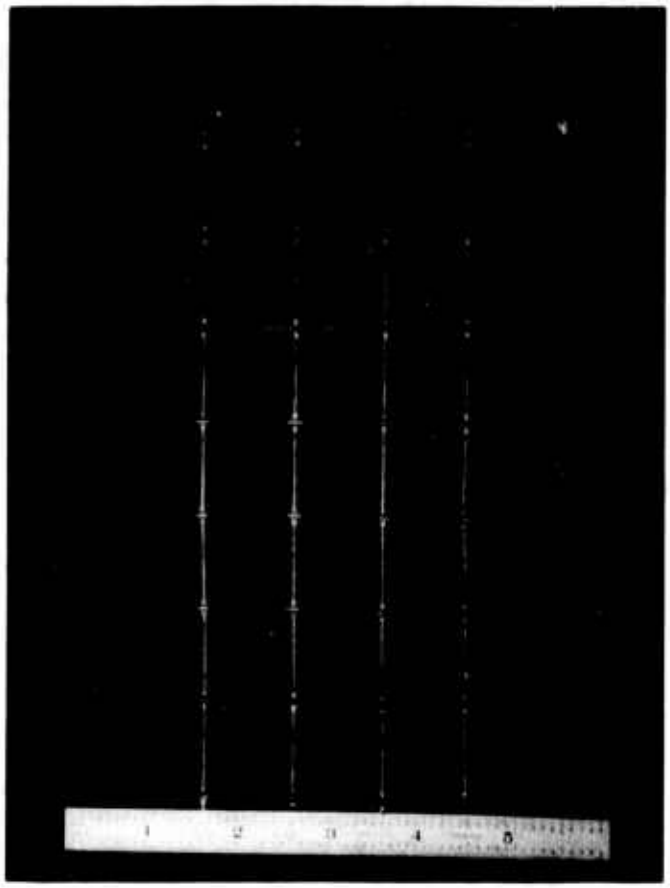

Fig. 5. Plane mesh reinforcement

Series F

Beams F-1 - F-4 contained small closed stirrups fabricated from 12-gage smooth steel wire as confining reinforcement. The stirrup spacing, 0.8 in., was selected to provide the same area of shear reinforcement as provided by the additional stirrups in series B.

Strain gages were attached to the longitudinal (tensile and compressive) reinforcement bars, and the leads were brought out at the sides and top of the beam. The concrete was placed in steel forms and consolidated with small internal vibrators. During the casting of each group of test beams, three standard test cylinders (6 by 12 in.) were also cast.

Upon completion of casting, all specimens were covered with burlap and moist-cured for 3 days. Then the forms and molds were removed, and the specimens were stored in a fog room for additional curing. At 14 days age, all specimens were removed from the fog room and air-cured until time of test at 28 days age.

Loading Apparatus

A rigid steel test frame was used for all beam tests with the beams supported on steel rollers as shown in fig. 6. A special

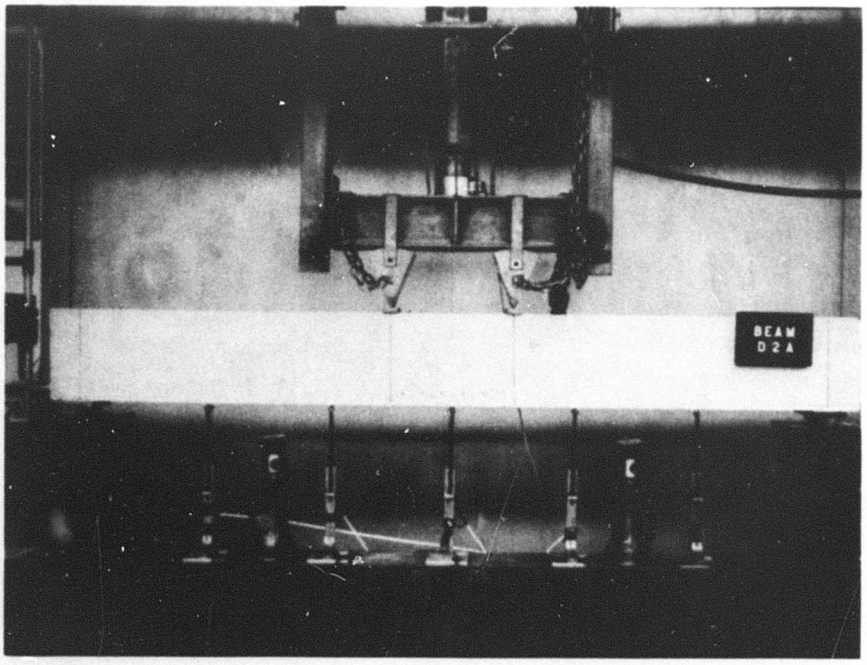

Fig. 6. Typical beam test setup

load-distribution beam incorporating a rocker system (fig. 7) was designed to ensure that loads were applied in a vertical plane even at extremely large deflections. Loads were supplied by means of a single hydraulic jack and the distribution beam that transmitted the load to the two loading points 6 in. off the beam center line. Steel pads,

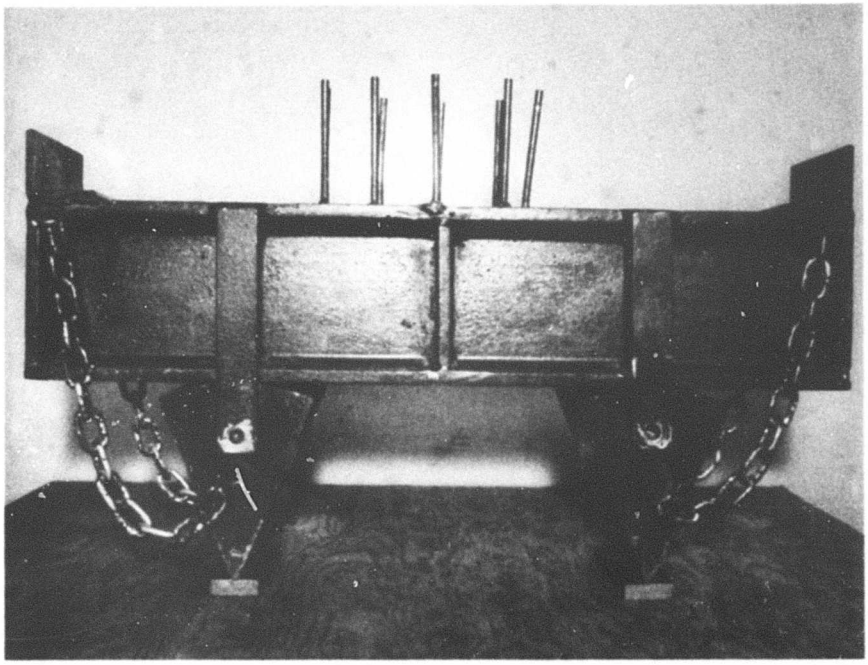

Fig. 7. Load-distribution beam

1 and 2-1/2 in. wide, served to distribute rocker loads and support reactions, respectively.

Instrumentation

Longitudinal strains in the tensile and compressive reinforcements were measured at midspan with bonded resistance strain gages. Concrete surface strains on top and at the sides of the beam at the level of reinforcement were measured at midspan with 2-in. gage-length mechanical strain gages. These strain measurements were obtained for correlation with measurements from future tests, and the results are not included in this report since the present area of interest is primarily ultimate load and beyond, at which point concrete spalling prevented further surface compressive strain measurements.

Potentiometers (6-in. range) were mounted on the test frame to

determine beam deflections at five points along the span. Output from the potentiometers and from a 30,000-lb-capacity load cell was fed into x-y and $x\text{-}y_1\text{-}y_2$ recorders to obtain continuous plots of load versus deflection. Deflections of the rigid test frame were monitored, and corrections to beam deflections were made when necessary.

A 50-ton-capacity hydraulic jack, a 2500-psi precision pressure gage, and a loading console were combined to apply and measure load.

Test Procedure

A beam was placed in the testing frame, and the load-distribution beam was situated on top of the test beam. Particular attention was given to alignment of the test beam and the load-distribution beam to ensure true axisymmetric loading.

After the five potentiometers had been mounted against the underside of the beam and all strain gages had been connected, loading was begun. Loads were applied in increments of 2000 lb (total load), with a complete set of concrete surface strain and steel reinforcement strain readings being made after each increase of load. Cracks were observed visually throughout the test, with significant changes in crack patterns being photographed. Generally, loading was continued beyond the maximum load-carrying capacity until either the load decreased to 10-15 percent of ultimate or the deflection reached the limits of the testing system (6-in. midspan or L/12), whichever occurred first.

Analysis Procedure

Since the value of ultimate concrete compressive strain is uncertain when concrete ductility is increased by confining reinforcement

and since the true maximum moment capacity of the section was desired rather than the moment that caused a specified ultimate strain, the iterative analysis procedure described in detail by Geymayer[13] was used in this investigation. Starting with 0.0005 in./in., assumed values for maximum concrete strain were increased in increments of 0.0005 in./in. until either the moment decreased to a point well below the maximum or an ultimate unit strain in the top fibers of 0.020 in./in. was attained. By consecutively taking different values for concrete strain, moment-curvature and load-deflection curves were obtained, as will be shown later. Briefly, the analysis procedure used is as follows:

a. Numerically integrate the experimentally evaluated stress-strain curves of the concrete (plate 26) computing a shape factor (k_1) for various values of concrete strain (ϵ_{co}).

b. For the same values of ϵ_{co}, determine the ratio of the depth to the resultant of concrete compressive force to depth of neutral axis. This ratio is designated as k_2 (fig. 8).

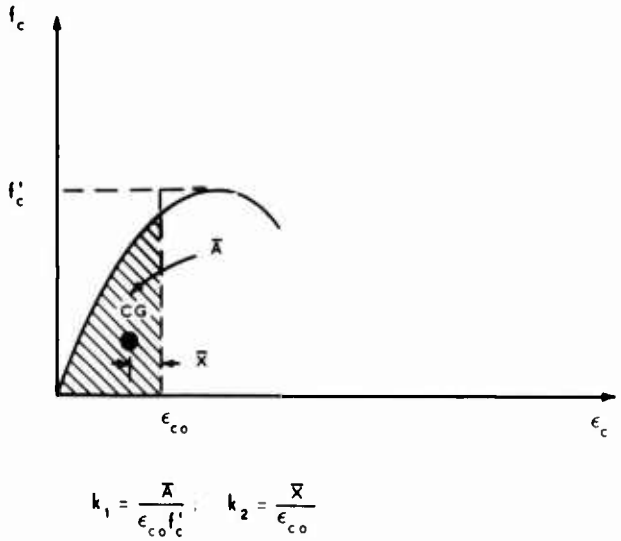

Fig. 8. Stress-strain curve

c. Let $\epsilon_{co} = 0.0005$ in./in.

d. Assume a value for kd . (Geometry and mechanics of a typical cross section containing only tensile reinforcement are shown in fig. 9).

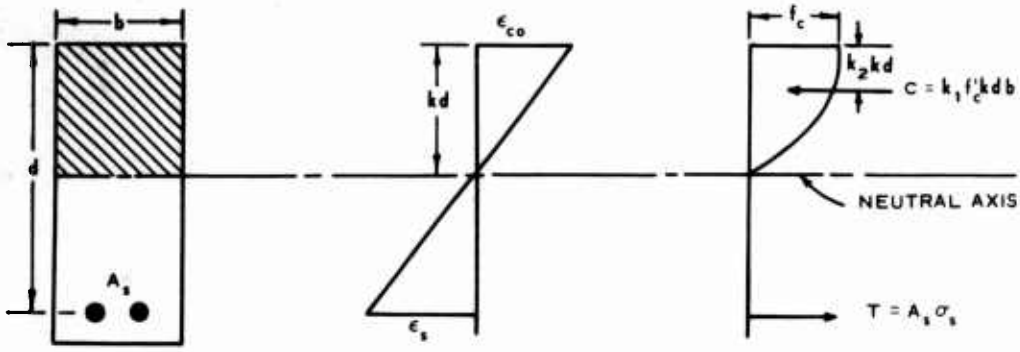

Fig. 9. Mechanics and geometry of cross section

e. Compute the total compressive force in the concrete (C)

$$C = k_1 f'_c \, kd \, b$$

f. Compute reinforcement strains within all layers of tensile and compressive reinforcement

$$\epsilon_{s_i} = \frac{\epsilon_{co}}{kd} (d_i - kd)$$

$$\epsilon'_s = \frac{\epsilon_{co}}{kd} (d' - kd)$$

and find the corresponding reinforcement stresses σ_{s_i} and σ'_s from the stress-strain curve of the reinforcement.

g. Compute the total tensile force carried by the tensile reinforcement

$$T_i = \sum_{1}^{n_r} A_{s_i} \sigma_{s_i} \qquad (\epsilon_{s_i} \leq \epsilon_{sh})$$

$$T_i = \sum_{1}^{n_r} A_{s_i} \sigma_{s_i} + \sum_{1}^{n_r} A_{s_i} (\epsilon_{s_i} - \epsilon_{sh}) E_{sh} \qquad (\epsilon_{s_i} > \epsilon_{sh})$$

$$(\sigma_{s_i} = f_y)$$

and the compressive force carried by the compressive reinforcement

$$T' = A_s' \sigma_s'$$

h. If $C + T' \neq \Sigma T_i$, assume a new kd and repeat the iteration beginning with step e. Repeat this operation until equilibrium of forces within the section is achieved within reasonable limits (e.g., 1 percent).

i. Compute the moment of all forces about the neutral axis

$$M = \sum_{1}^{n_r} T_i (d_i - kd) + T' (kd - d') + C (kd - k_2 kd)$$

j. Compute the curvature

$$\phi = \frac{\epsilon_{co}}{kd}$$

k. Increase ϵ_{co} in increments of 0.0005 in./in. and repeat the iteration analysis beginning with step d.

To facilitate the computations outlined in the iteration analysis, a computer program was written for a GE-265. The program was written in BASIC language for a time-sharing system. Program input consisted of experimentally evaluated stress-strain relations for the concrete and longitudinal reinforcement, beam size, and amount and geometry of the longitudinal steel. Program output included concrete strain, distance from neutral axis to top fiber, curvature, moment, and strain in the tensile reinforcement. Theoretical moment-curvature curves computed for each test beam using this analysis procedure are shown in plates 27-30.

Using the moment-curvature relations previously obtained, the

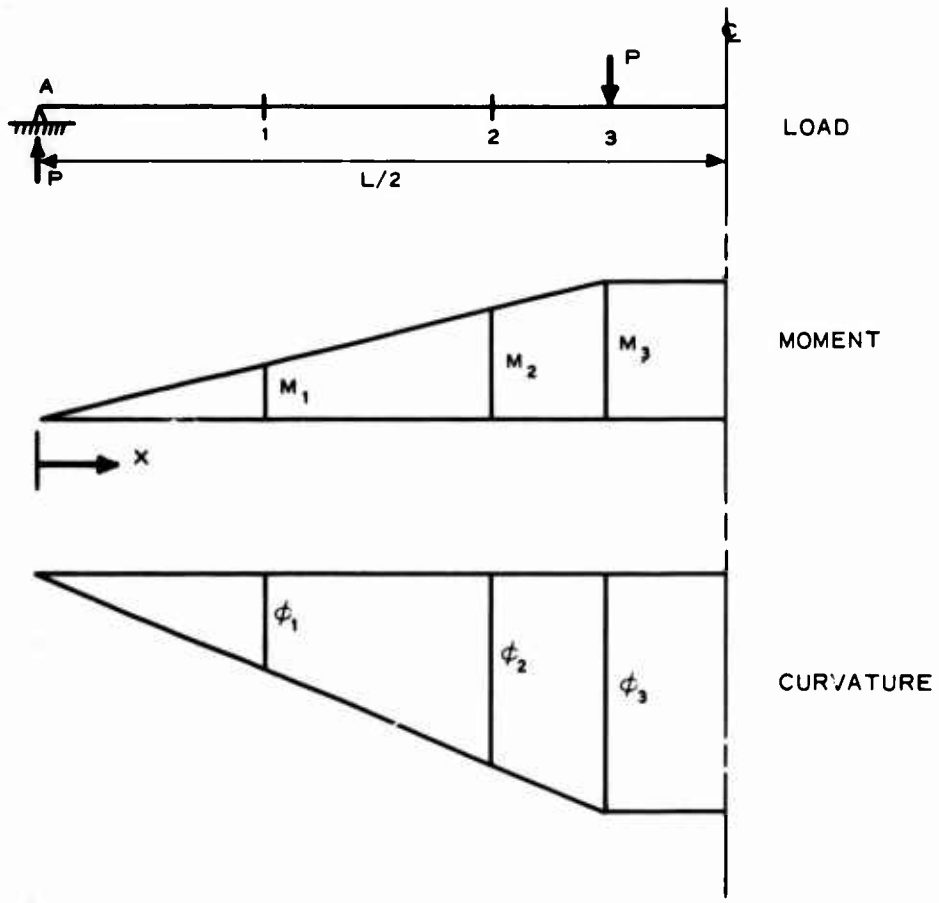

Fig. 10. Moment-curvature distribution

curvature distribution along a beam can be plotted (fig. 10). Double integration of the curvature distribution eventually yields the bending line of the beam for the given moment distribution. For the simply supported, symmetrically loaded beams tested in this investigation, the midspan deflection is:

$$Y_m = \theta_A \frac{L}{2} - \int_0^{L/2} \phi_{(x)} \left(\frac{L}{2} - x\right) dx$$

Load-deflection curves computed in this manner are compared with portions of the experimental results in plates 31-54.

Test Results

Complete load-deflection characteristics of the test beams are

shown in plates 55-82. From these relations, the actual ductility ratios, i.e., the ratios of the maximum deflections of the beam at the point of collapse to the maximum elastic deflections, were computed and are shown in table 3. In some cases, the exact point of collapse was difficult to determine. As a result, collapse deflections were defined as those corresponding to 90 percent of the yield moment (after spalling). In the cases where the moment did not drop to this level, the maximum deflection was used. Yield, spalling, and ultimate moments are presented in table 2. Also in table 2, actual ultimate moments are compared with theoretical ultimate moments computed with (1) the iterative analysis procedure described earlier and (2) an ultimate strength analysis assuming a Whitney stress block and an ultimate concrete strain of 0.003 in./in. Theoretical and measured midspan deflections of each test beam are compared in plates 31-54. Photographs 1-19 show failure patterns and plastic hinging developed in selected beams.

Series A

The four beams (A-1 - A-4) in this series, which were control specimens without confining compressive reinforcement, failed within 1.8 percent of their predicted failure loads, generally in an essentially compressional mode. Individual beam behavior is described briefly below.

Beam A-1. An underreinforced section ($p/p_b = 0.57$), this beam exhibited the conventional failure pattern of initial reinforcement yield followed by compressional failure of the concrete. As in all beams in this series, the actual ductility ratio was considerably less than ratios predicted by equations presented in the Air Force Design

Manual,[16] which were based on tests of reinforced concrete beams using a structural grade of steel.

Beam A-2. The additional reinforcement in this beam ($p/p_b = 0.88$) increased the rate at which the concrete crushed after initial reinforcement yield. As a result, the ductility ratio was less than half of that in beam A-1.

Beam A-3A. This beam was similar to beam A-2 with the exception that it contained compressive reinforcement. Comparing ductility ratios for beams A-2 and A-3A indicates that compressive reinforcement contributes to a beam's ductility as expected. This increase probably would have been somewhat greater except for premature buckling of the compressive reinforcement (photograph 1a).

Beam A-4. This overreinforced section ($p/p_b = 1.18$) failed in a brittle manner due to crushing of the concrete and, as expected, possessed very little ductility (1.8 actual ductility ratio).

Series B

The four beams (B-1 - B-4) in this series, each containing vertical stirrups throughout the entire length, failed within 2.3 percent of the predicted failure load. As in series A, all failures were generally in an essentially compressional mode. In this series, the concrete crushing was generally confined to a 6-in. length about the beam center line, whereas in series A, the concrete tended to crush along the entire length (12 in.) between load points. Again, as in series A, actual ductility ratios were considerably less than the predicted ratios. Individual beam behavior is described briefly below.

Beam B-1. This beam behaved in nearly the same manner as beam A-1, with only a small increase in ductility.

Beam B-2. Again, as in design 1, the addition of vertical stirrups between the load points had little effect on the beam behavior.

Beam B-3. This beam exhibited a slight increase in ductility, probably due to the additional restraint against buckling of the compressive steel provided by the vertical stirrups (photograph 1b).

Beam B-4. This overreinforced section performed in nearly the same manner as beam A-4. As a result, ductility ratios of beams A-4 and B-4 were identical.

Series C

The four beams (C-1 - C-4) in this series contained helical confining compressive reinforcement in the hinging region between load points. These beams behaved in essentially the same manner as comparable beams without confining reinforcement up to the spalling moment. Spalling moment is defined as the initial peak in the load-deflection relation. At this point, the concrete cover to the helix started to spall, and loads decreased in amounts ranging from 8 percent (beam C-1) to 20 percent (beam C-4) before stabilizing. With the transfer of stresses from the spalled concrete cover to the confined concrete core completed, loads, with the exception of that of beam C-4, started to increase. In the underreinforced sections, the ultimate moment actually exceeded the spalling moment. In each beam, the confined concrete core bounded by the helix remained relatively intact (photographs 2-5) even after beam deflections up to L/13. Obviously, the ability of the confined concrete to continue carrying load after spalling of the cover greatly improved the load-deflection characteristics of each beam. As a result, significant increases in ductility were obtained when compared with series A beams without confining compressive reinforcement.

Individual beam behavior is described briefly below.

Beam C-1. Due to spalling of the concrete cover, the moment dropped approximately 8 percent from the initial peak or spalling moment (179.0 in.-kips) prior to increasing uniformly to an ultimate moment of 199.5 in.-kips, or an increase of approximately 11 percent over the spalling moment. This indicates that, in addition to increasing the ductility significantly, proper confining compressive reinforcement slightly increases the ultimate moment capacity of an underreinforced section.

Beam C-2. Concrete in the top of this beam, a nearly balanced section ($p/p_b = 0.95$), began to crush almost immediately after yielding of the tensile reinforcement. As a result of this crushing, the moment decreased to 94 percent of spalling moment before stabilizing. At this point, the moment started increasing and peaked at 96 percent of spalling moment before diminishing rapidly due to localized crushing of the concrete core. Compared with beam A-2 (no confining reinforcement) the helix provided an increase in ductility of more than 300 percent.

Beam C-3. After attaining a spalling moment of 262.5 in.-kips, the concrete cover started crushing, and the moment dropped to 90 percent of the spalling moment. Stabilizing at this point, the moment began to increase, peaking at an ultimate moment of 286.5 in.-kips, or an increase of approximately 9 percent over the spalling moment. At ultimate, the compression steel strain was well beyond the yield point, and only the confined core of concrete remained to act with the steel in carrying the compressive force (photograph 6). Apparently, the compressive steel buckled at this point, causing a localized failure of the helix (photograph 4). As a result, the concrete core started crushing

at the point of helix failure, and the moment decreased rapidly.

Beam C-4. The helix in this beam shifted downward during consolidation of the concrete and was well below its optimum position near the compressive surface (photograph 5). As a result, spalling of the increased concrete cover caused the moment to drop below 90 percent of the yield moment before stabilizing. Consequently, the ductility ratio determined as previously described was identical with that of a comparable beam without confining compressive reinforcement. However, taking the collapse deflections as those corresponding to 80 percent of yield load results in ductility ratios of 2.2 and 6.7 for beams A-4 and C-4, respectively. This indicates that the helical binding provided more than three times the ductility obtained without confining compressive reinforcement. Even though the beam still failed by crushing of the concrete, helical binding in this overreinforced section transformed the brittle failure mode normally associated with such beams into an essentially plastic failure mode.

Series D

Beams D-1 - D-4 contained plane mesh at 0.9-in. horizontal spacing as confining compressive reinforcement in the hinging region. These beams behaved in essentially the same manner as comparable beams in series C, with the exception that the drop in load due to spalling of the concrete cover was generally smaller than the drop in series C. This is attributed to the fact that the unconfined concrete area outside the helix was larger than that outside the plane mesh. As in series C, the confined concrete core in the hinging region of all beams except beam D-2A remained relatively intact (photographs 7-10). Comparing these beams with those without confining compressive reinforcement

clearly demonstrates the ability of plane mesh to increase the ductility of reinforced concrete beams greatly. In addition, the plane mesh increases the ultimate strength of underreinforced beams by increasing the ultimate compressive strain capacity of the concrete. Individual beam behavior is described briefly below.

Beam D-1. The moment in this underreinforced section ($p/p_b = 0.63$) dropped approximately 6 percent from the spalling moment due to crushing of the concrete cover. After the compressive force had been transferred to the confined concrete core, the moment increased to an ultimate of 207 in.-kips, an increase of approximately 11 percent over the spalling moment. The ductility ratio, essentially the same as for beam C-1, was four times that of a comparable beam without confining compressive reinforcement.

Beam D-2A. As expected, the concrete in the top of this beam began to crush very soon after yielding of the reinforcement. However, the moment stabilized after spalling and had started to increase slightly when a localized failure in the mesh occurred (photograph 8). This failure allowed the confined concrete to crush, and the moment decreased rapidly.

Beam D-3. This beam failed in a manner similar to that of beam C-3. At spalling moment, the concrete cover to the mesh began crushing, and the moment dropped to 96 percent of the spalling moment. As the confined concrete and the compressive reinforcement assumed the total compressive force in the beam, moment started increasing to a peak of 319.5 in.-kips, an increase of more than 18 percent over the spalling moment. Apparently, the compressive reinforcement buckled at this point, rupturing a portion of the plane mesh, and the moment decreased rapidly.

Beam D-4. As in beam C-4, the confining compressive reinforcement transformed the normally brittle failure of an overreinforced section into an essentially plastic failure which gave warning of imminent collapse.

Series E

Beams E-1 - E-4 were similar to the beams in series D except that the plane mesh confining compressive reinforcement had a horizontal spacing of 0.5 in. Generally, the beams in this series performed in essentially the same manner as those previously discussed that contained confining compressive reinforcement (series C and D). However, an examination of the test results clearly indicated that the beams in this series were considerably more ductile than those of any other series investigated. Series E beams exhibited ductility ratios ranging up to more than nine times those of comparable beams without confining reinforcement.

Beam E-1. This underreinforced section ($p/p_b = 0.68$) exhibited a spalling moment of 184.5 in.-kips. Due to yielding of the reinforcement and subsequent crushing of the concrete cover to the mesh, the moment dropped to 95 percent of the spalling moment. After transfer of the compressive force to the confined concrete, moment started increasing and was still increasing when the loading system became unstable at 6.1-in. (L/12) deflection. Moment at this point was 226.5 in.-kips, or approximately 23 percent more than the spalling moment. The ductility ratio of more than 22.2 was the largest for any beam in the investigation. Plastic hinge formation at various loads is shown in photograph 11. It is apparent from photograph 12 that the confined concrete remained intact after considerable bending. No mesh failures were

observed. This was the only beam tested in which the stress outside the constant moment section was sufficiently high to cause concrete spalling outside the hinging region (photographs 11 and 12).

Beam E-2A. This slightly underreinforced section ($p/p_b = 0.82$) exhibited a failure pattern typical of that of underreinforced beams with confining reinforcement--initial yielding of tensile reinforcement followed by a drop in load due to crushing of concrete cover, transfer of compressive force to confined concrete, then increasing moment due to strain hardening of tensile reinforcement until strain capacity of the confined concrete is exceeded. In this case, several failures at mesh joints were observed which apparently allowed the confined concrete to crush at an advanced state of strain. Plastic hinge formation at various loads is shown in photograph 13.

Beam E-3. This was the only beam tested of design 3 in which the compressive reinforcement did not buckle. However, it appears from the load-deflection curve (plate 69) that the beam may have been approaching this critical state when the test was discontinued due to instability of the distribution beam at such a large deflection. As in other beams of this series, beam E-3 exhibited the greatest ductility of any beam of its design in the investigation. The hinging section at failure is shown in photograph 14.

Beam E-4. This overreinforced section ($p/p_b = 1.49$) exhibited nearly four times the ductility of the underreinforced section without confining compressive reinforcement tested in this investigation. Obviously, the plane mesh confining reinforcement transformed the brittle failure of beam A-4 into a truly plastic failure which gave ample warning of imminent collapse. The hinging region at failure is shown in

photograph 15. Considering that overreinforced sections normally have little or no ductility, the ductility ratio of 16.5 obtained in this test seems incredible.

Series F

Beams F-1 - F-4 contained small, closely spaced, rectangular, closed stirrups as confining reinforcement. The load-deflection curves for beams of this series show that the closed stirrups used in this investigation were decidedly less efficient than the other types of confining compressive reinforcement investigated. Examination of the hinging region of these beams (photographs 16-19) reveals that the rectangular stirrups were of inadequate rididity and tended to deform into oval shapes at elevated strains, thus allowing the confined concrete to crush. Individual beam behavior is described briefly below.

Beam F-1. This underreinforced section ($p/p_b = 0.61$) exhibited greater ductility than a comparable beam (A-1) without confining reinforcement. However, the ductility was somewhat less than that obtained with beams of similar design containing the other types of confining reinforcement investigated. Apparently the stirrups deformed outward (photograph 16) under the bursting pressure of the confined concrete, allowing the confined concrete to crush with a subsequent rapid decrease in load.

Beam F-2. The drop in load due to crushing of the concrete cover was sufficient to penalize this beam when ductility ratios were determined as previously described. However, the moment tended to stabilize a lower load, and computation of the ductility ratio at 80 percent of yield load yielded a value of 4.5, or more than twice that at 90 percent of yield load. Still the ductility ratio was less than half that of the

beam F-1 ratio due to the additional reinforcement in this beam, which increased the rate of concrete crushing after initial reinforcement yield.

Beam F-3. It was difficult to determine whether buckling of the compressive reinforcement or crushing of the confined concrete occurred first in this beam. However, because the compressive steel buckled in a horizontal plane, it is believed that the stirrups deformed outward, allowing the concrete to crush with subsequent buckling of the steel and a rapid decrease in the load.

Beam F-4. The rectangular stirrups did little to improve the brittle failure mode normally associated with an overreinforced section. Consequently, this beam was only slightly more ductile than comparable beams without confining reinforcement.

Discussion of Test Results

Beam behavior

In general, the significant points in the test behavior of all beams followed a typical sequence. Generalized moment-deflection curves for beams with and without confining compressive reinforcement are shown in fig. 11. Points 1-5 define the five behavior stages which define the moment-deflection response of the beams.

Point 1 represents the stage of first cracking in the beam. Generally, the cracking moments ranged from 15-30 percent of the yield moment.

The next stage in the sequence of beam behavior was the yield moment (point 2). This point represented either initial yielding of the tensile reinforcement in the underreinforced sections or initial

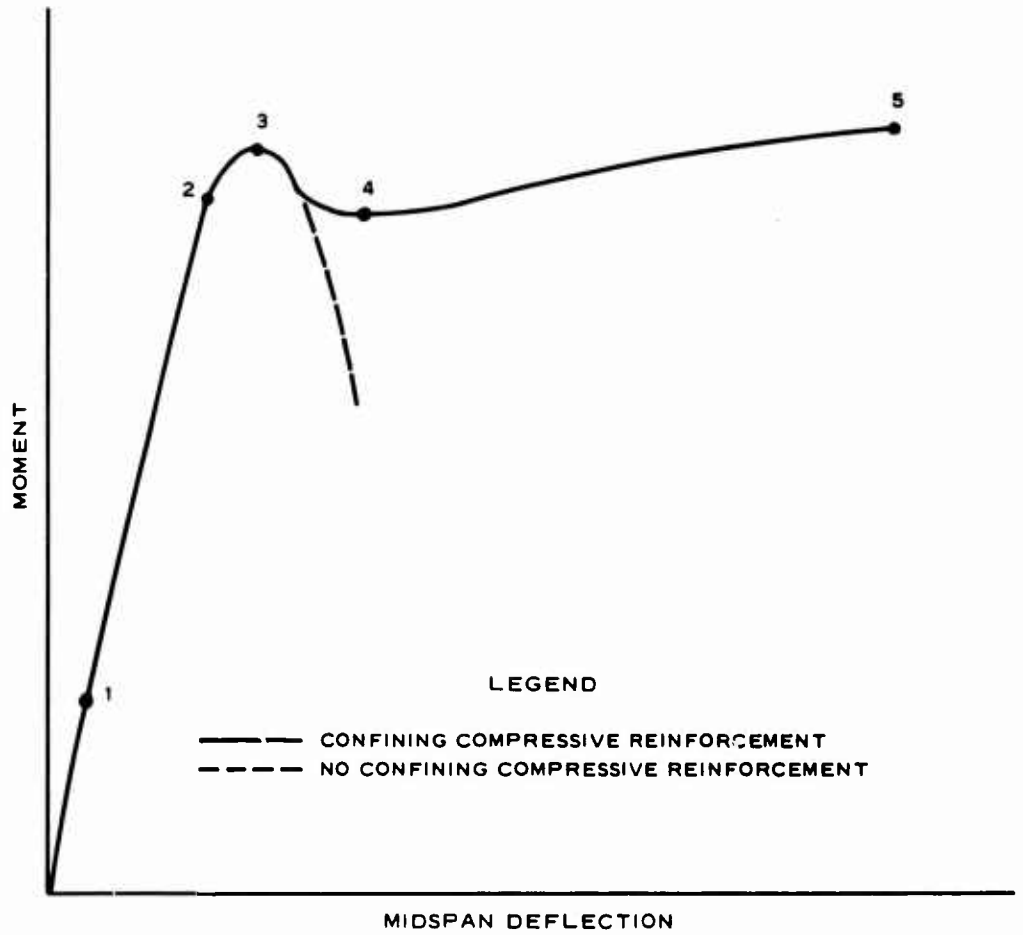

Fig. 11. Generalized moment-deflection curves

concrete cracking on the compressive surface in the overreinforced sections. As would be expected, this point marked the boundary between elastic and inelastic behavior.

Up to the spalling moment (point 3), beams with and without confining compressive reinforcement behaved in essentially the same manner. However, concrete crushing at this stage marked the ultimate moment for all beams without confining reinforcement, whereas some beams with the most efficient confining reinforcement were able to attain ultimate moments in excess of their spalling moments. As a rule, the spalling moments were only slightly higher than the yield moments.

In the beams containing confining compressive reinforcement, the confined concrete core was, in general, capable of sustaining the compressive force in a beam sufficiently to halt the decrease in moment due to spalling of the concrete cover. The point at which this transfer of compressive force to the confined concrete core was completed was designated as the stabilizing moment (point 4). With the confining reinforcement in the correct position, stabilizing moments generally ranged from 90-98 percent of the spalling moments. As expected, the larger the unconfined compressive area the larger the drop in moment.

The final stage in the behavior of beams with confining compressive reinforcement was the ultimate moment (point 5). Usually, this stage was terminated by localized failure of the confining reinforcement and subsequent crushing of the confined concrete, which allowed the load to diminish rapidly.

Ductility

The ability of confining compressive reinforcement to greatly increase the ductility of both underreinforced and overreinforced concrete beams is clearly demonstrated by the results of this investigation. All beams with confining reinforcement underwent much larger deformations before collapse than comparable beams without such reinforcement. In addition, the most efficient confining reinforcement (plane mesh) transformed the brittle failure mode normally associated with an overreinforced section into a plastic failure mode which gave ample warning of imminent collapse.

As shown in table 3, the actual ductility ratios for the beams of conventional design (series A and B) were considerably less than those predicted by equations given in the Air Force Design Manual.[16]

These equations were developed from tests of reinforced concrete beams using a structural grade of steel with a yield point of approximately 40 ksi. It appears that the use of higher strength reinforcement such as that used in this investigation necessitates a slight modification in these equations. Multiplying the present equations by the ratios of the yield strengths results in predicted values which are in much better agreement with actual values than those previously determined (table 4).

The ductility of beams with compression steel was increased as compared with the ductility of beams without compression steel, the increase being a function of the amount and spacing of secondary reinforcement provided as restraint against premature buckling of the compression steel. At best, the ductility increase achieved by the addition of compression steel (with closely spaced stirrups to prevent premature buckling) was less than 500 percent. By comparison, a ductility increase of more than 800 percent was achieved with closely spaced mesh reinforcement (no compressive reinforcement) even in an overreinforced section. Also, the latter case required less steel.

Ultimate moments

For the beams of conventional design (series A and B), actual ultimate moments were within 2.3 percent of the moments predicted by the iteration analysis procedure. In this group of beams, the ultimate moments predicted according to the stress block method were within 6 percent of those predicted by the iteration analysis procedure, with the larger differences being in the overreinforced sections. This indicates, as has been shown by Dunham and Gesund,[17] that the shape of the compressive stress block has little influence on the ultimate moment of concrete beams with conventional reinforcement.

In the beams containing confining compressive reinforcement (series C-F), actual ultimate moments were within 13.9 percent of the moments predicted by the iteration analysis procedure, with the largest differences being in the underreinforced sections. In this group of beams, the ultimate moments predicted by the stress block method were within 16 percent of those predicted by the iteration analysis procedure. In all beams the stress block method yielded the most conservative values, while, with one exception (beam C-2), the iteration analysis procedure yielded values between those of the stress block method and the actual ultimate moment.

Of the twelve beams containing the more efficient confining reinforcement (plane mesh and helix), eight exhibited ultimate moments in excess of their spalling moments. These increases in moment after crushing and spalling of the concrete cover ranged from approximately 1 percent (beam E-2A) to more than 23 percent (beam E-1). In general, these reserves in moment capacity were due to the increased strain capacity of the confined concrete core, which resulted in strain hardening in the tensile reinforcement.

Load-deflection relations

Measured midspan deflections were generally slightly less than computed deflections in the early stages of loading. In the middle loading stages, the two deflections were very nearly equal. As loads approached the yield point, measured deflections generally exceeded the computed deflections. Up to the yield point, agreement of measured and computed deflection was generally considered satisfactory. Beyond the yield point, computed deflections were somewhat smaller than measured deflections for the conventionally reinforced beams (series A and B).

However, in the remaining beams containing confining reinforcement, agreement of computed and measured deflections continued to be quite satisfactory, in some cases incredible, well beyond the yield load.

Economical aspects

It appears that the primary concern about using confining reinforcement such as the plane mesh is the added cost, both material and fabrication. The plane mesh at 0.5-in. horizontal spacing (series E), which provides the greatest ductility, results in a secondary reinforcement ratio of 1.3 percent in the hinging region. However, under the test conditions it was necessary to provide confining reinforcement in less than 25 percent of the span. Thus, based on the total beam, the secondary reinforcement ratio drops to approximately 0.3 percent. Since a mesh spacing of 0.9 in. (series D) provided shear reinforcement equivalent to that provided by the stirrups in the conventional design, it is obvious that the 0.5-in. plane mesh spacing provides an excess of such reinforcement. Omitting the bottom 5 in. of the interior legs in alternating meshs would have reduced the secondary reinforcement ratio to less than 0.3 percent and still provided adequate shear reinforcement.

The beams tested in this investigation should be considered as models of beams for actual service. As a result, the horizontal mesh spacing of 0.5 in. could be increased to a minimum of 1 in. and possibly 2 in. in a prototype specimen. This would ease the congestion in hinging regions and allow the use of normal maximum-size aggregate. Considering the increased wire diameter required in the prototype, it is contemplated that the mesh could be obtained from conventional welded wire fabric in a rather simple manner.

Whether or not confining reinforcement should be used in practice

to improve the ductility of reinforced concrete members depends upon the type of structure and the loading conditions for which it is designed. In the case of structures which must resist dynamic loads whose probability of occurrence is small, economy in design dictates that design must be based on collapse and energy-absorption concepts rather than strength. Therefore, the increased ductility resulting from the proper use of confining reinforcement such as plane mesh can and should be used to advantage in this area.

CHAPTER V: CONCLUSIONS AND RECOMMENDATIONS

Conclusions

Rectangular concrete prisms properly confined by lateral reinforcement exhibited considerable load-carrying capacity up to strains in excess of two percent, or more than six times the strain usually considered as ultimate for concrete.

The ductility of conventionally designed beams reinforced with high-strength steel was considerably less than that predicted by the current equation based on structural grade steel. Reducing ductility ratios obtained in the present manner by the ratio of reinforcement yield strengths (structural grade over high strength) significantly improved the agreement between computed and measured values.

The ability of confining compressive reinforcement, particularly plane mesh, to significantly increase the ductility of reinforced concrete beams using high-strength steel was clearly demonstrated by the results of the tests reported herein. Plane mesh confining compressive reinforcement transformed the brittle failure normally associated with an overreinforced section into a plastic failure which gave ample warning of imminent collapse. This increased ductility can and should be used to advantage in structural designs based on collapse and energy-absorption concepts.

The addition of compression steel increased ductility as compared with the ductility of beams without compression steel, the increase being a function of the amount and spacing of secondary reinforcement provided as restraint against premature buckling of the compression steel. However, a significantly larger increase in ductility can be

achieved with a closely spaced plane mesh without the addition of compression steel.

The iterative analysis procedure gave satisfactory results with respect to ultimate moments and allowed an accurate prediction of load-deflection relations of reinforced concrete beams containing confining compressive reinforcement.

Recommendations

As previously stated, the beams tested in this investigation should be considered as models of the members used in actual practice. Therefore, minimum horizontal mesh spacings in prototype members would probably be 1-2 in., or much larger than the 0.5-in. minimum spacing used in this investigation. Considering the effect of this spacing on congestion in the hinging region, tests should be conducted on prototype members to ascertain the maximum allowable spacing.

Because confining compressive reinforcement seems to have considerable promise in designs based on collapse and energy-absorption concepts, an investigation of the effect of confining reinforcement on the behavior of dynamically loaded beams should be initiated to evaluate the potential of such reinforcement in protective construction.

Additional tests should be performed to investigate the effect of confining reinforcement on tensile hinging regions and beam-column connections in reinforced concrete members.

Other types of confining compressive reinforcement, such as multiple helices and sinusoidal meshes should be investigated. Also, the effectiveness of random fiber reinforcement in improving ductility should be investigated.

BIBLIOGRAPHY

1. Winter, G., "Properties of Steel and Concrete and the Behavior of Structures," Transactions, American Society of Civil Engineers, 126, Part II, Paper 3264 (1961), 1054-1100.

2. Flexural Mechanics of Reinforced Concrete, Proceedings of the International Symposium, Miami, Fla., Nov. 10-12, 1964. American Society of Civil Engineers, 1965.

3. Richart, F. E., A. Brandtzaeg, and R. L. Brown, The Failure of Plain and Spirally Reinforced Concrete in Compression. University of Illinois, Engineering Experiment Station, Bulletin No. 190, 1929, Urbana, Ill.

4. Richart, F. E., and R. L. Brown, An Investigation of Reinforced Concrete Columns. University of Illinois, Engineering Experiment Station, Bulletin No. 267, 1934, Urbana, Ill.

5. Richart, F. E., and others, The Effect of Eccentric Loading, Protective Shells, Slenderness Ratios, and Other Variables in Reinforced Concrete Columns. University of Illinois, Engineering Experiment Station, Bulletin No. 368, 1947, Urbana, Ill.

6. Weigler, H., and J. Henzel, "Untersuchungen uber die Tragfahigkeit netzbewehrter Bentonsaulen," Deutscher Ausschuss Fuer Stahlbeton, Verlag Von Wilhelm Ernst and Sohn, Berlin, Heft 174 (1965).

7. Chan, W. W. L., "The Ultimate Strength and Deformation of Plastic Hinges in Reinforced Concrete Frameworks," Magazine of Concrete Research, London, 7, No. 21 (November 1955), 121-132.

8. Roy, H. E. H., and M. A. Sozen, "Ductility of Concrete," Flexural Mechanics of Reinforced Concrete (see Reference 2, 213-224).

9. Bertero, V. V., and C. Felippa, Discussion of "Ductility of Concrete" (see Reference 2, 227-235).

10. Szulceynski, T., and M. A. Sozen, Load-Deformation Characteristics of Concrete Prisms with Rectilinear Transverse Reinforcement. University of Illinois, Civil Engineering Studies, Structural Research Series No. 224, 1961, Urbana, Ill.

11. Base, G. D., "Helical Reinforcement in the Compression Zone of Concrete Beams," Concrete and Constructional Engineering, London, 57, No. 12 (December 1962), 456-460.

12. Base, G. D., and J. B. Read, "Effectiveness of Helical Binding in the Compression Zone of Concrete Beams," Proceedings, American Concrete Institute, 62, No. 7 (July 1965), 763-781.

13. Geymayer, H. G., Static Tests of Reinforced Concrete Beams; Development of Iterative Analysis Procedure and Tests of Beams Reinforced with Steel Aluminum, and Fiber Glass, With and Without Helical Compressive Reinforcement. U. S. Army Engineer Waterways Experiment Station, CE, Technical Report No. 6-818, Report 1, March 1968, Vicksburg, Miss.

14. Warwaruk, J., and R. L. Ward, Effect of Confinement of Concrete on Behavior of Prestressed Beams. American Society of Civil Engineers Structural Engineering Conference, Conference Preprint 501, May 8-12 1967, Seattle, Wash.

15. Soliman, M. T. M., and C. W. Yu, "The Flexural Stress-Strain Relationship of Concrete Confined by Rectangular Transverse Reinforcement," Magazine of Concrete Research, London, 19, No. 61 (December 1967), 223-238.

16. Newmark, N. M., and J. D. Haltiwanger, Air Force Design Manual; Principles and Practices for Design of Hardened Structures. Air Force Special Weapons Center, Technical Documentary Report No. AFSWC-TDR-62-138, December 1962, Kirtland Air Force Base, N. Mex.

17. Dunham, C. W., and H. Gesund, "Yield Moments of Reinforced Concrete Beams and Columns," Proceedings, American Concrete Institute, 56 (March 1960), 837-851.

Table 1

Prism Reinforcements

Specimen No.	Shape	U. S. Steel Wire Gage No.	Mesh Size, in.	Weight g	Remarks
1-A	Circular	14	1 × 1	168	Horizontal rings inside longitudinal wires
1-B				168	
2-A	Circular	14	1 × 1	172	Horizontal rings outside longitudinal wires
2-B				173	
3-A	Square	14	1 × 1	224	
3-B				223	
4-A	Circular	14	1 × 2	150	
4-B				151	
5-A	Square	14	1 × 2	181	
5-B				181	
6-A	Circular	16	2 × 2-5/8	61	
6-B				61	
7-A	Square	16	2 × 2-5/8	78	
7-B				78	
8-A	Circular	23	1/4 × 1/4	118	Interwoven hardware cloth
8-B				122	
9-A	Square	23	1/4 × 1/4	147	
9-B				145	
10-A	Circular	19	1/2 × 1/2	134	
10-B				140	
11-A	Square	19	1/2 × 1/2	159	
11-B				154	
12-A	Circular	17	5/8 × 5/8	178	
12-B				181	
13-A	Square	17	5/8 × 5/8	207	
13-B				210	
14-A	Circular	12	--	311	Helix; 1/2-in. pitch
14-B				308	
15-A	Circular	12	--	203	Helix; 1-in. pitch
15-B				192	
16-A	Circular	12	--	122	Helix; 1-1/2-in. pitch
16-B				141	
17-A	Circular	12	--	107	Helix; 2-in. pitch
17-B				122	
18-A	Circular	16	--	110	Helix; 1/2-in. pitch
18-B				112	
19-A	Circular	16	--	65	Helix; 1-in. pitch
19-B				63	
20-A	Circular	16	--	56	Helix; 1-1/2-in. pitch
20-B				61	
21-A	Circular	16	--	54	Helix; 2-in. pitch
21-B				53	
22-A	Circular	14	2 × 1	135	Horizontal rings outside longitudinal wires
22-B				133	
23-A	Square	14	2 × 1	165	Horizontal rings outside longitudinal wires
23-B				170	
24-A	Circular	14	1 × 1	216	Single cross braces at 2 in.
24-B				220	
25-A	Square	14	1 × 1	299	Double cross braces at 2 in.
25-B				298	
26-A	Square	14	1 × 2	252	Double cross braces at 2 in.
26-B				256	
27-A	Square	16	2 × 2-5/8	99	Double cross braces at 4 in.
27-B				98	
29-A	Square	14	1 × 1	238	Thirteen 3-in. squares at 1-in. vertical spacing
29-B				238	

(Continued)

Table 1 (Concluded)

Specimen No.	Shape	U. S. Steel Wire Gage No.	Mesh Size, in.	Weight g	Remarks
30-A 30-B	Square	17	5/8 × 5/8	173 176	Thirteen 3-in. squares at 1-in. vertical spacing
31-A 31-B	Square	17	5/8 × 5/8	259 260	Four 3- × 12-in. sheets at 1-in. horizontal spacing
32-A 32-B	Square	23	1/4 × 1/4	149 147	Four 3- × 12-in. sheets at 1-in. horizontal spacing
33-A 33-B	Square	14	1 × 1	229 229	Horizontal rings inside longitudinal wires
34-A 34-B	Square	14	1 × 2	182 184	
35-A 35-B	Circular	14	1 × 2	147 148	
36-A 36-B	Circular	14	2 × 1	133 131	
37-A 37-B	Square	14	2 × 1	165 167	
42-A 42-B	Circular	14	--	148 144	Helix; 1/2-in. pitch
43-A 43-B	Circular	14	--	81 86	Helix; 1-in. pitch
44-A 44-B	Circular	14	--	72 71	Helix; 1-1/2-in. pitch
45-A 45-B	Circular	14	--	61 52	Helix; 2-in. pitch
50-A 50-B	Square	14	1 × 1	428 435	Twenty-five 3-in. squares at 1/2-in. vertical spacing
51-A 51-B	Square	14	1 × 1	177 177	Nine 3-in. squares at 1-1/2-in. vertical spacing
52-A 52-B	Square	17	5/8 × 5/8	342 344	Twenty-five 3-in. squares at 1/2-in. vertical spacing
53-A 53-B	Square	17	5/8 × 5/8	143 143	Nine 3-in. squares at 1-1/2-in. vertical spacing
54-A 54-B	Square	23	1/4 × 1/4	229 228	Twenty-five 3-in. squares at 1/2-in. vertical spacing
55-A 55-B	Square	23	1/4 × 1/4	133 132	Thirteen 3-in. squares at 1-in. vertical spacing
56-A 56-B	Square	23	1/4 × 1/4	103 101	Nine 3-in. squares at 1-1/2-in. vertical spacing
57-A 57-B	Circular	12	--	361 374	4-in.-diam helix; 1/2-in. pitch
58-A 58-B	Circular	12	--	233 208	4-in.-diam helix; 1-in. pitch
59-A 59-B	Circular	16	--	110 110	4-in.-diam helix; 1/4-in. pitch
60-A 60-B	Circular	16	--	69 72	4-in.-diam helix; 1-in. pitch
61-A 61-B	Square	12	--	527 520	Thirteen 12-gage wires at 1-in. vertical spacing around four 1/4-in.-diam rods forming a 3-in. square
62-A 62-B	Square	12	--	419 416	Seven 12-gage wires at 2-in. vertical spacing arranged similarly to those in specimen 61
63-A 63-B	Square	12	--	385 384	Five 12-gage wires at 3-in. vertical spacing arranged similarly to those in specimen 61
64-A 64-B	Square	12	--	368 366	Four 12-gage wires at 4-in. vertical spacing arranged similarly to those in specimen 61
65-A 65-B	Square	12	--	334 333	Two 12-gage wires at 12-in. vertical spacing arranged similarly to those in specimen 61

Table 2

Summary of Beam Test Results

Beam	Type of Confining Reinforcement	Concrete Strength* psi	Actual Yield Moment in.-kip	Actual Spalling Moment in.-kip	Ultimate Moment, in.-kip: Theoretical, Stress Block**	Theoretical, Iteration†	Actual	Deviation†† %
A-1	None	3290	187.5	195.0	193.0	196.0	195.0	-0.5
A-2		3290	268.5	268.5	263.8	270.5	268.5	-0.7
A-3A		3630	273.0	280.5	272.7	275.6	280.5	+1.8
A-4		3630	240.0	247.5	232.3	246.1	247.5	+0.6
B-1	No. 2 stirrups at 4-in. spacing	2970	180.0	189.0	186.4	189.7	189.0	-0.4
B-2		2970	252.8	255.0	253.8	261.0	255.0	-2.3
B-3		3140	267.0	276.0	270.0	273.4	276.0	+1.0
B-4		3630	234.0	241.5	227.8	240.8	241.5	+0.3
C-1	3-in.-diam helix	3230	174.0	179.0	179.5	183.0	199.5	+9.0
C-2		3230	240.0	240.0	244.6	251.9	240.0	-4.7
C-3		3230	261.0	262.5	271.6	281.0	286.5	+2.0
C-4		2930	202.5	207.0	200.8	213.8	207.0	-3.2
D-1	1- × 1-in. plane mesh at 0.9-in. spacing	3140	180.0	186.0	182.8	186.4	207.0	+11.0
D-2A		3220	235.5	242.2	238.6	245.5	242.2	-1.3
D-3		3010	270.0	270.0	275.1	280.6	319.5	+13.9
D-4		2740	219.0	226.5	203.7	220.9	226.5	+2.5
E-1	1- × 1-in. plane mesh at 0.5-in. spacing	3010	175.5	184.5	176.0	205.3	226.5‡	+10.3
E-2A		3220	247.5	260.2	238.1	261.5	262.5	+0.4
E-3		2930	234.0	243.0	251.4	297.3	289.5	-2.7
E-4		2930	216.0	222.0	201.5	228.8	225.0	-1.7
F-1	12-gage stirrups at 0.8-in. spacing	2940	170.2	175.5	166.6	176.7	175.5	-0.7
F-2		3220	241.5	247.5	233.3	240.8	247.5	+2.8
F-3		2940	240.0	253.5	242.7	259.8	253.5	-2.5
F-4		2940	219.0	235.1	199.3	224.8	235.1	+4.6

Note: "A" designates beam was repeated due to cracking during handling, improper fabrication, etc.

* Average of 3 tests on standard 6- × 12-in. cylinders.

** Analysis was based on Whitney stress block and 0.003-in./in. maximum concrete strain.

† The iteration analysis procedure is described in Chapter IV.

†† Deviation of actual load from the theoretical load calculated according to iteration method.

‡ Moment was still increasing when deflection exceeded capacity of test apparatus.

Table 3

Theoretical and Actual Ductility Ratios

Beam No.	p , %	p' , %	$\frac{p - p'}{p_b}$	Ductility Ratios	
				Theoretical*	Actual
A-1	1.16		0.57	8.6	4.4
A-2	1.77		0.88	5.6	2.0
A-3A	1.88	0.63	0.56	8.0	3.7
A-4	2.85		1.18	3.5	1.8
B-1	1.19		0.65	8.4	5.5
B-2	1.79		0.98	5.6	1.7
B-3	1.85	0.62	0.64	8.1	5.5
B-4	2.90		1.20	3.4	1.8
C-1	1.24		0.63	8.1	17.0
C-2	1.88		0.95	5.3	6.8
C-3	1.86	0.62	0.63	8.1	11.3
C-4	2.90		1.49	3.4	1.8**
D-1	1.22		0.63	8.2	17.6
D-2A	1.84		0.86	5.4	11.4
D-3	1.84	0.61	0.66	8.1	13.4
D-4	2.79		1.53	3.6	6.0
E-1	1.26		0.68	7.9	22.2†
E-2A	1.82		0.82	5.5	15.2
E-3	1.83	0.61	0.63	8.2	20.2†
E-4	2.90		1.49	3.4	16.5
F-1	1.24		0.61	8.1	10.8
F-2	1.85		0.84	5.4	2.0**
F-3	1.85	0.62	0.61	8.1	11.4
F-4	2.89		1.43	3.5	2.8

* Computed according to procedures described in Air Force Design Manual.[16]

** As a result of large drops in load due to spalling of the concrete, determination of ductility ratios as described in Chapter IV seems to penalize these beams. As evident from the load-deflection curves, computation of ductility ratios at 80% yield load would result in values of 6.7 and 4.5 for beams C-4 and F-2, respectively.

† Deflection exceeded capacity of test apparatus before beam reached point of collapse; therefore, ductility ratio shown is somewhat conservative.

Table 4

Ductility Ratios for Conventionally Reinforced Beams

Design No.	p - p'* %	Ductility Ratios		
		Theoretical		
		Present**	Proposed†	Actual
1	1.18	8.5	5.1	5.0
2	1.78	5.6	3.4	1.8
3	1.24	8.1	4.8	4.6
4	2.88	3.5	2.1	1.8

* Averages of series A and B.

** Computed according to Air Force Design Manual.[16]

$$\mu = \frac{10}{p - p'}$$

† Computed according to $\mu = \frac{10}{p - p'}\left(\frac{40}{fy}\right)$.

a. Beam A-3A

b. Beam B-3

Photograph 1. Buckling of compressive reinforcement in beams A-3A and B-3

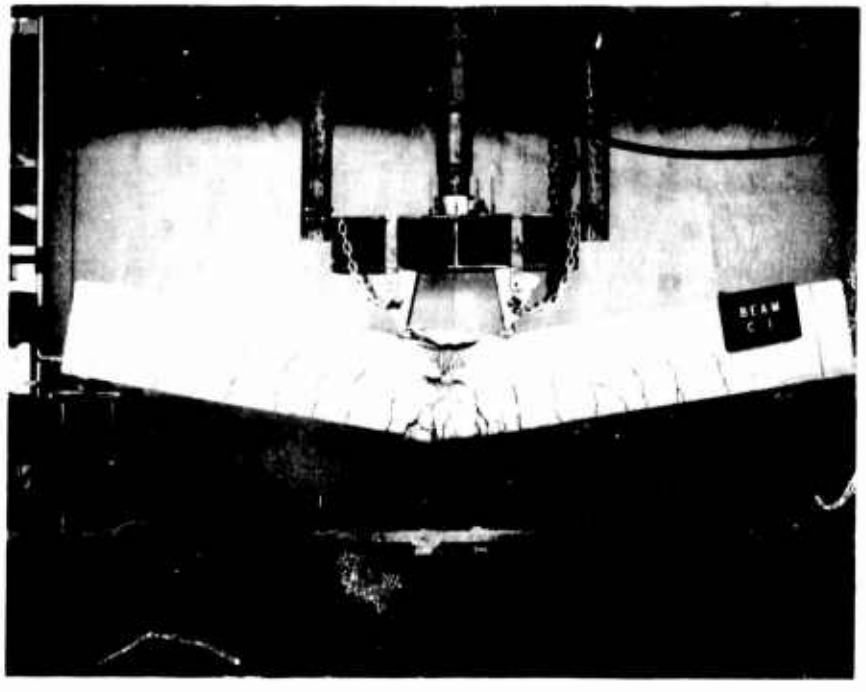

a. Overall view

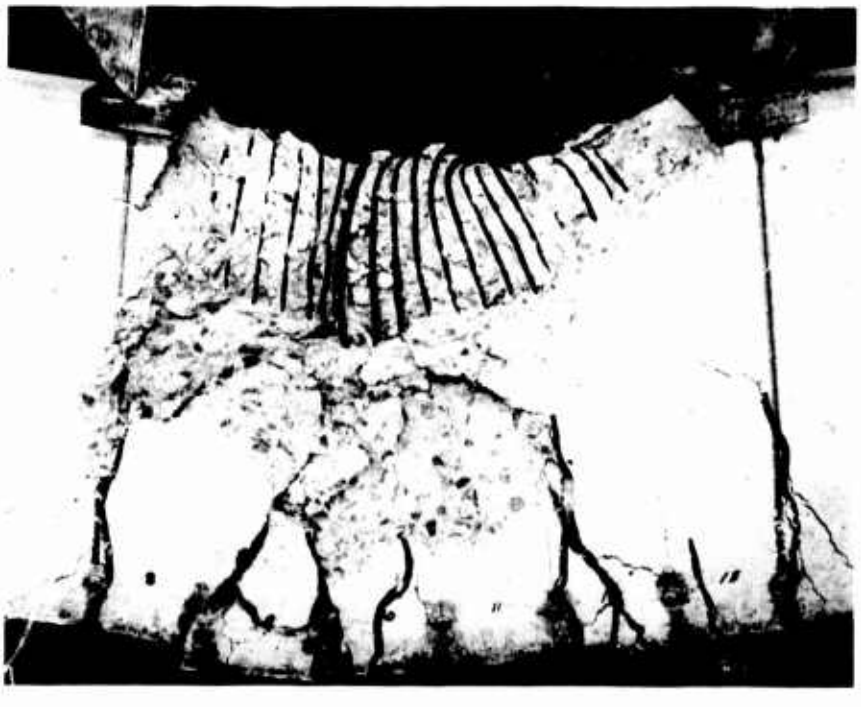

b. Close-up of midspan section

Photograph 2. Beam C-1 at failure

Photograph 3. Beam C-2 hinging region

Photograph 4. Beam C-3 hinging region

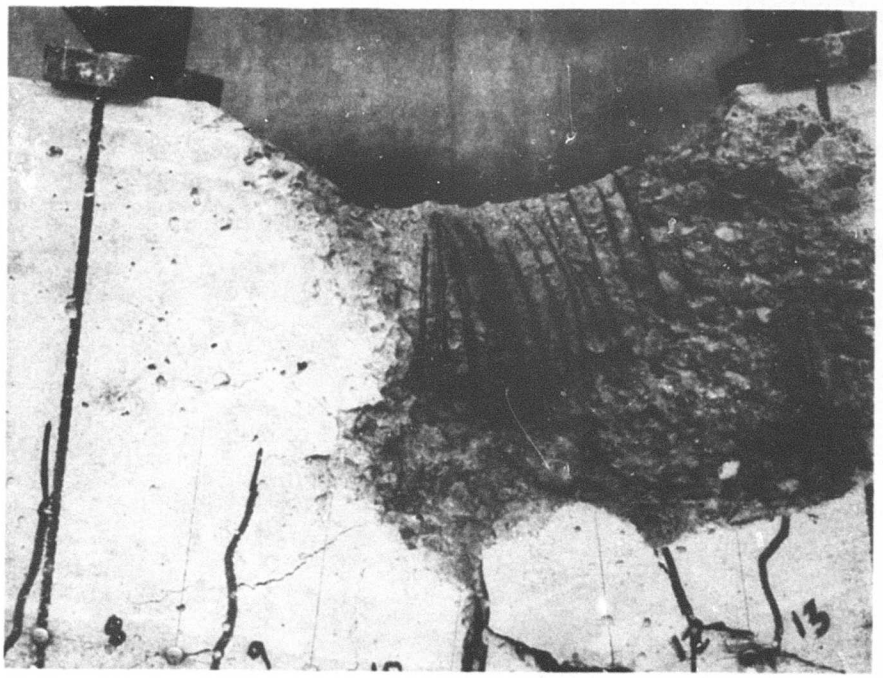

Photograph 5. Beam C-4 hinging region

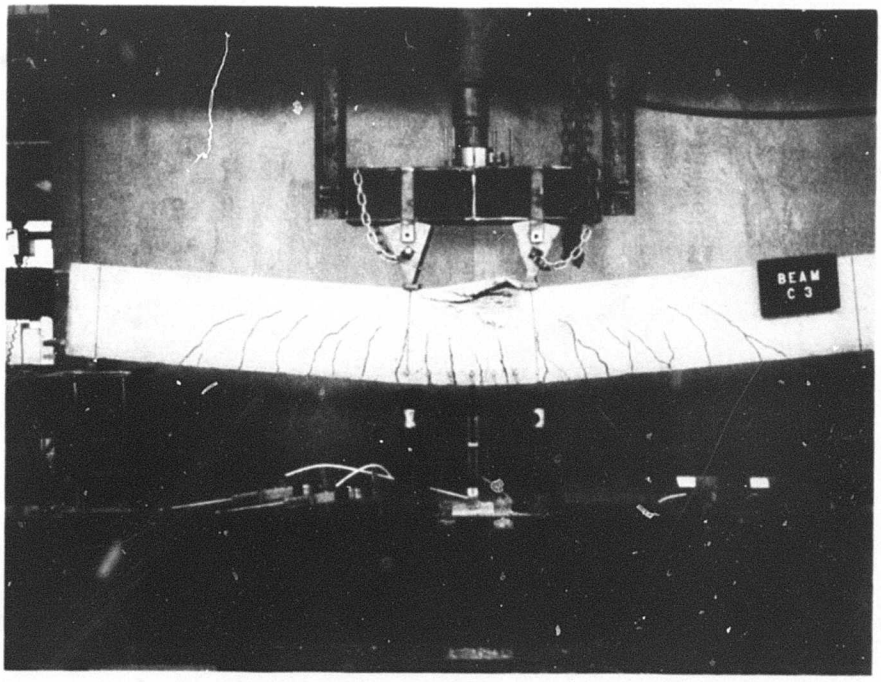

Photograph 6. Beam C-3 at 19,000-lb load

BLANK PAGE

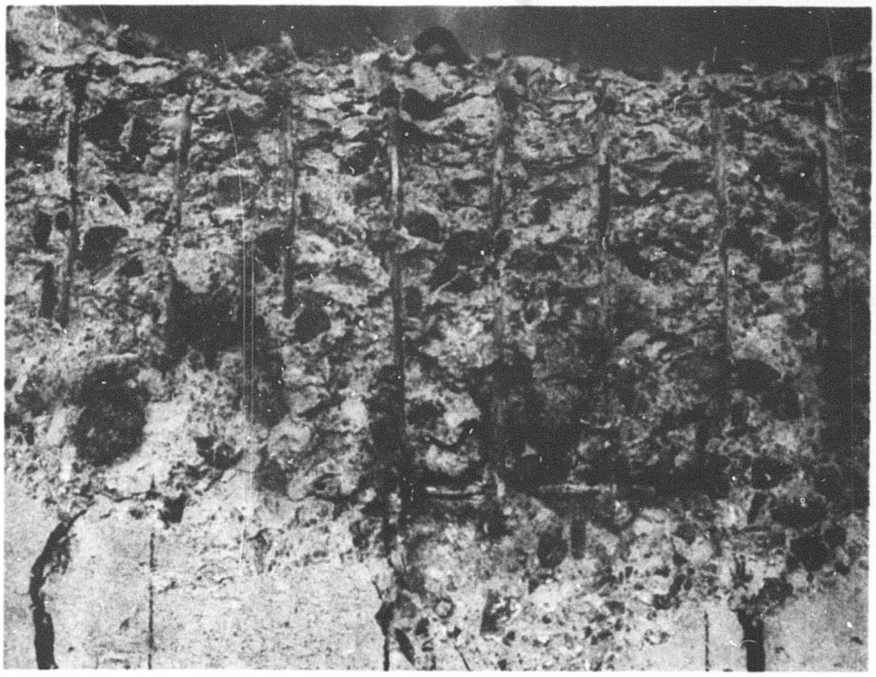

Photograph 7. Beam D-1 hinging region

Photograph 8. Beam D-2A hinging region

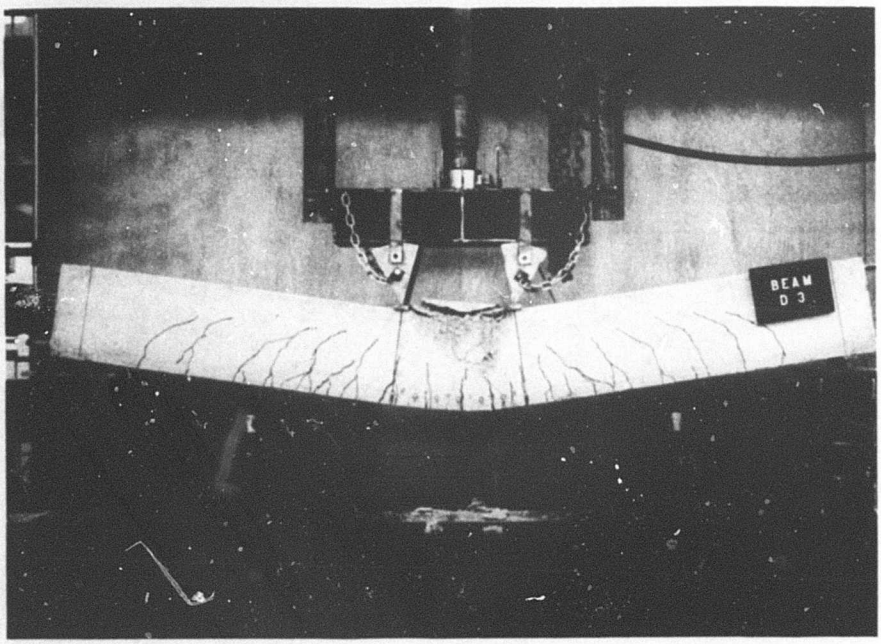

a. Overall view

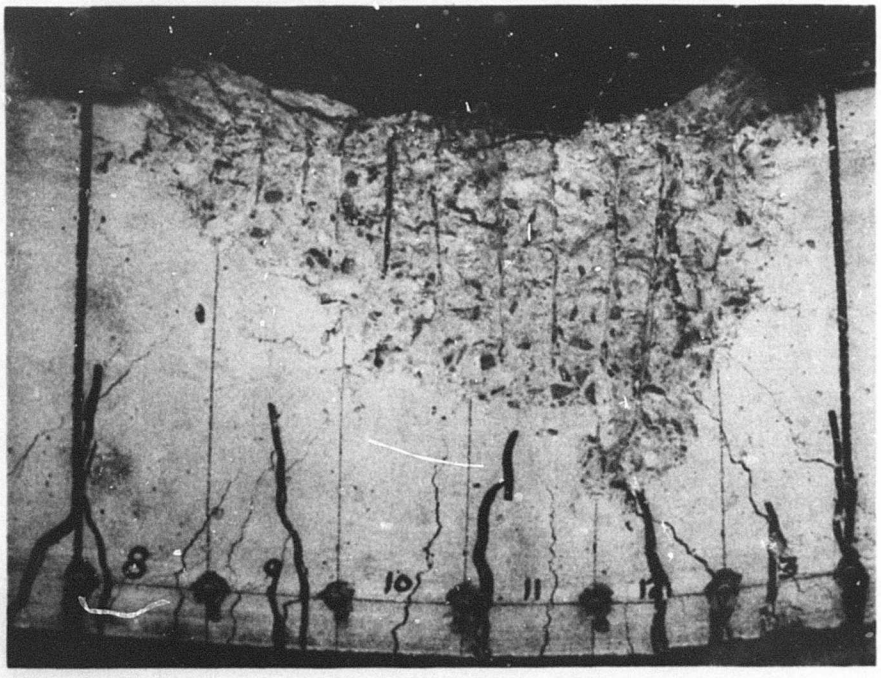

b. Hinging region

Photograph 9. Beam D-3 at failure

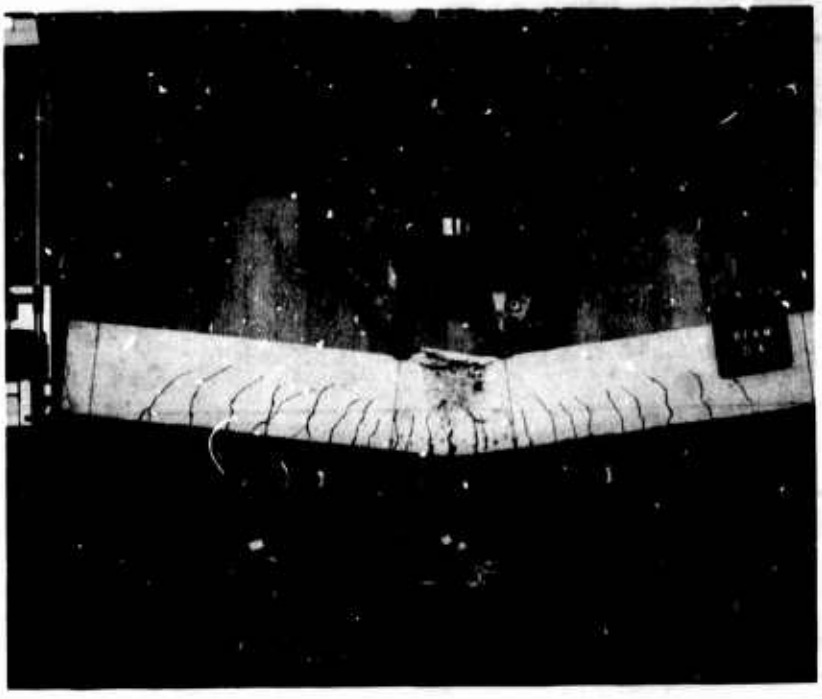

a. Overall view

b. Hinging region

Photograph 10. Beam D-4 at failure

a. Total load, 11,000 lb

b. Total load, 12,500 lb

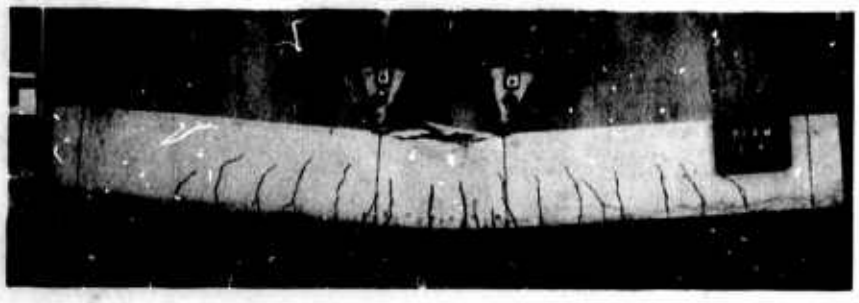

c. Total load, 13,500 lb

d. Total load, 14,500 lb

e. Total load, 15,000 lb

Photograph 11. Development of hinge in beam E-1

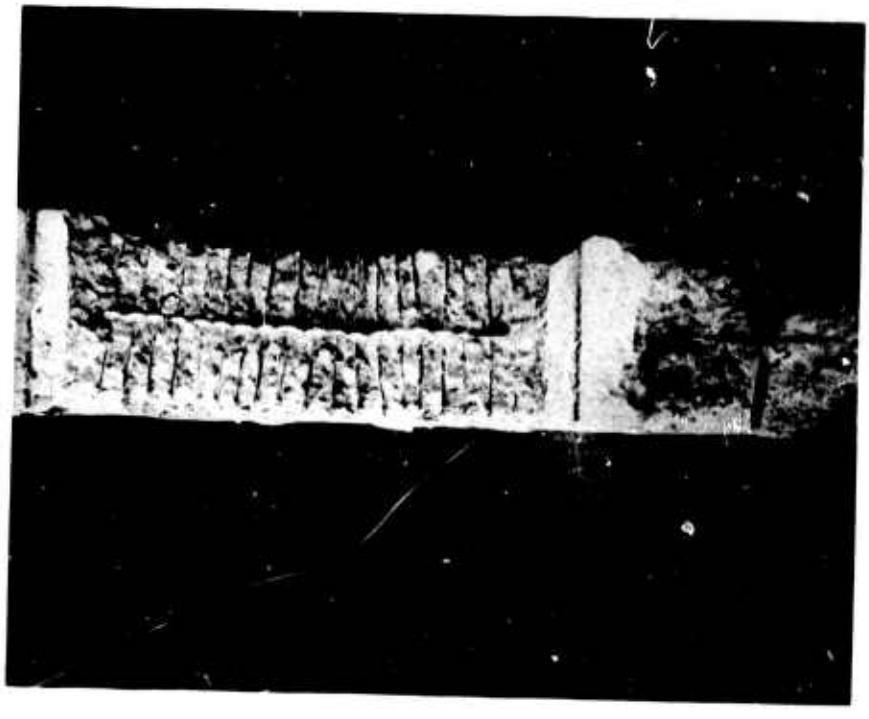

Photograph 12. Compressive surface of beam E-1

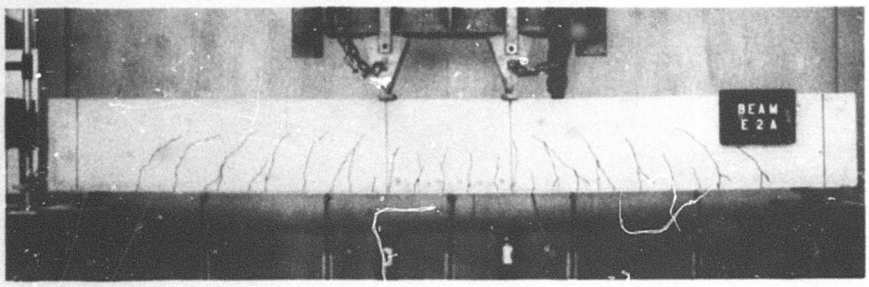

a. Total load, 16,000 lb

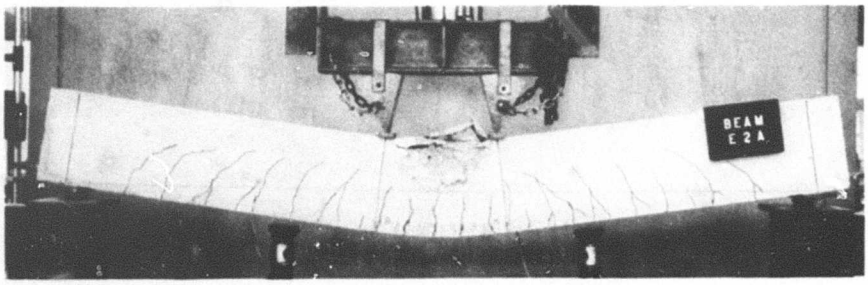

b. Total load, 17,300 lb

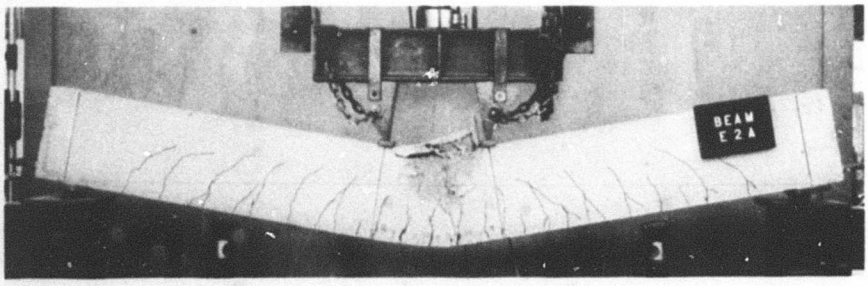

c. Total load, 3000 lb

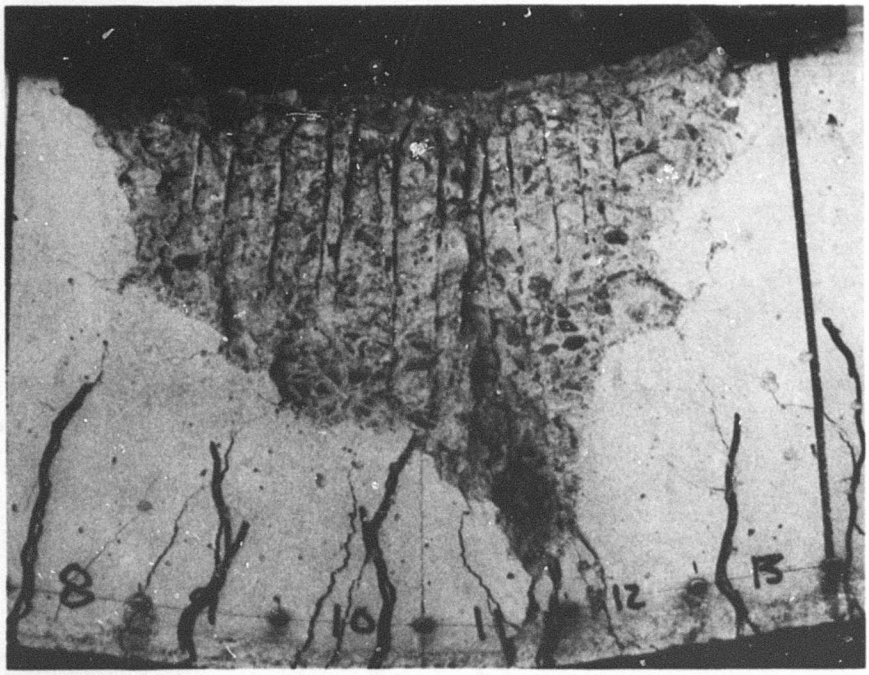

d. Hinging region

Photograph 13. Development of hinge in beam E-2A

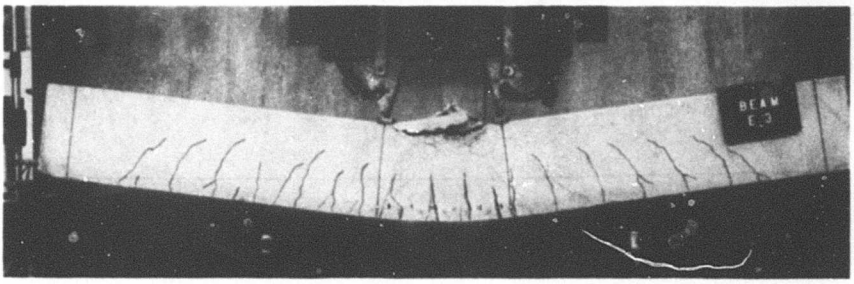

a. Total load, 19,000 lb

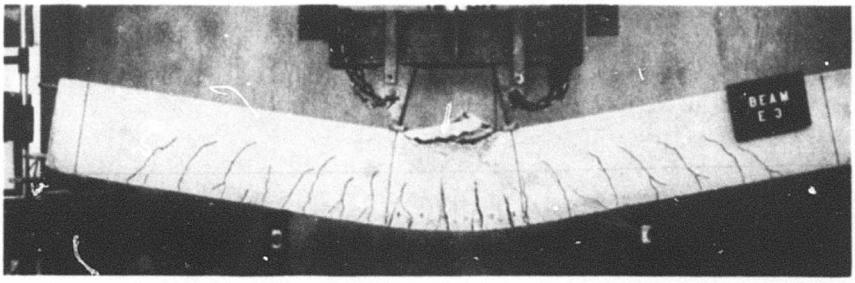

b. Total load, 17,900 lb

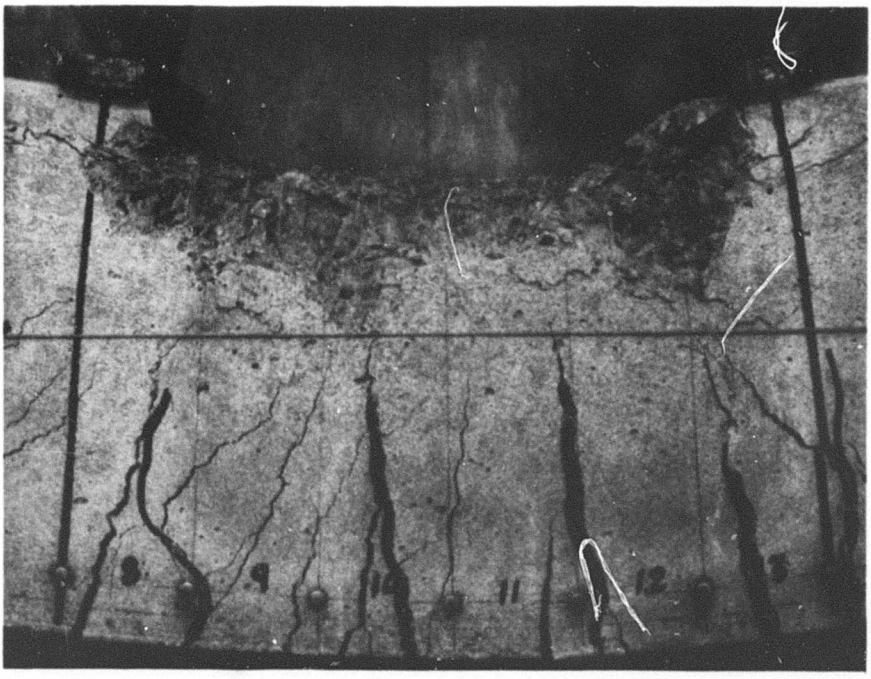

c. Hinging region

Photograph 14. Development of hinge in beam E-3

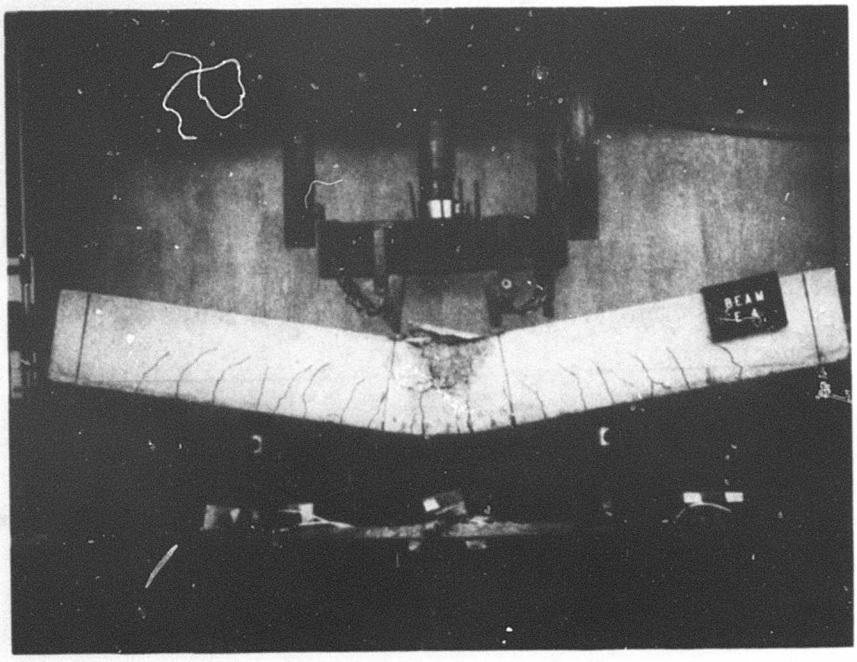

a. Overall view

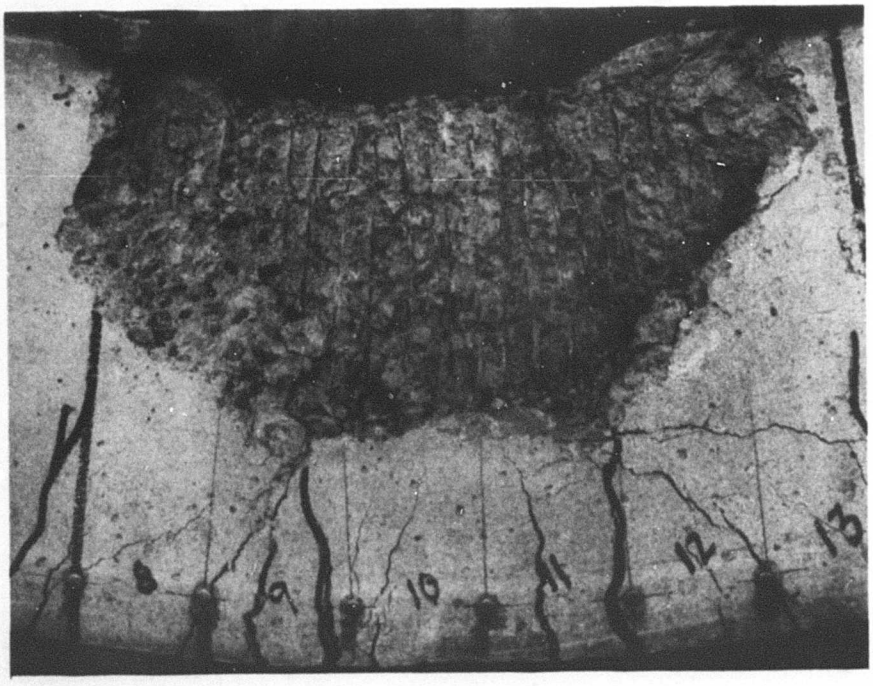

b. Hinging region

Photograph 15. Beam E-4 at failure

Photograph 16. Hinging region in beam F-1

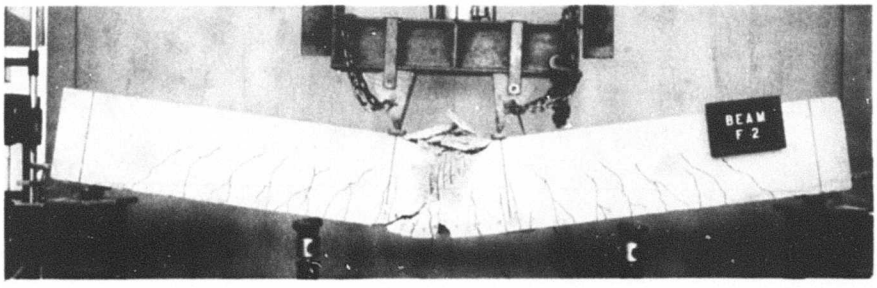

a. Overall view

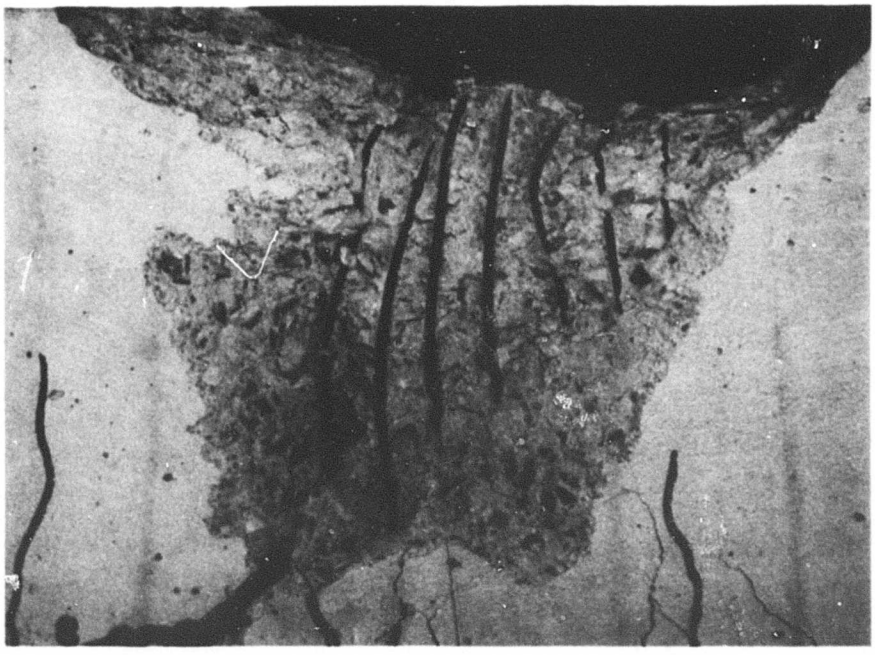

b. Hinging region

Photograph 17. Beam F-2 at failure

Photograph 18. Beam F-3 hinging region

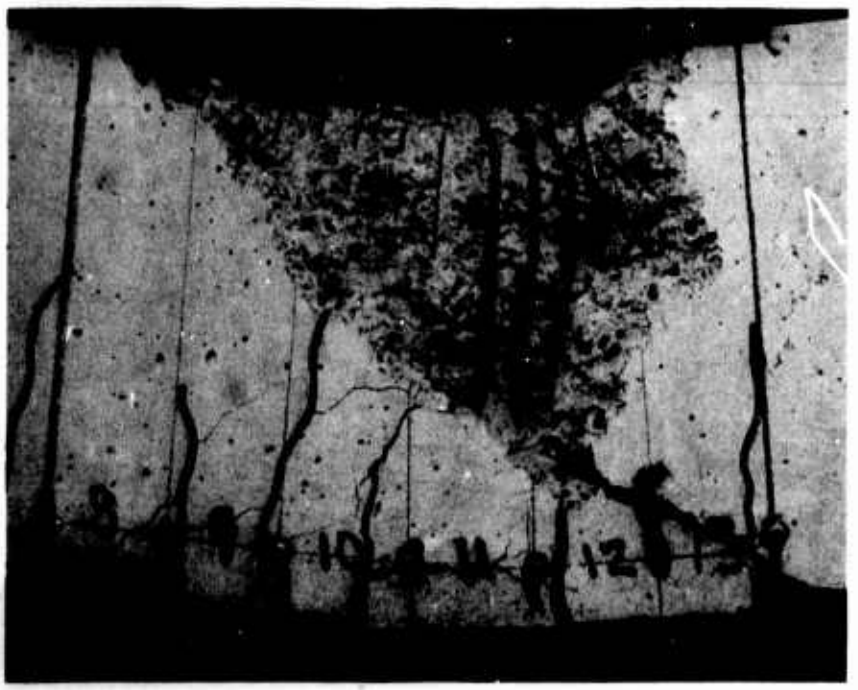

Photograph 19. Beam F-4 hinging region

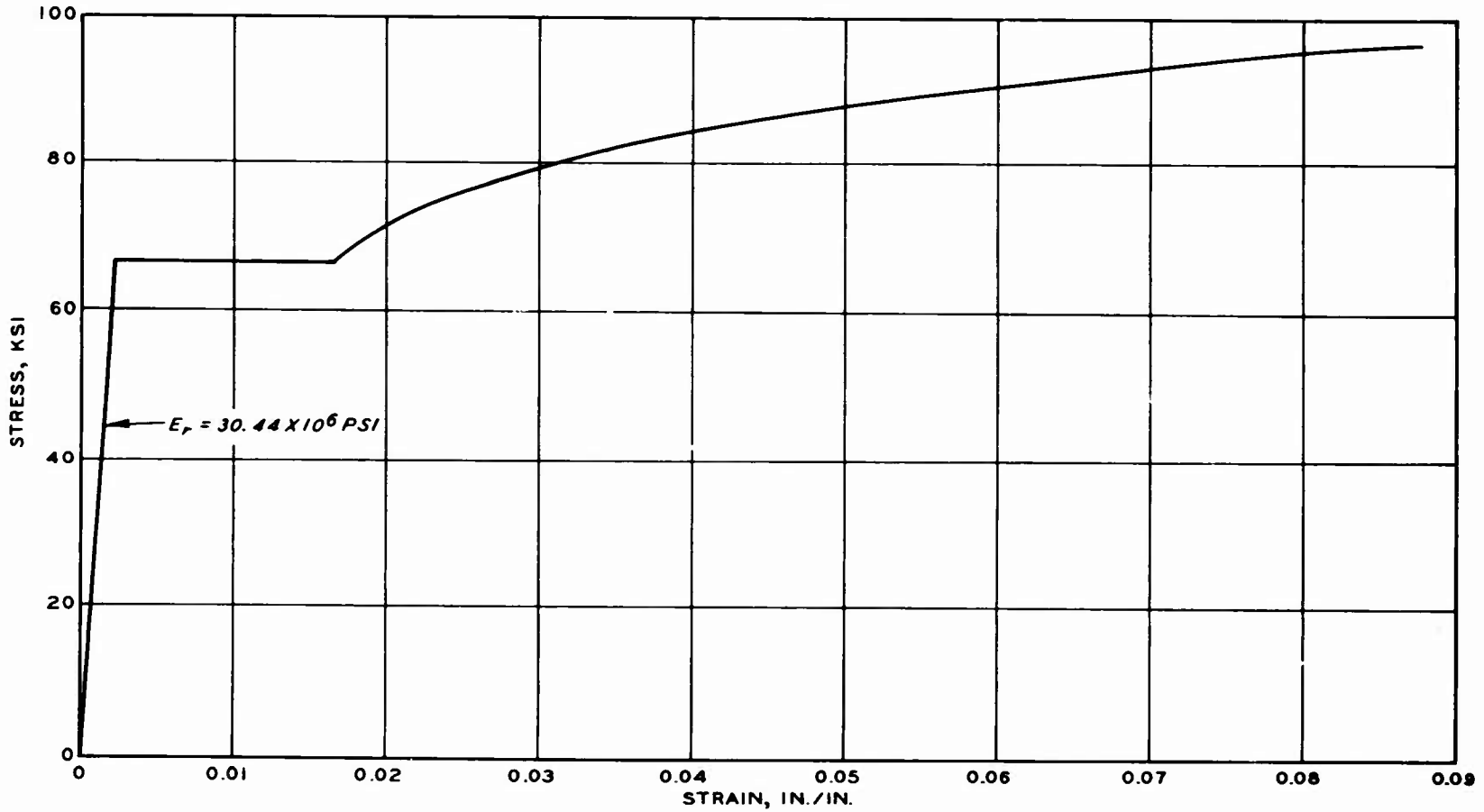

STRESS – STRAIN CURVE
LONGITUDINAL REINFORCEMENT

PLATE I

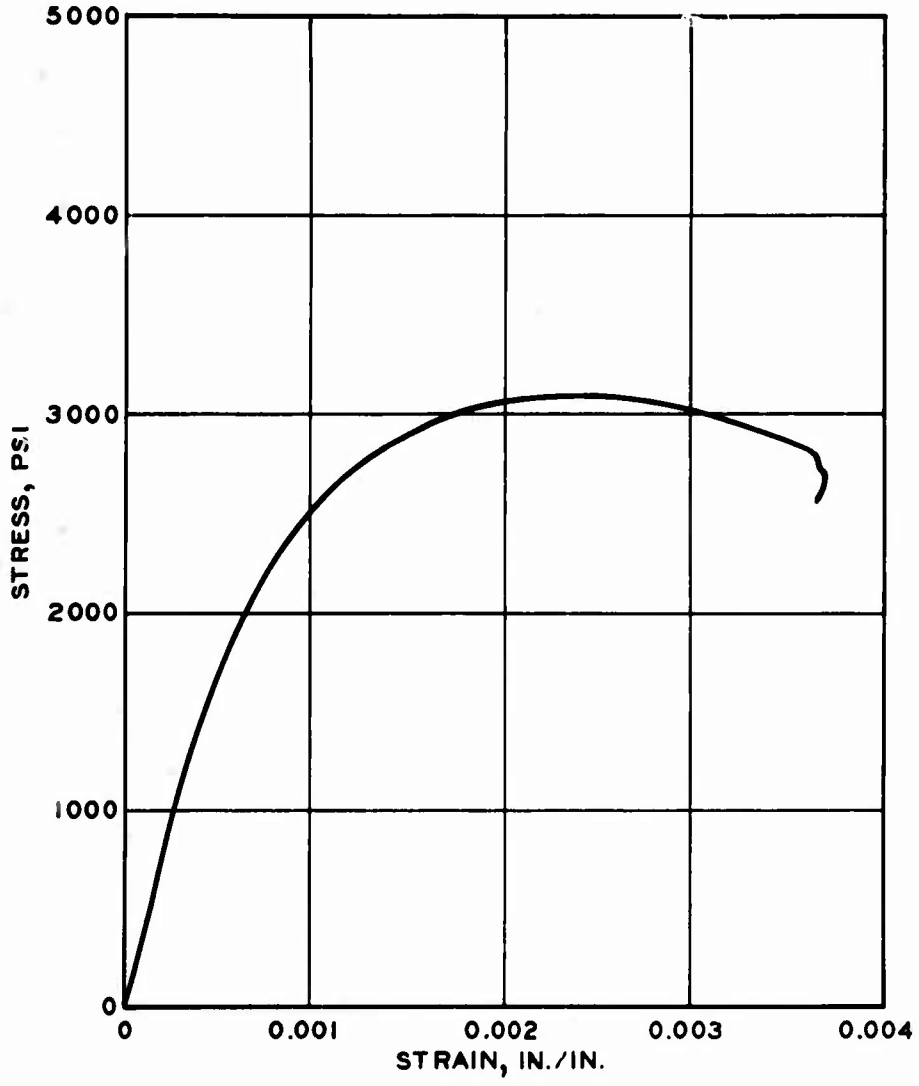

STRESS-STRAIN CURVE
CONCRETE

PLATE 2

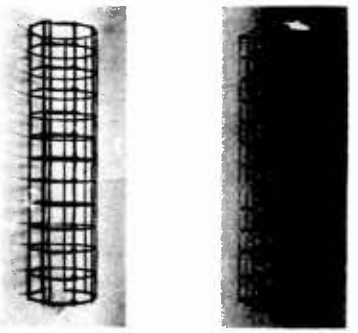

SPECIMEN NO.	1	33
REINFORCEMENT WEIGHT, G	168	229

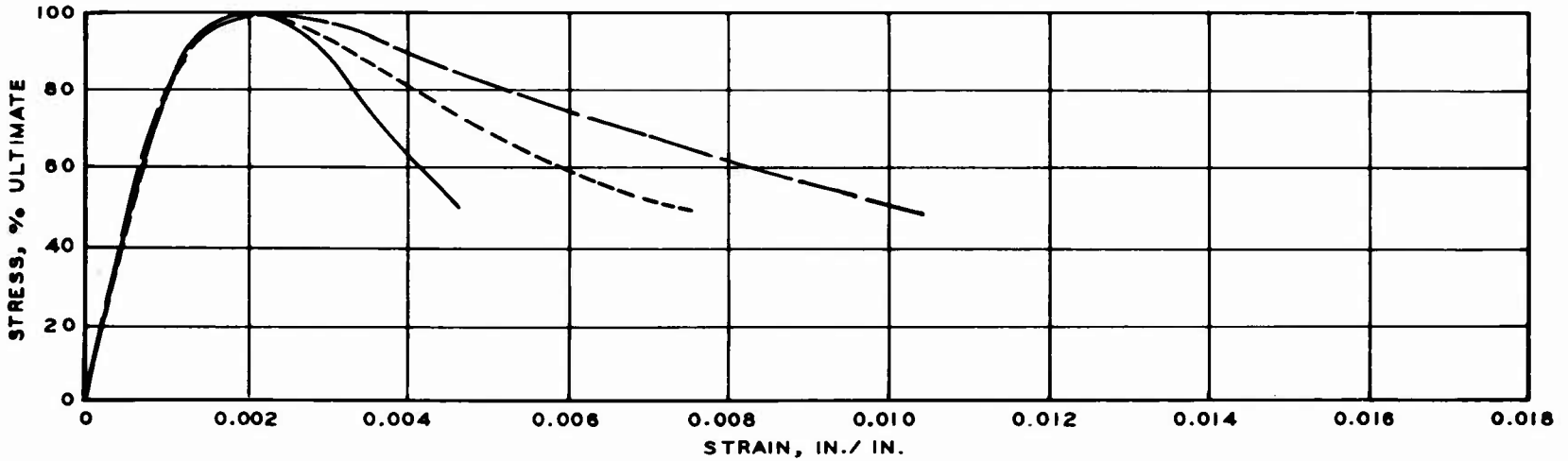

LEGEND

CONTROL

1

33

STRESS-STRAIN CURVES

TUBULAR MESHES
SPECIMENS 1 AND 33

PLATE 3

PLATE 4

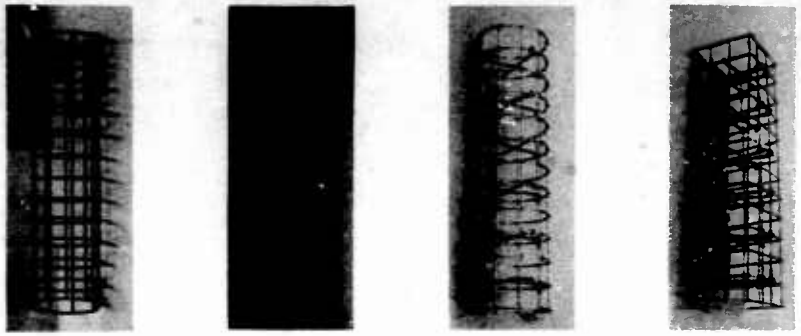

SPECIMEN NO.	2	3	24	25
REINFORCEMENT WEIGHT, G	172	224	218	298

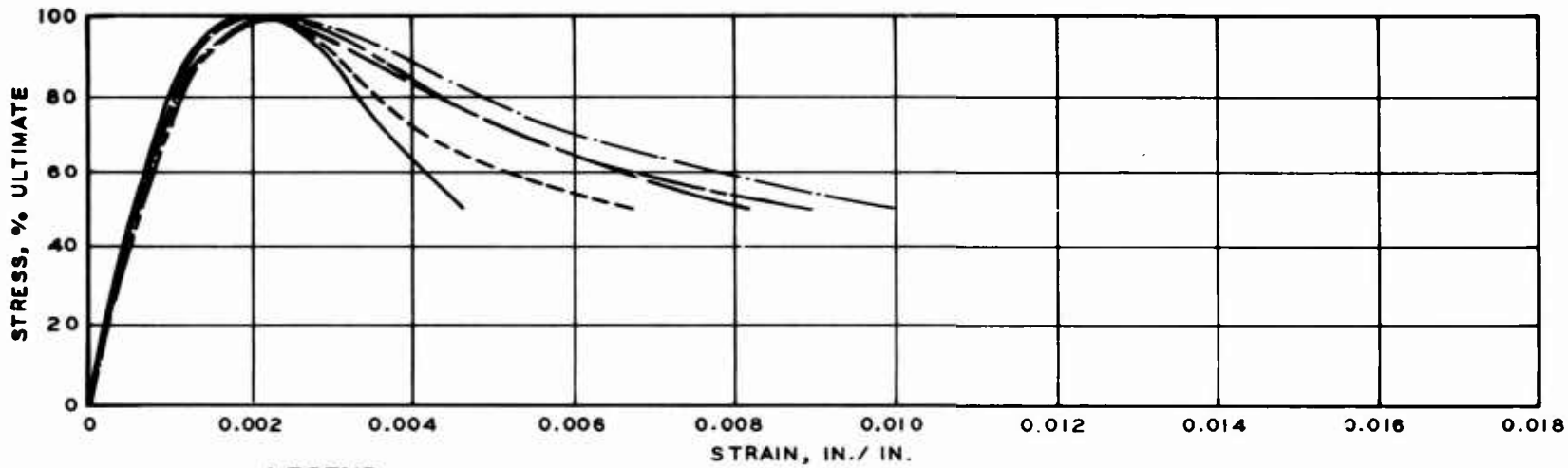

LEGEND

CONTROL
2
3
24
25

STRESS-STRAIN CURVES
TUBULAR MESHES
SPECIMENS 2, 3, 24, AND 25

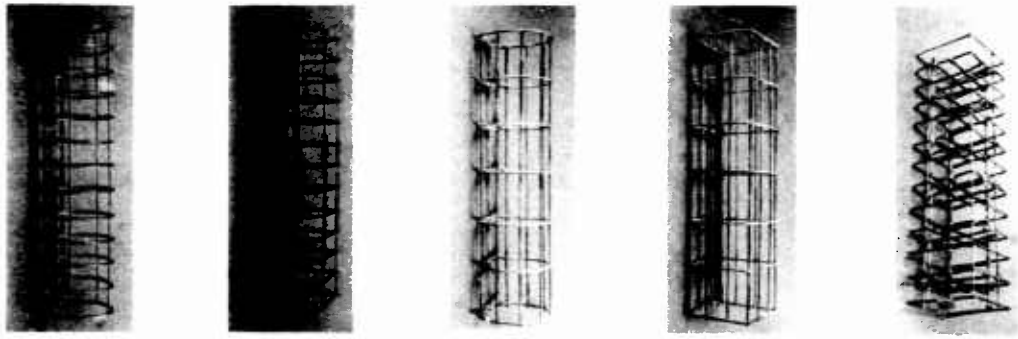

SPECIMEN NO.	4	5	22	23	26
REINFORCEMENT WEIGHT, G	150	181	134	168	254

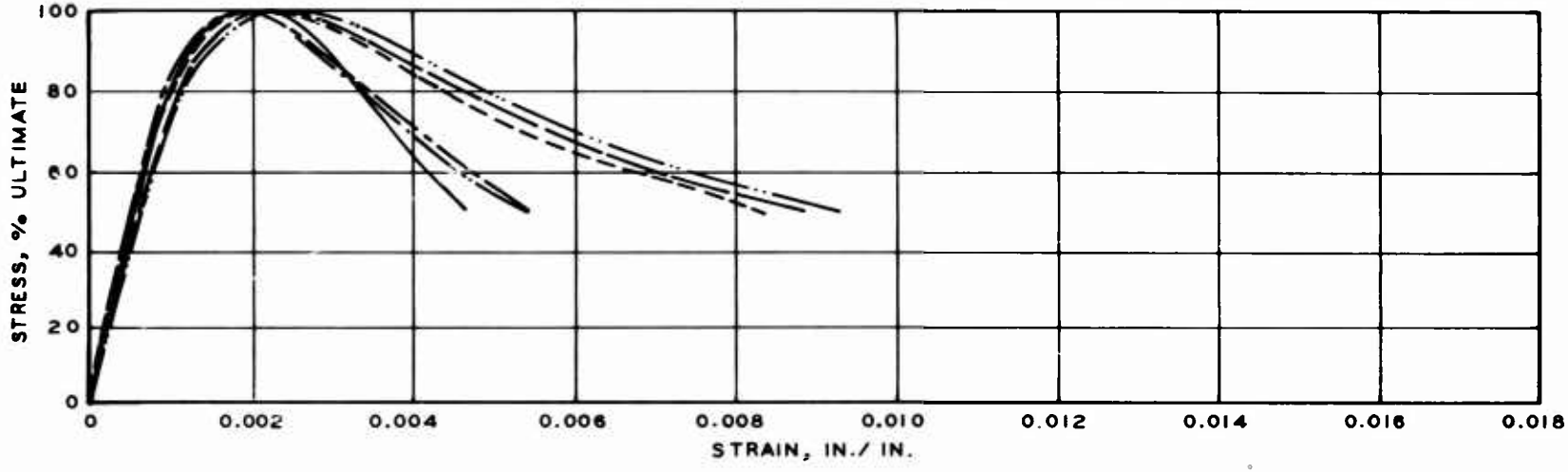

LEGEND

———	CONTROL	— — —	22
- - - -	4	— · —	23
— —	5	— ·· —	26

STRESS-STRAIN CURVES
TUBULAR MESHES
SPECIMENS 4, 5, 22, 23, AND 26

PLATE 5

PLATE 6

SPECIMEN NO.	6	7	27
REINFORCEMENT WEIGHT, G	61	78	98

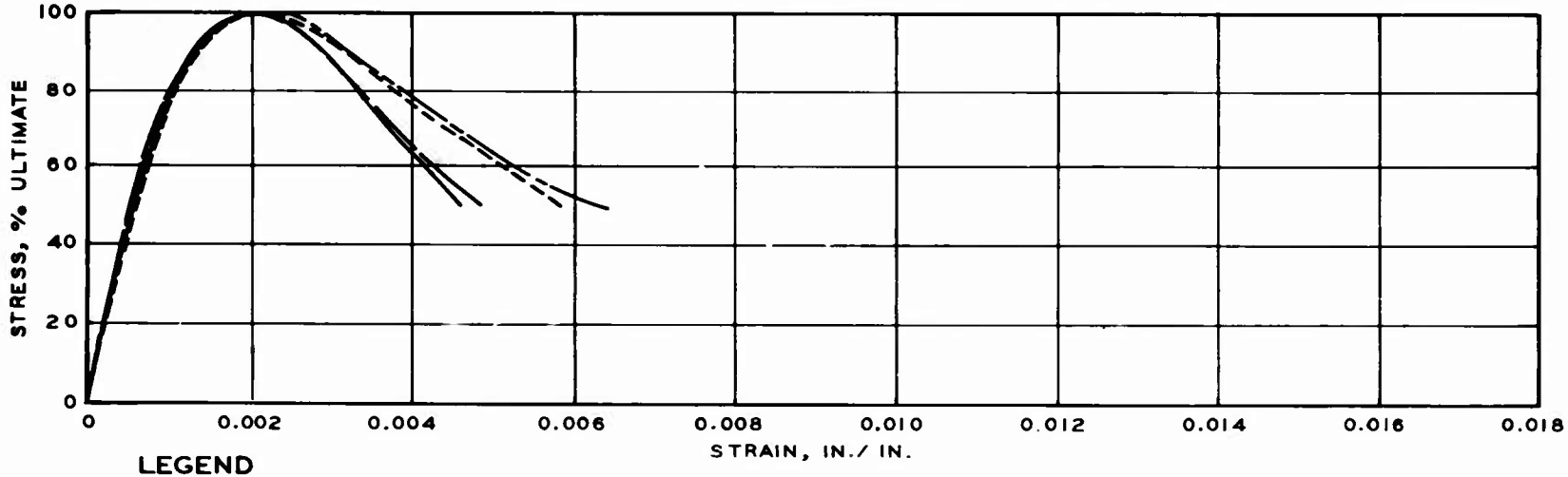

LEGEND

——— CONTROL
– – – – 6
— — — 7
— – — 27

STRESS-STRAIN CURVES
TUBULAR MESHES
SPECIMENS 6, 7, AND 27

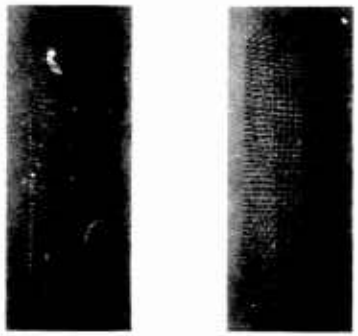

SPECIMEN NO.	8	9
REINFORCEMENT WEIGHT, G	120	148

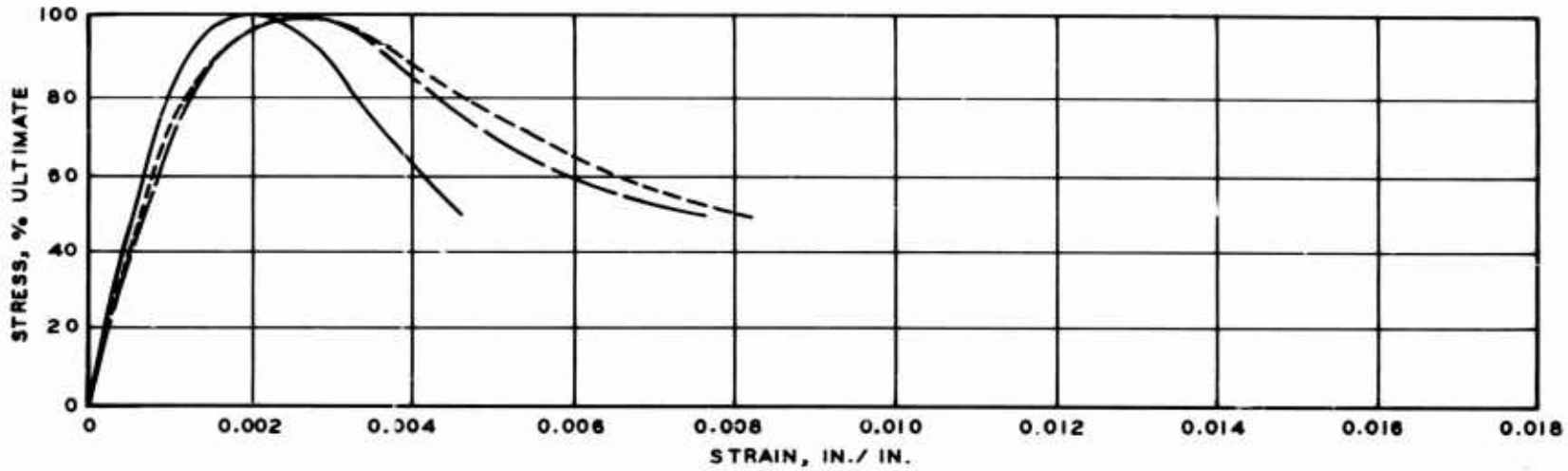

LEGEND

——— CONTROL

– – – – 8

— — 9

STRESS-STRAIN CURVES
TUBULAR MESHES
SPECIMENS 8 AND 9

PLATE 7

PLATE 8

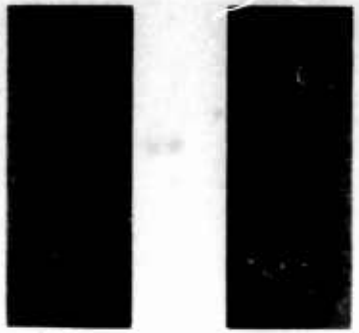

SPECIMEN NO.	10	11
REINFORCEMENT WEIGHT, G	138	158

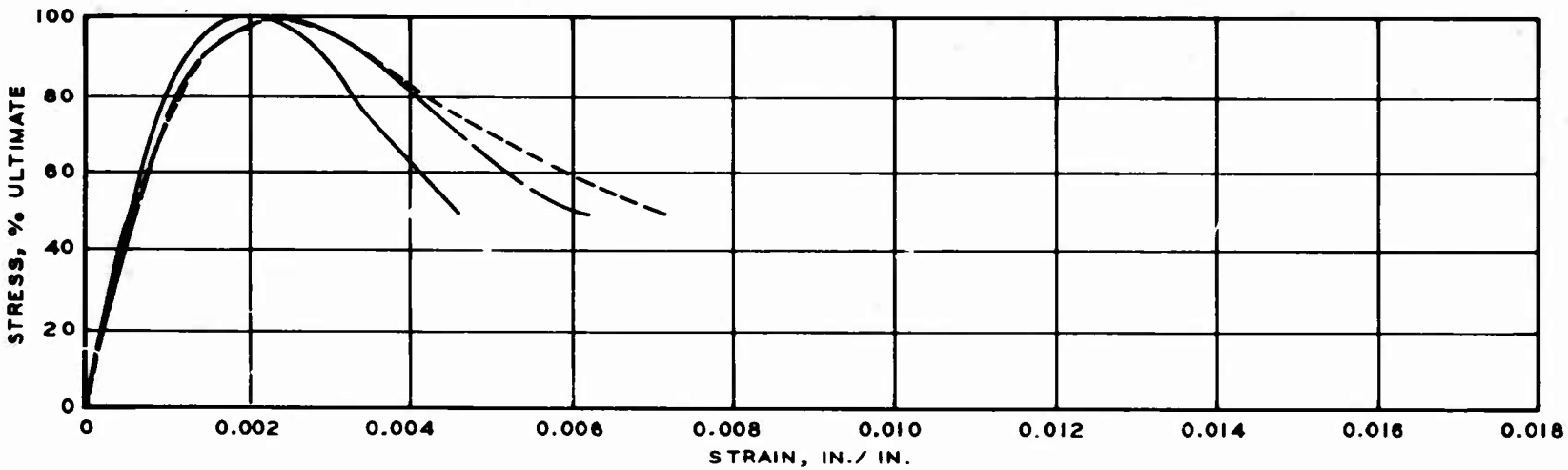

LEGEND

——— CONTROL
– – – – 10
— — 11

STRESS-STRAIN CURVES
TUBULAR MESHES
SPECIMENS 10 AND 11

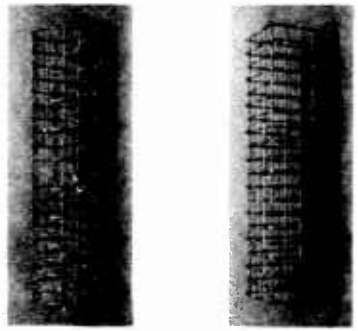

SPECIMEN NO.	12	13
REINFORCEMENT WEIGHT, G	180	208

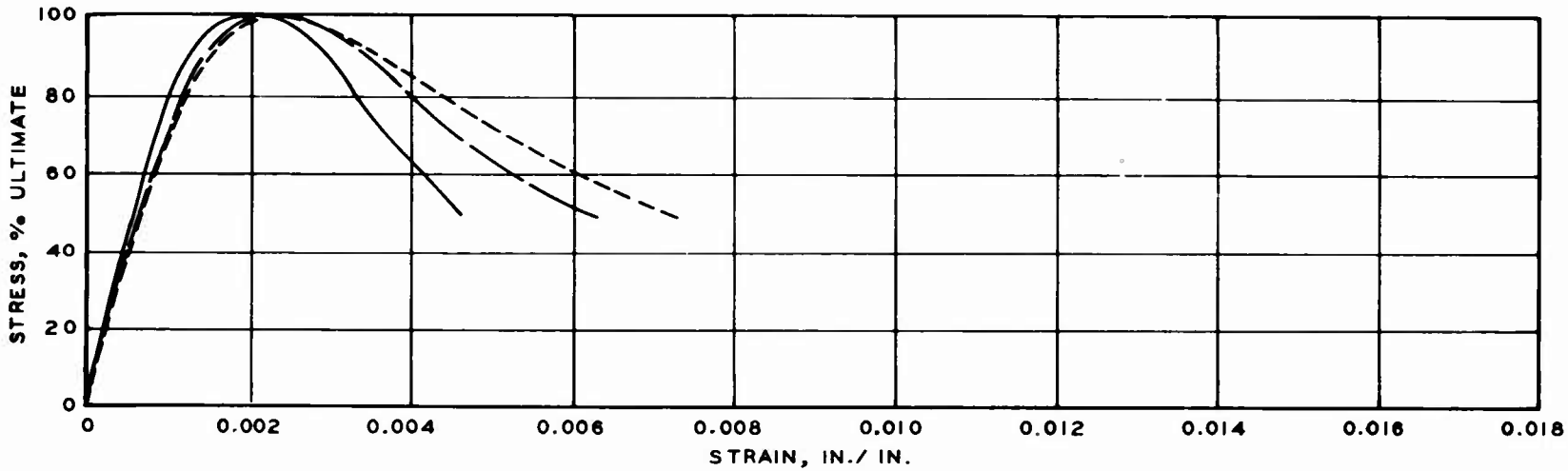

LEGEND

——— CONTROL
- - - - 12
— — 13

STRESS-STRAIN CURVES
TUBULAR MESHES
SPECIMENS 12 AND 13

PLATE 9

PLATE 10

SPECIMEN NO.	34	35	36	37
REINFORCEMENT WEIGHT, G	183	148	132	166

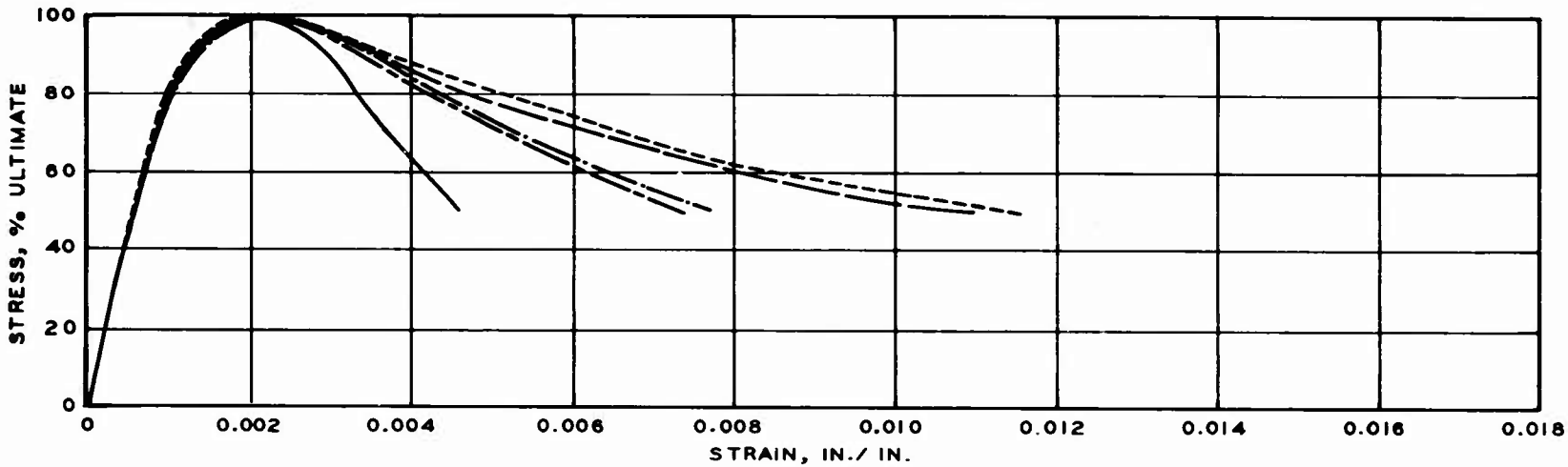

LEGEND

CONTROL
34
35
36
37

STRESS-STRAIN CURVES
TUBULAR MESHES
SPECIMENS 34, 35, 36, AND 37

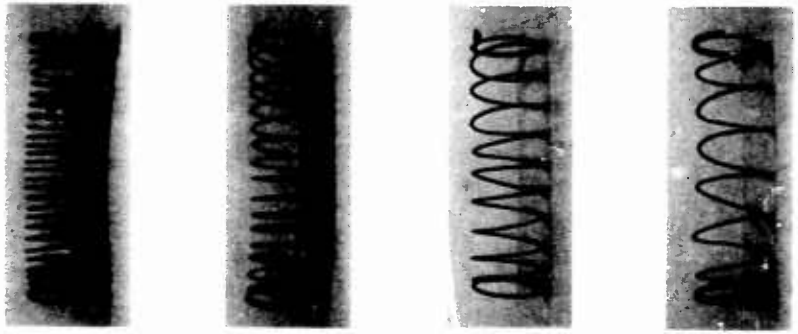

SPECIMEN NO.	14	15	16	17
REINFORCEMENT WEIGHT, G	310	198	132	114

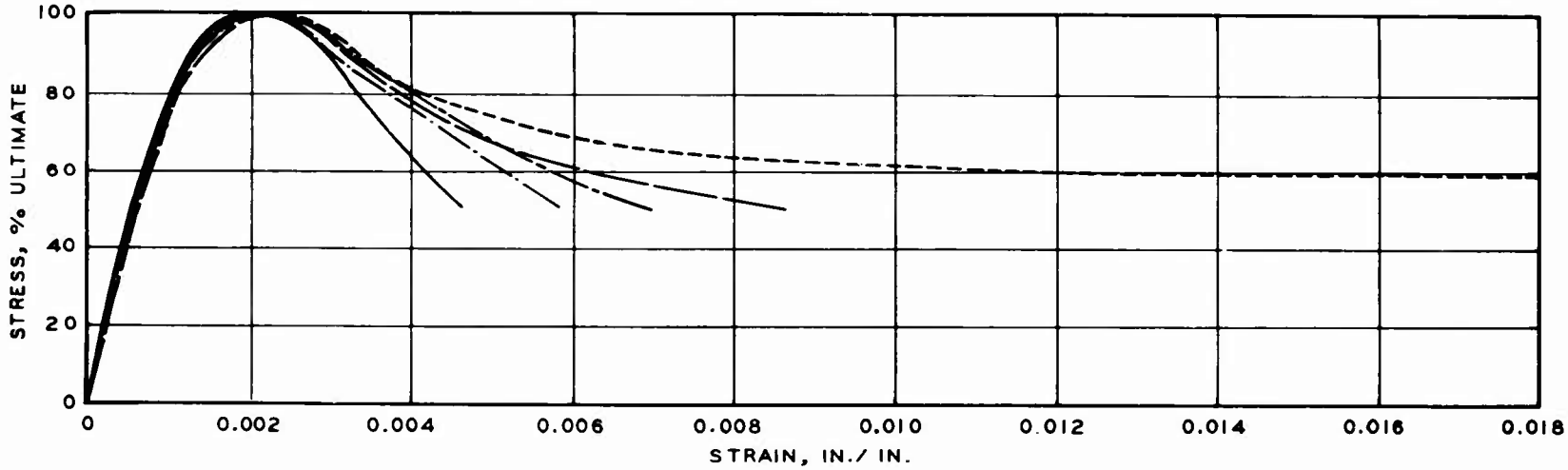

LEGEND

CONTROL
14
15
16
17

STRESS-STRAIN CURVES

HELICES
SPECIMENS 14, 15, 16, AND 17

PLATE 11

PLATE 12

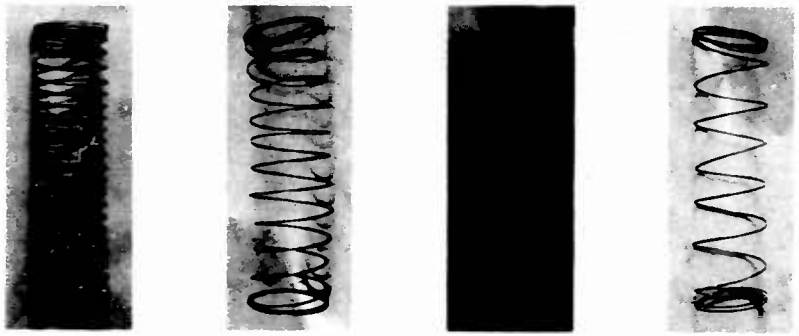

SPECIMEN NO.	42	43	44	45
REINFORCEMENT WEIGHT, G	146	84	72	56

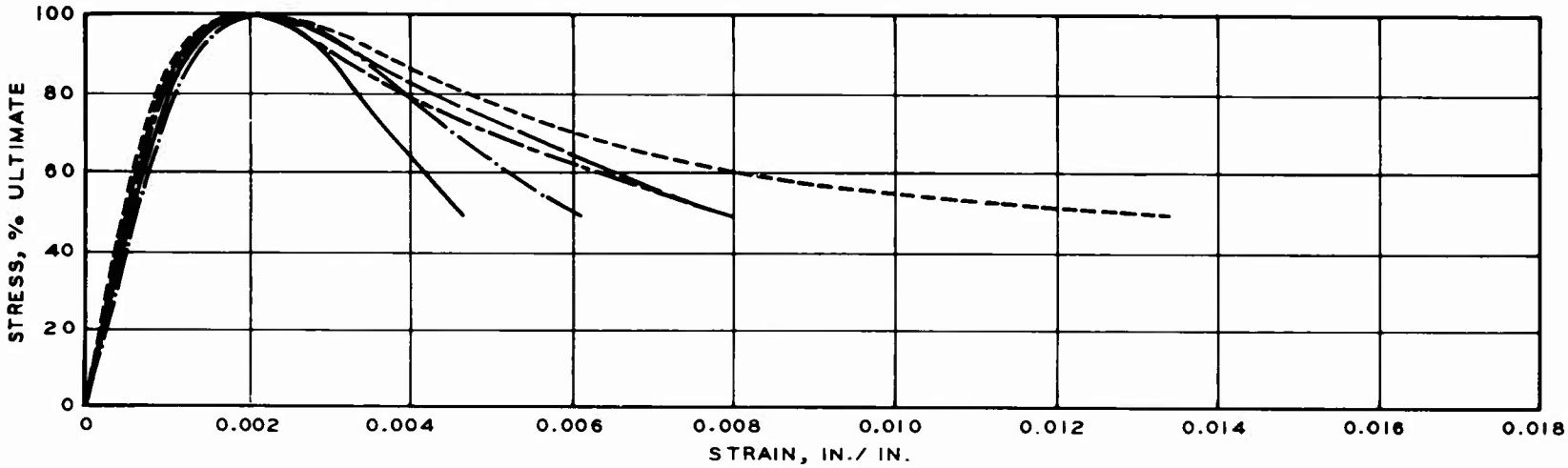

LEGEND

CONTROL
42
43
44
45

STRESS-STRAIN CURVES

HELICES
SPECIMENS 42, 43, 44, AND 45

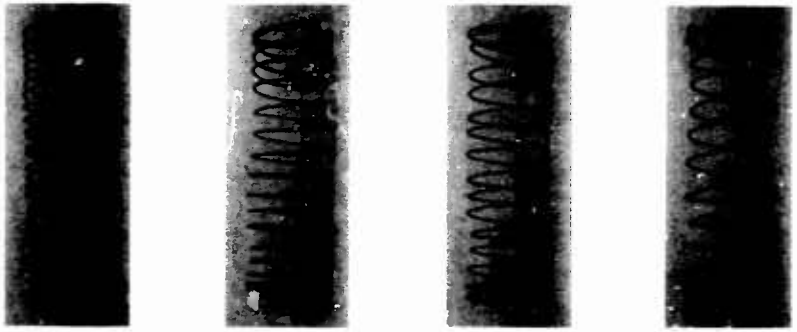

SPECIMEN NO.	18	19	20	21
REINFORCEMENT WEIGHT, G	111	64	58	54

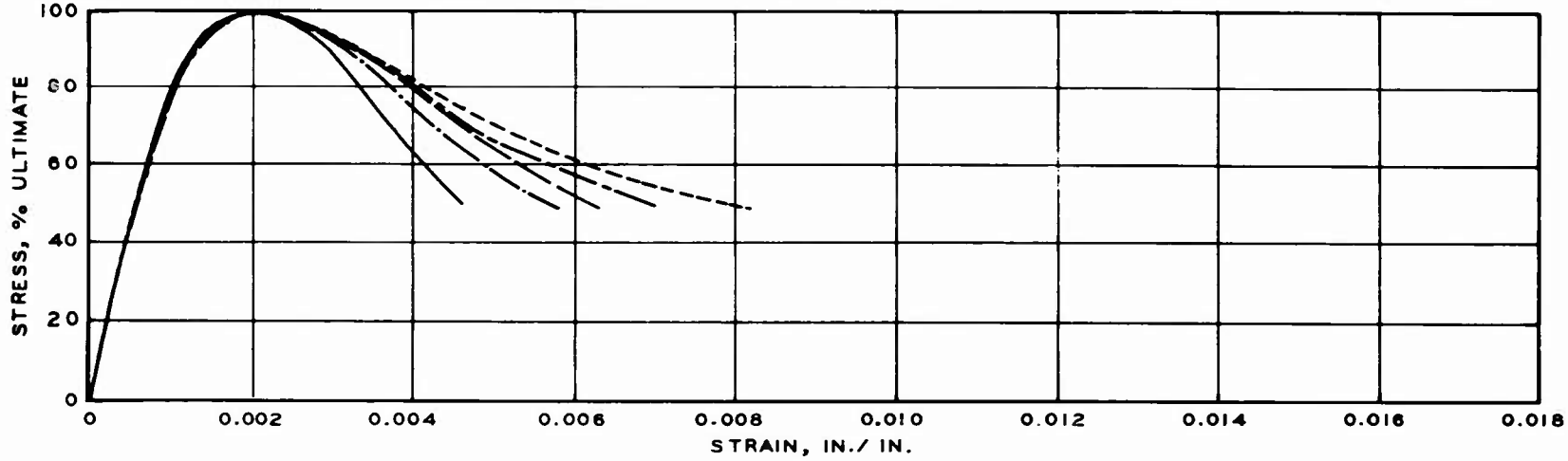

LEGEND

CONTROL
18
19
20
21

STRESS-STRAIN CURVES

HELICES
SPECIMENS 18, 19, 20, AND 21

PLATE 13

PLATE 14

SPECIMEN NO.	57	58	59	60
REINFORCEMENT WEIGHT, G	368	220	110	70

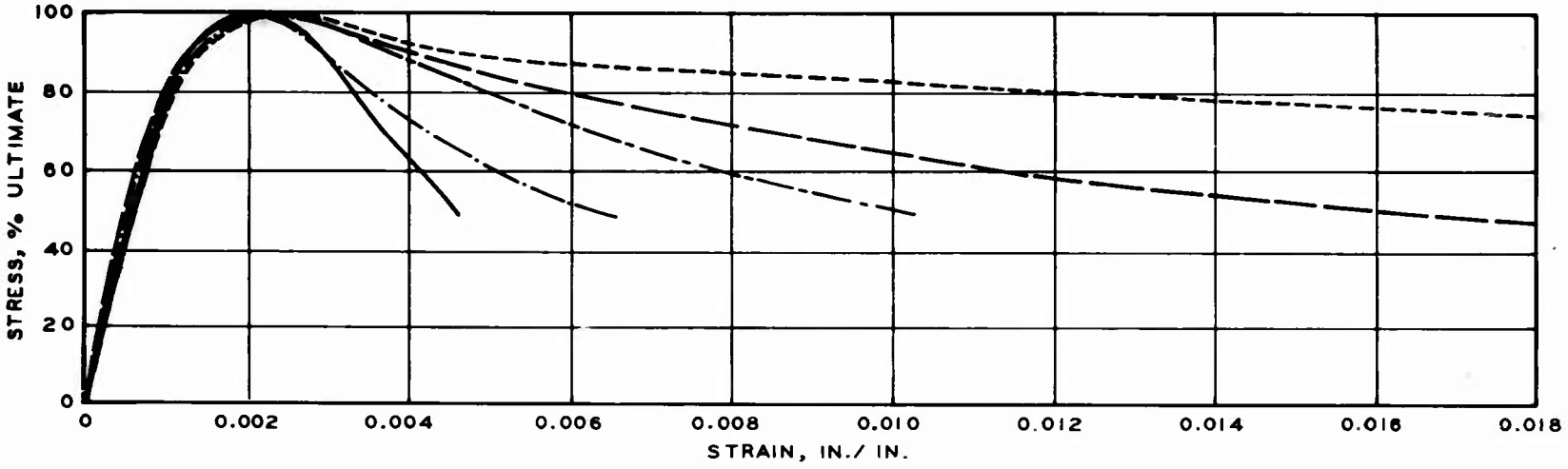

LEGEND

CONTROL
57
58
59
60

STRESS-STRAIN CURVES

HELICES
SPECIMENS 57, 58, 59, AND 60

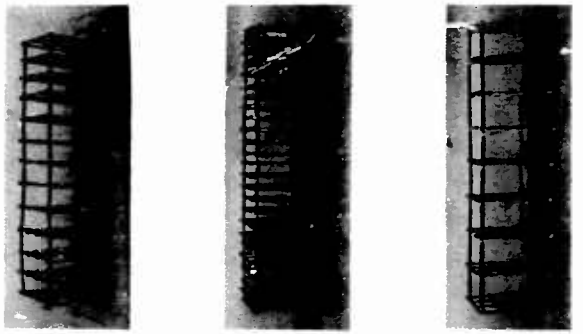

SPECIMEN NO.	29	50	51
REINFORCEMENT WEIGHT, G	238	432	177

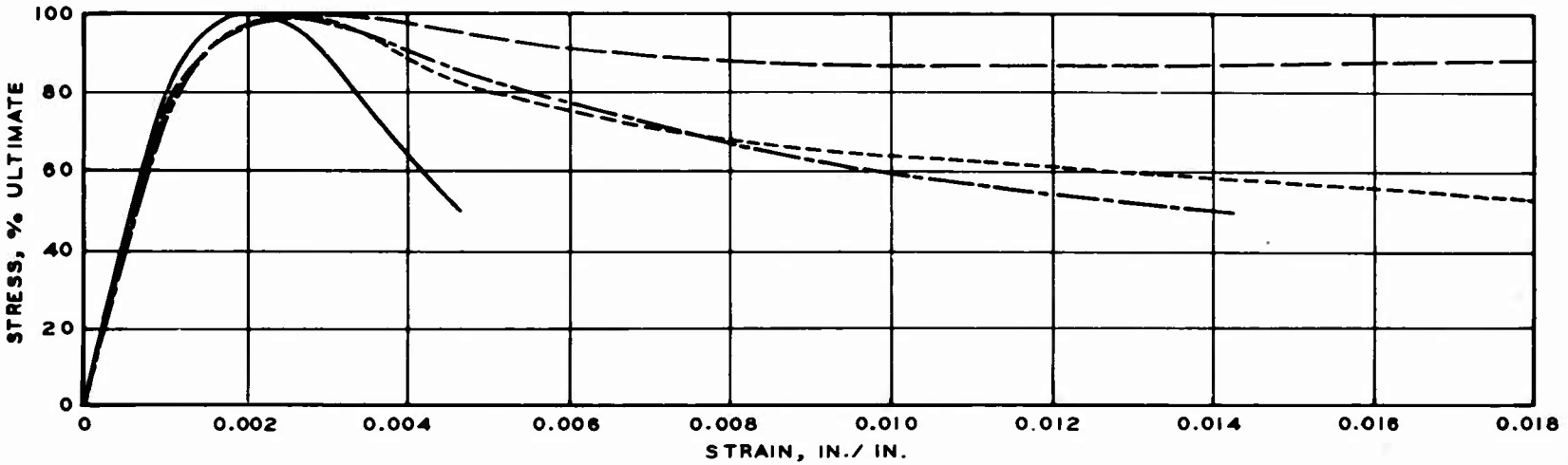

LEGEND

——— CONTROL
– – – – 29
— — — 50
— – — 51

STRESS-STRAIN CURVES

PLANE MESHES
SPECIMENS 29, 50, AND 51

PLATE 15

PLATE 16

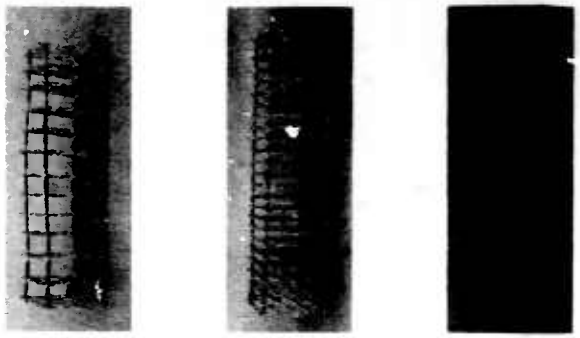

SPECIMEN NO.	30	52	53
REINFORCEMENT WEIGHT, G	174	343	143

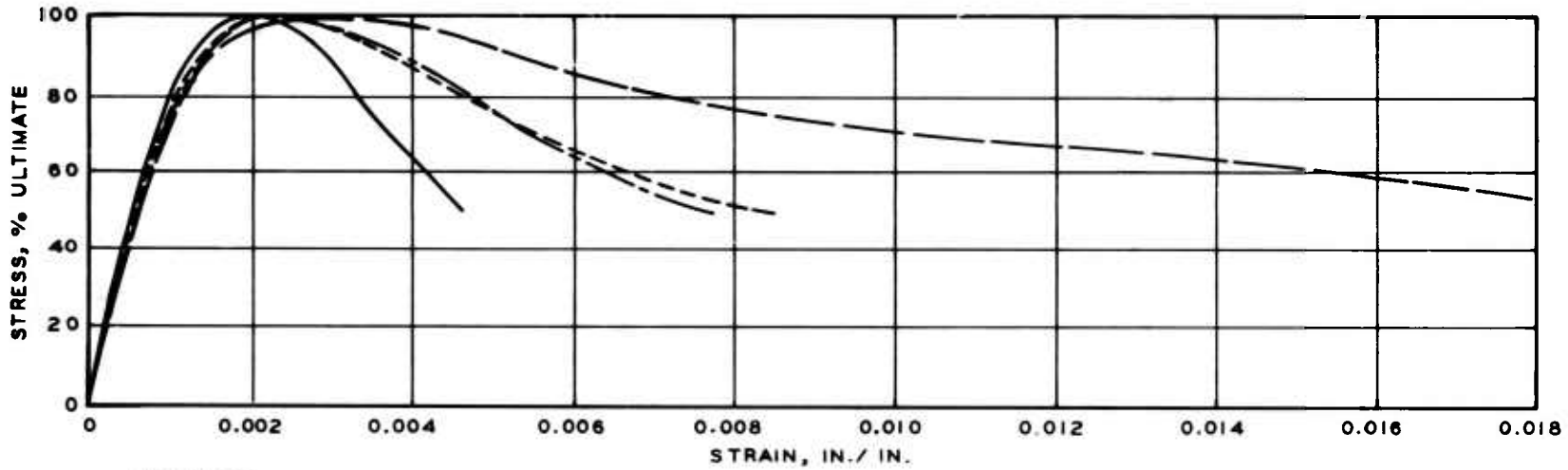

LEGEND

——— CONTROL
– – – – 30
— — 52
— – — 53

STRESS-STRAIN CURVES
PLANE MESHES
SPECIMENS 30, 52, AND 53

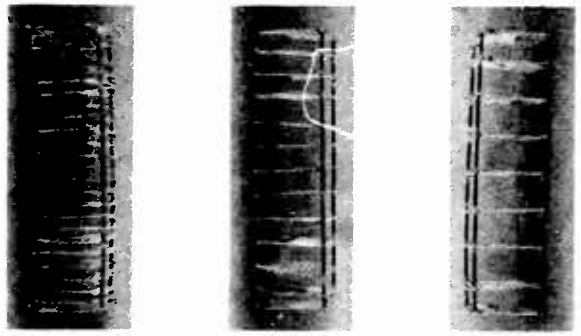

SPECIMEN NO.	54	55	56
REINFORCEMENT WEIGHT, G	228	132	102

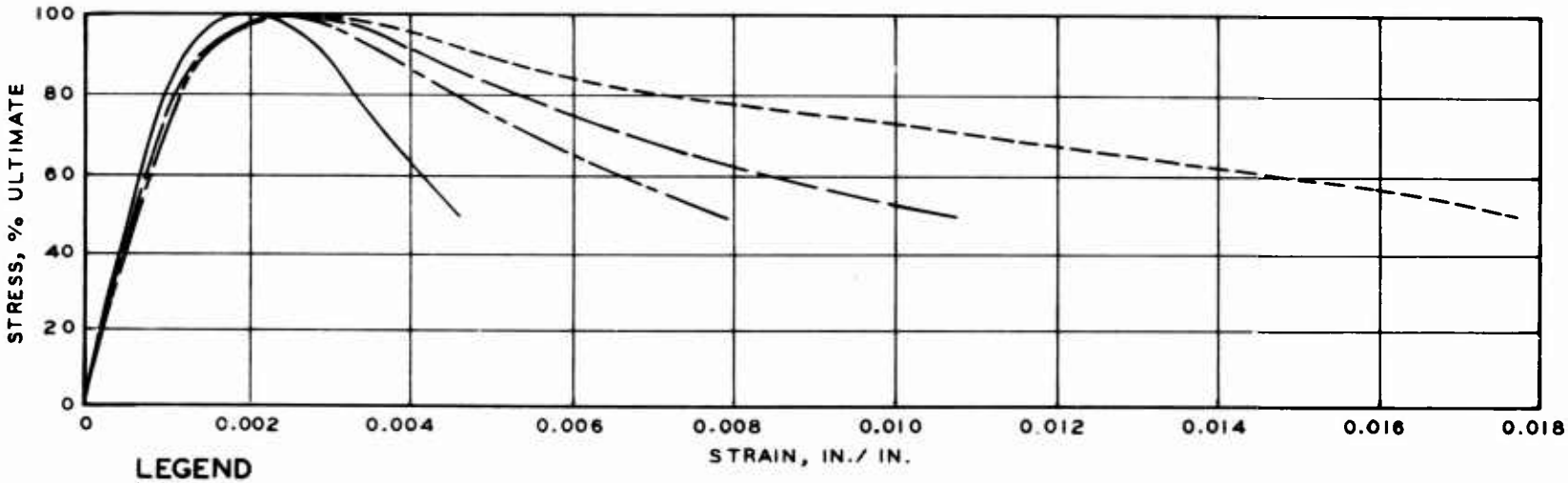

LEGEND

——— CONTROL
- - - - 54
— — 55
— - — 56

STRESS-STRAIN CURVES
PLANE MESHES
SPECIMENS 54, 55, AND 56

PLATE 17

PLATE 18

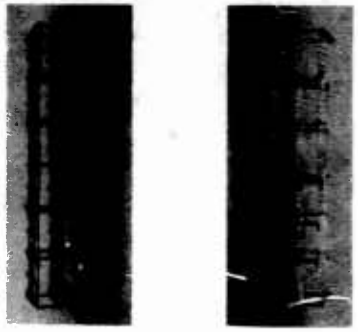

SPECIMEN NO.	31	32
REINFORCEMENT WEIGHT, G	260	148

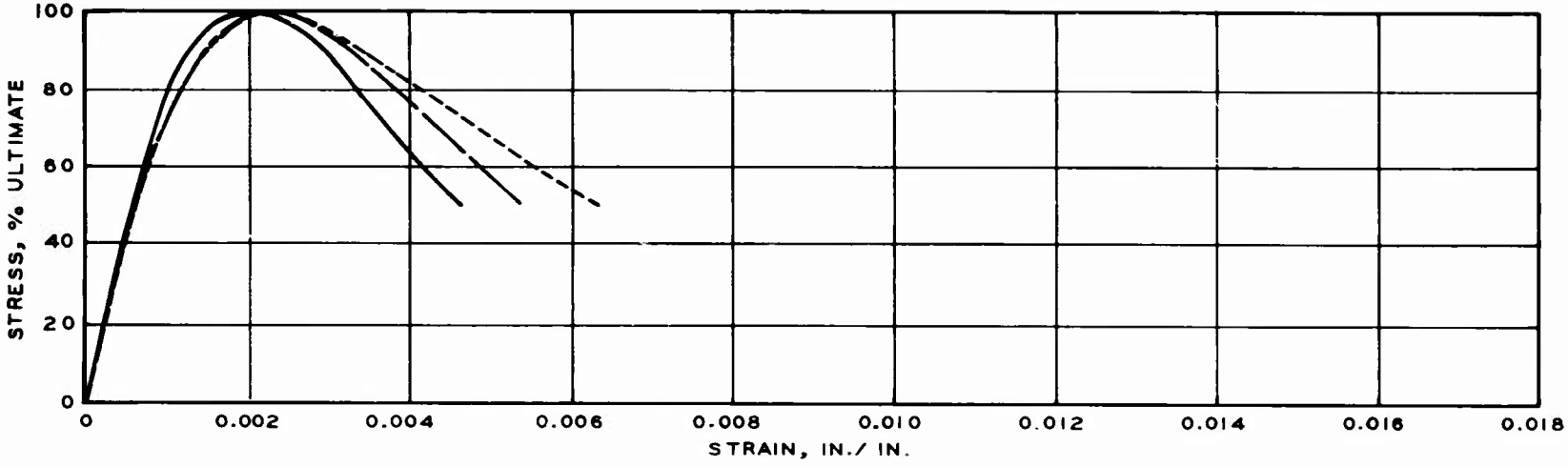

LEGEND

——— CONTROL
– – – – 31
— — 32

STRESS-STRAIN CURVES
PLANE MESHES
SPECIMENS 31 AND 32

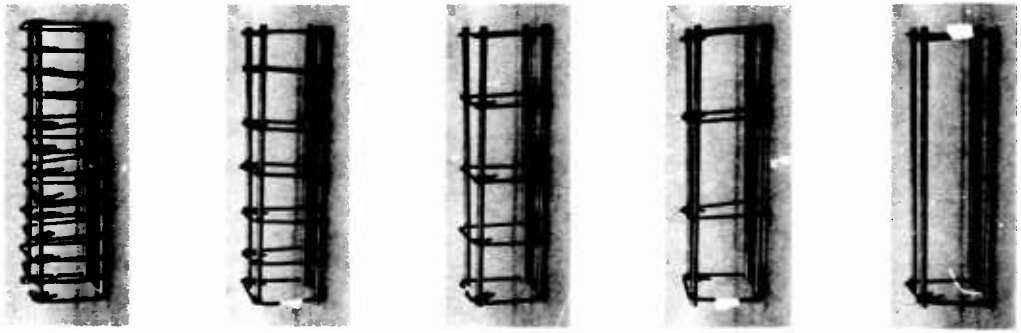

SPECIMEN NO.	61	62	63	64	65
REINFORCEMENT WEIGHT, G	524	418	384	367	333

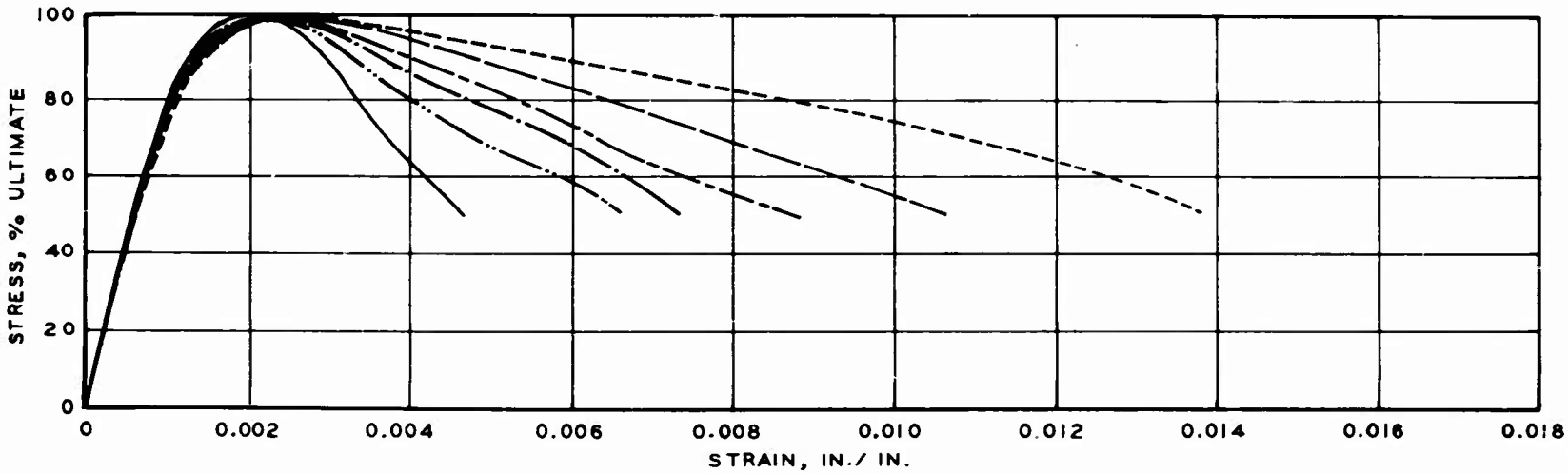

LEGEND

CONTROL
61
62
63
64
65

STRESS-STRAIN CURVES

LATERAL TIES

SPECIMENS 61, 62, 63, 64, AND 65

PLATE 19

PLATE 20

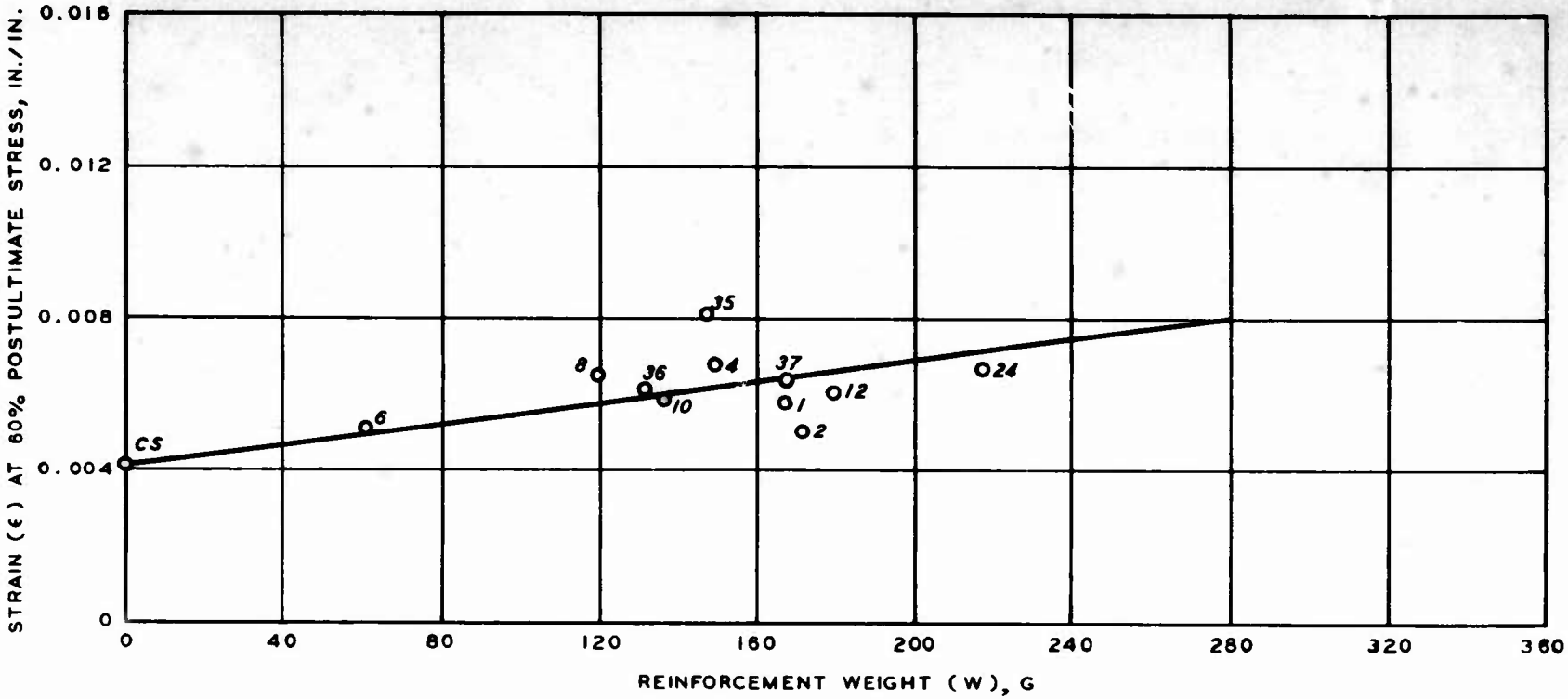

EFFICIENCY OF CIRCULAR TUBULAR MESH CONFINING REINFORCEMENT

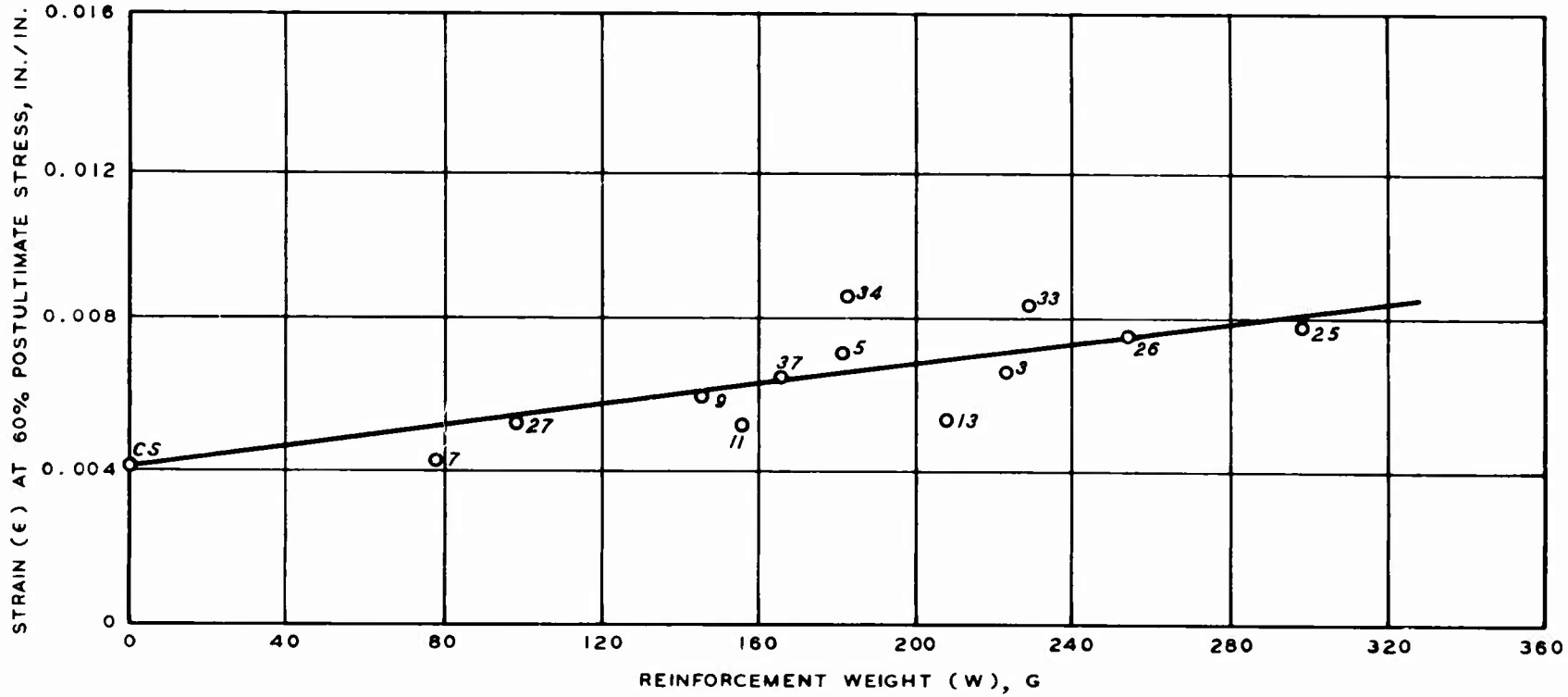

EFFICIENCY OF SQUARE TUBULAR MESH CONFINING REINFORCEMENT

PLATE 21

PLATE 22

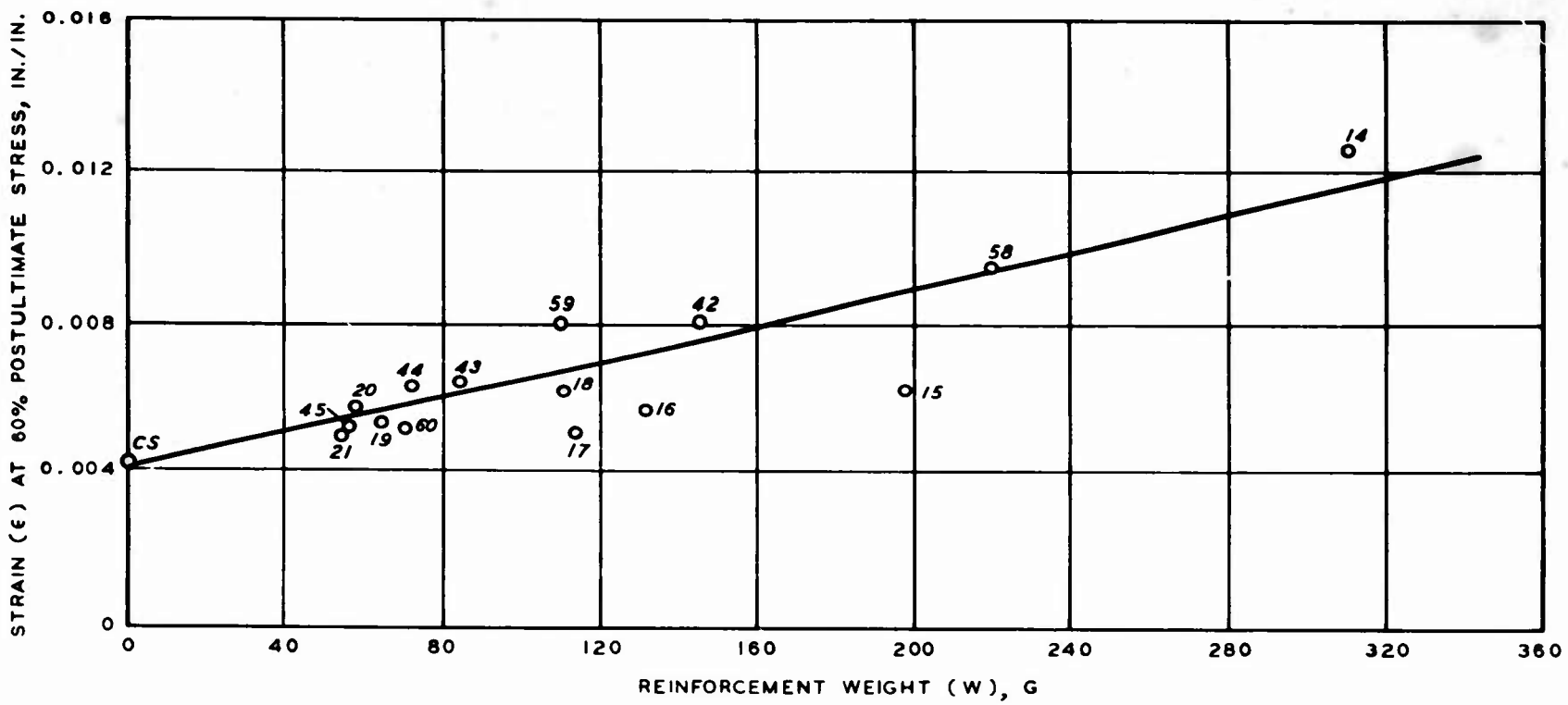

EFFICIENCY OF HELICAL
CONFINING REINFORCEMENT

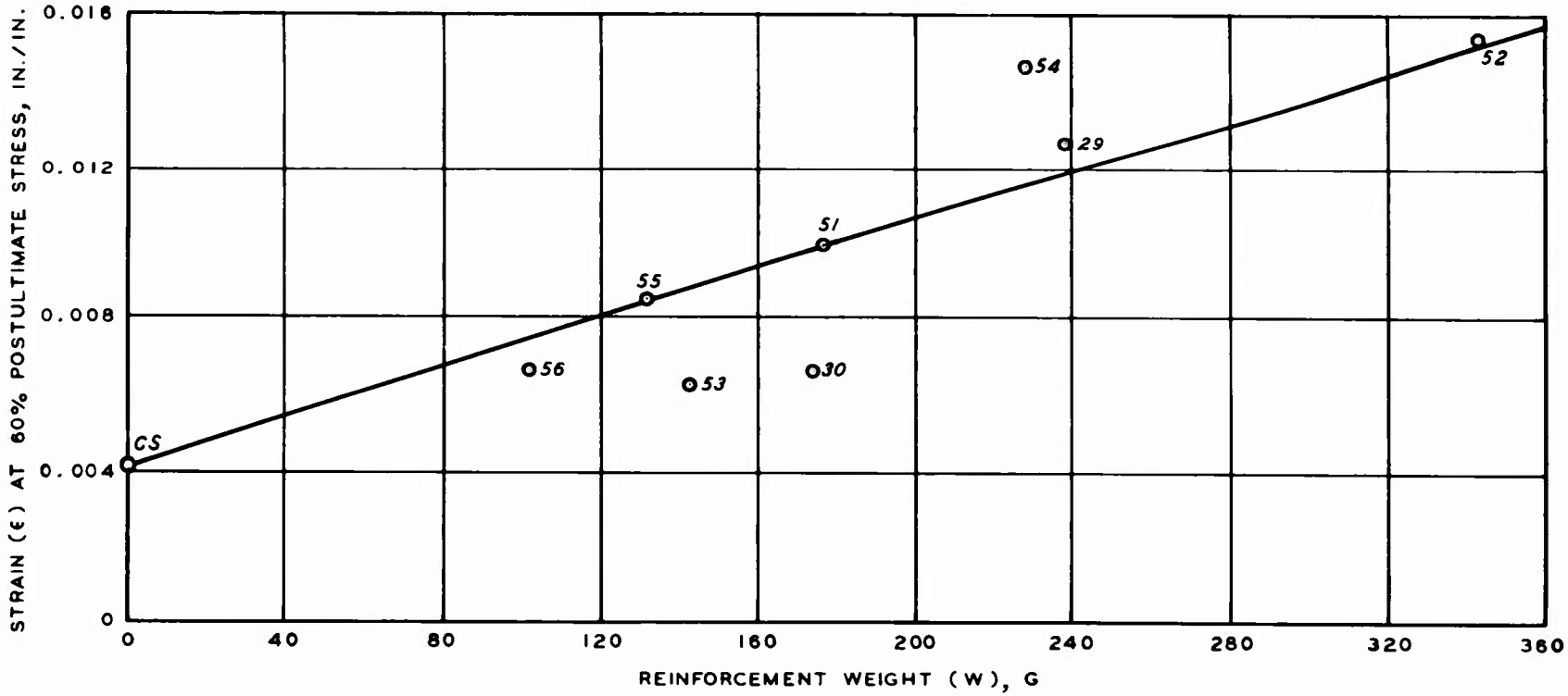

EFFICIENCY OF HORIZONTAL PLANE MESH CONFINING REINFORCEMENT

PLATE 23

PLATE 24

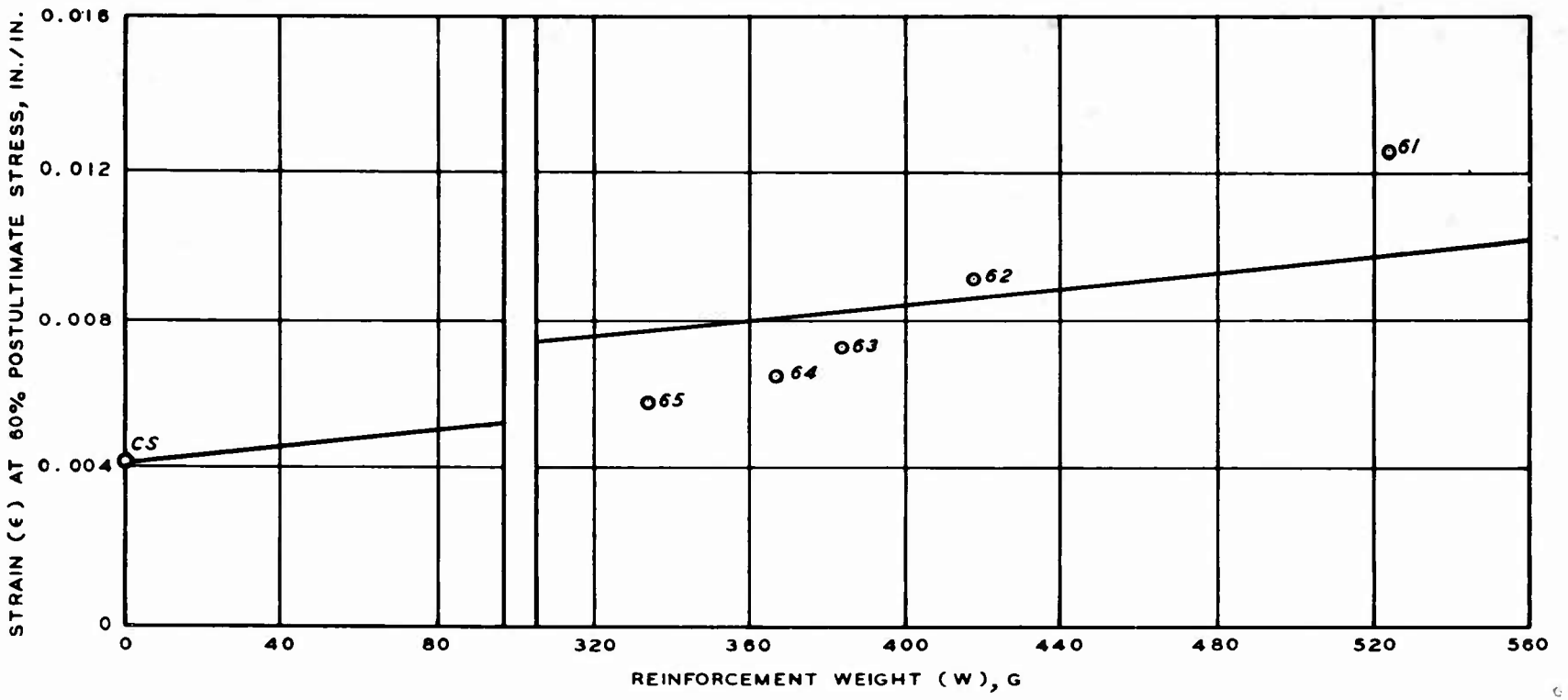

EFFICIENCY OF LATERAL
TIE CONFINING REINFORCEMENT

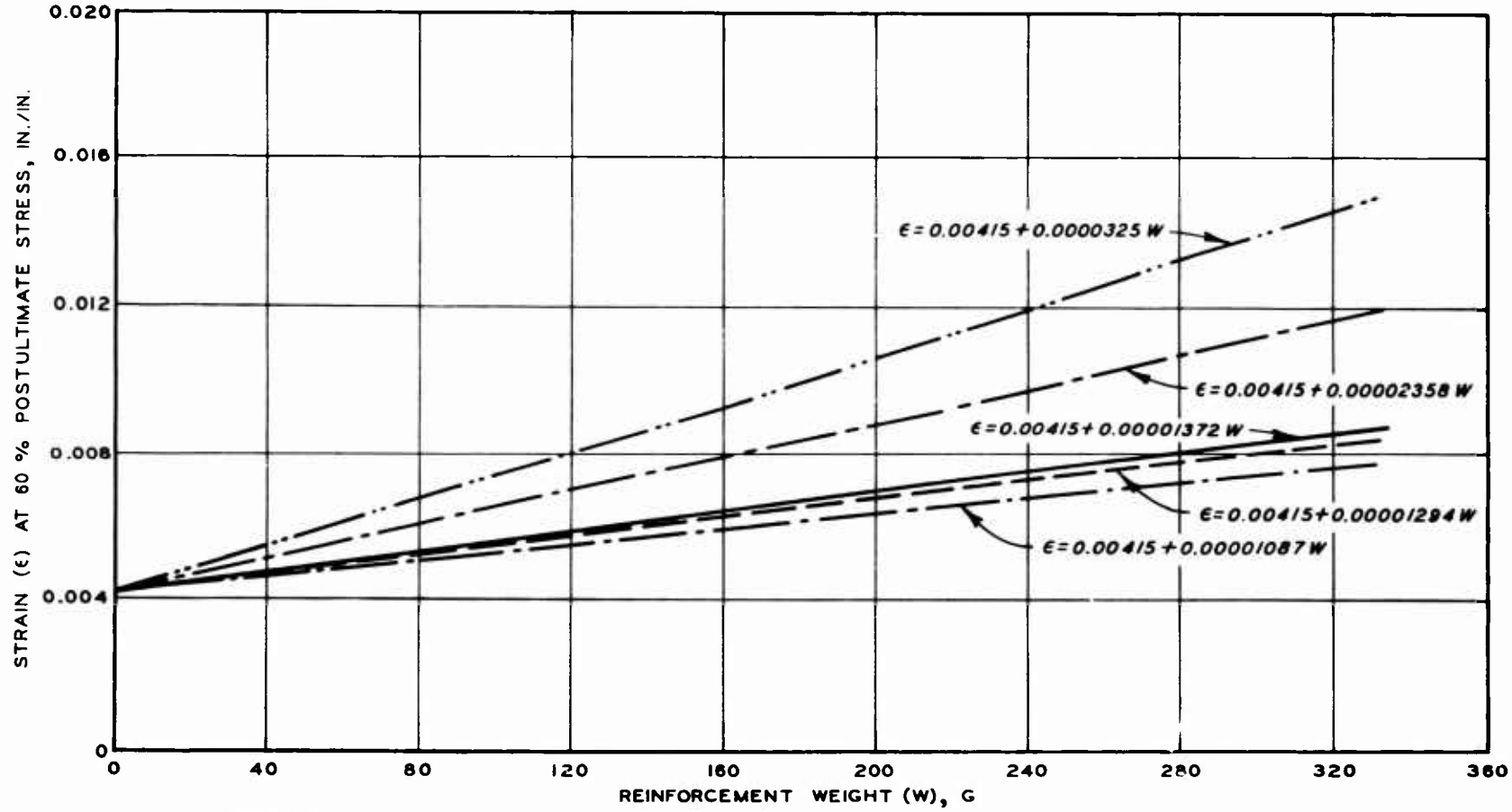

EFFICIENCY OF DIFFERENT TYPES OF CONFINING REINFORCEMENT

PLATE 25

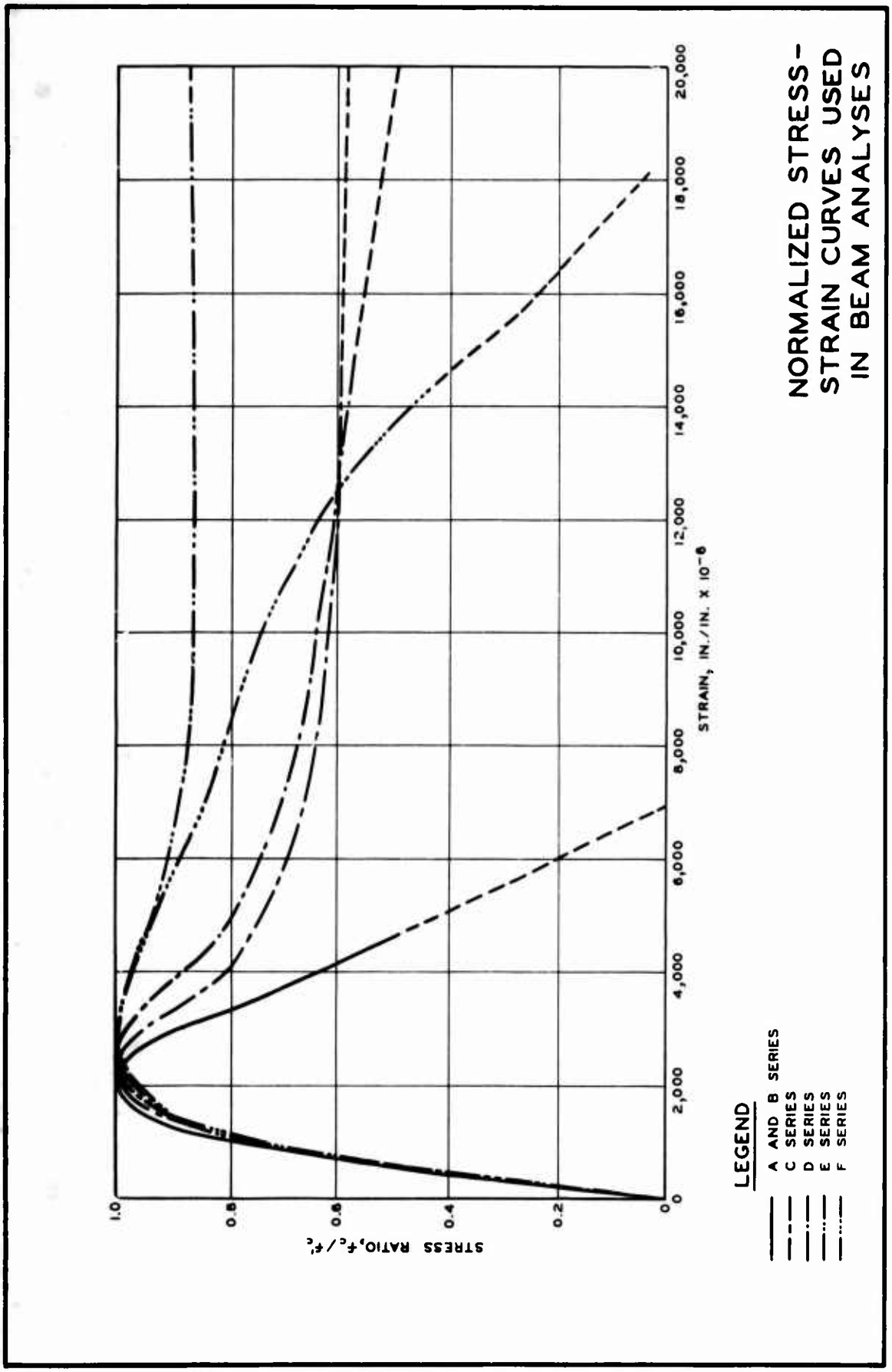
NORMALIZED STRESS-STRAIN CURVES USED IN BEAM ANALYSES
LEGEND
A AND B SERIES
C SERIES
D SERIES
E SERIES
F SERIES
STRESS RATIO, f_c / f'_c
0
0.2
0.4
0.6
0.8
1.0
STRAIN, IN./IN. x 10^{-6}
0
2,000
4,000
6,000
8,000
10,000
12,000
14,000
16,000
18,000
20,000

PLATE 26

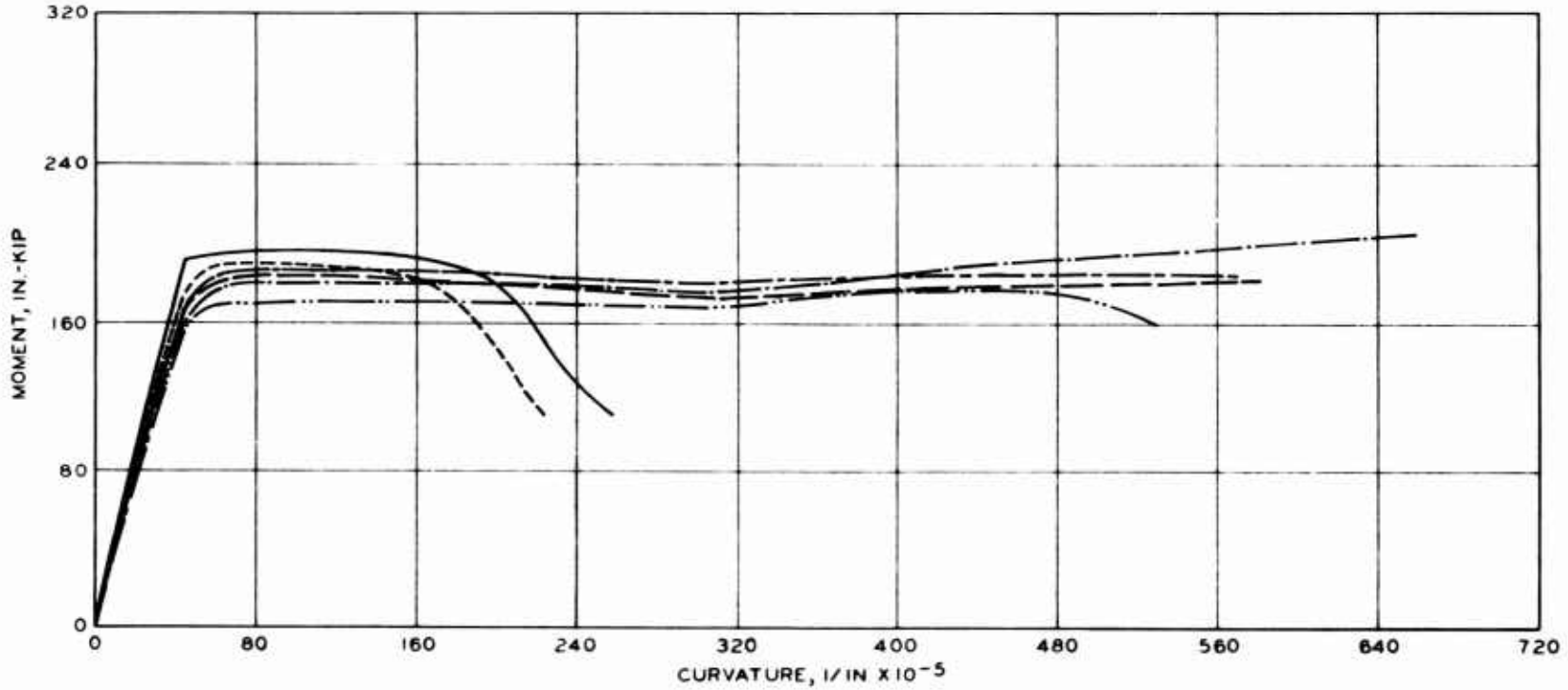

LEGEND

A-1
B-1
C-1
D-1
E-1
F-1

THEORETICAL MOMENT - CURVATURE RELATIONS
DESIGN I

PLATE 27

PLATE 28

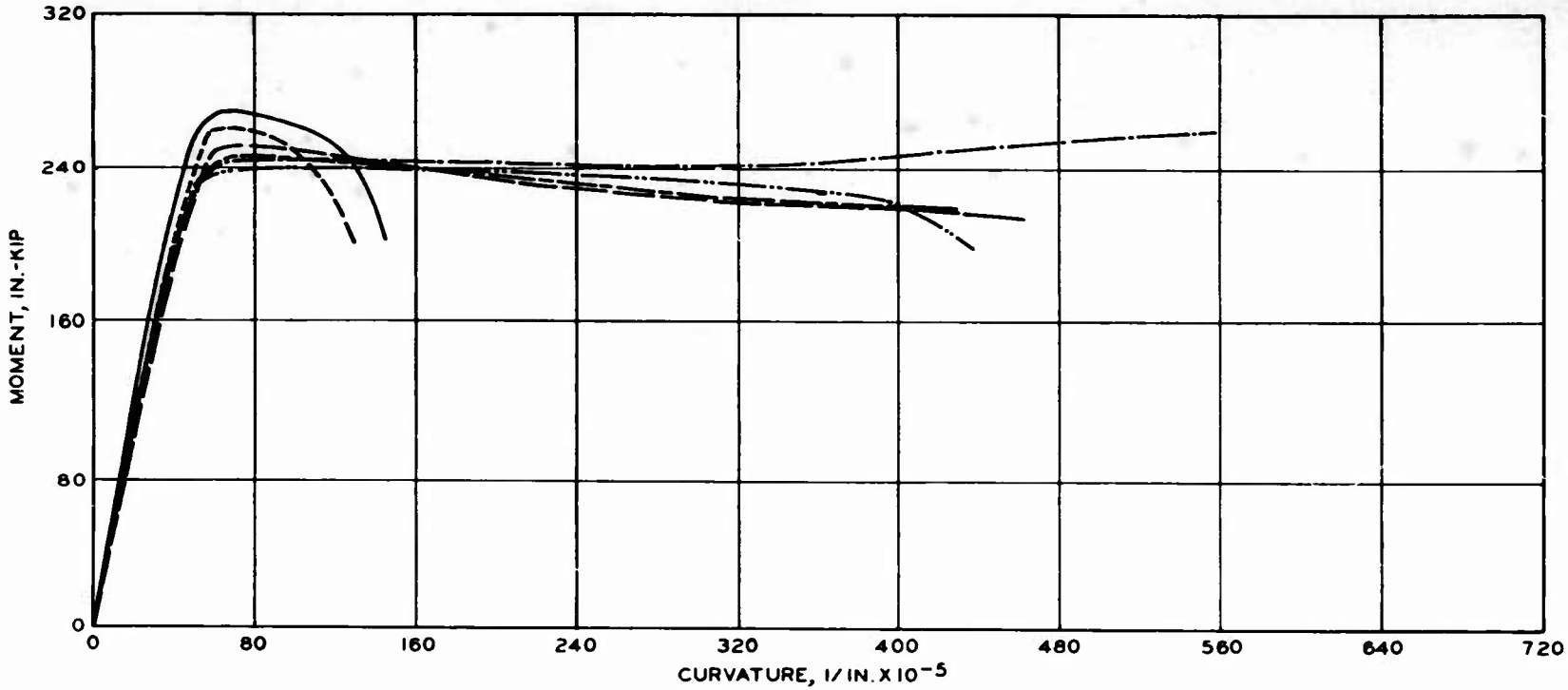

LEGEND

- A-2
- B-2
- C-2
- D-2A
- E-2A
- F-2

THEORETICAL MOMENT – CURVATURE RELATIONS
DESIGN 2

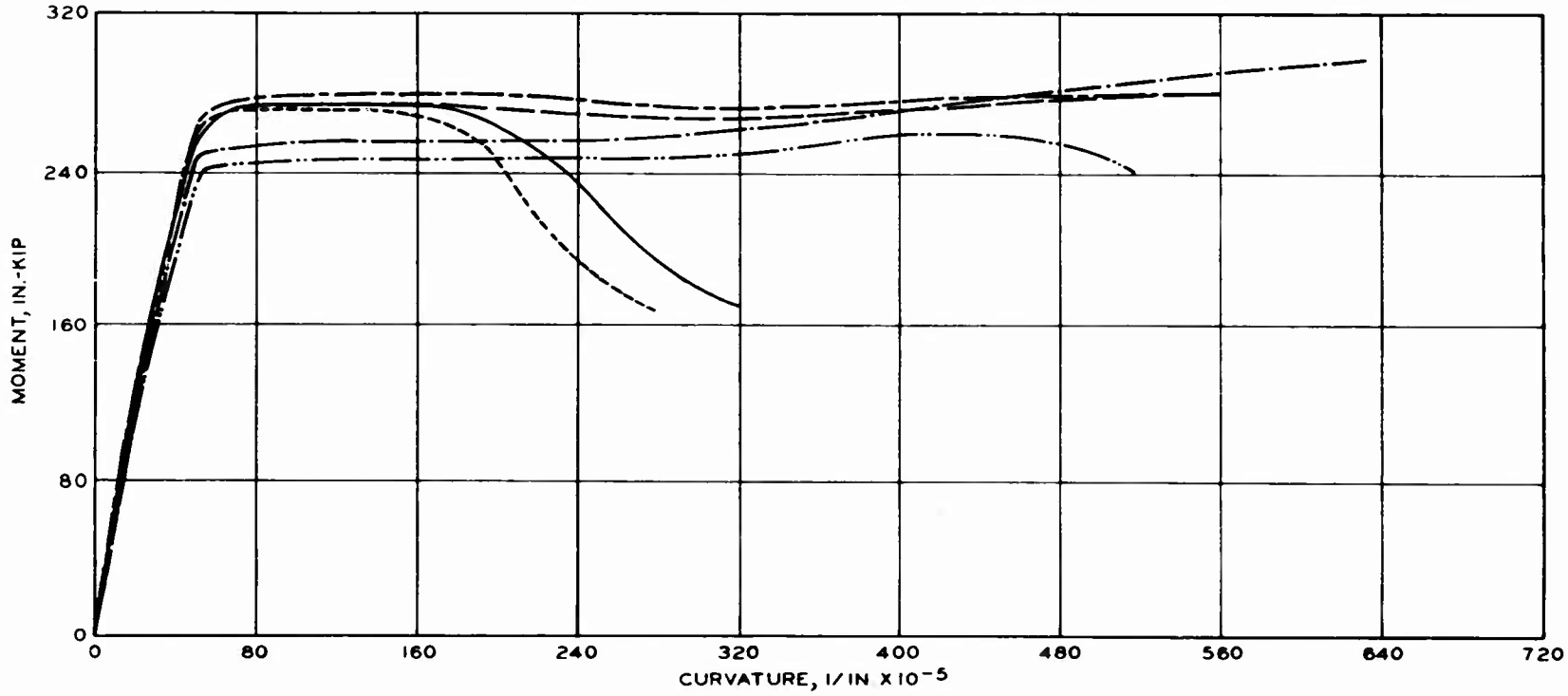

LEGEND

- A-3A
- B-3
- C-3
- D-3
- E-3
- F-3

THEORETICAL MOMENT - CURVATURE RELATIONS
DESIGN 3

PLATE 29

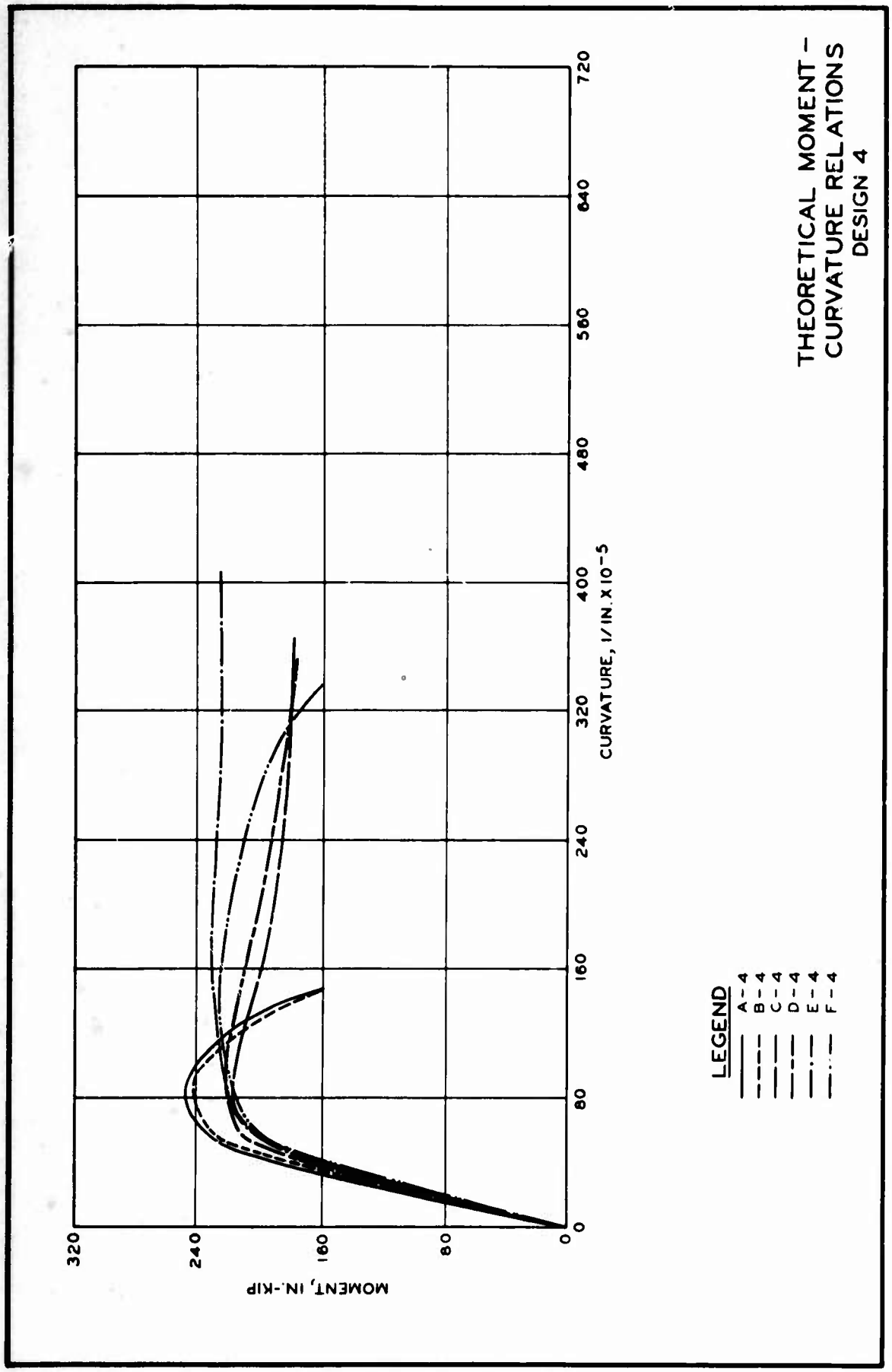
THEORETICAL MOMENT - CURVATURE RELATIONS
DESIGN 4
LEGEND
A-4
B-4
C-4
D-4
E-4
F-4
MOMENT, IN.-KIP
0
80
160
240
320
CURVATURE, 1/IN. X 10⁻⁵
0
80
160
240
320
400
480
560
640
720

PLATE 30

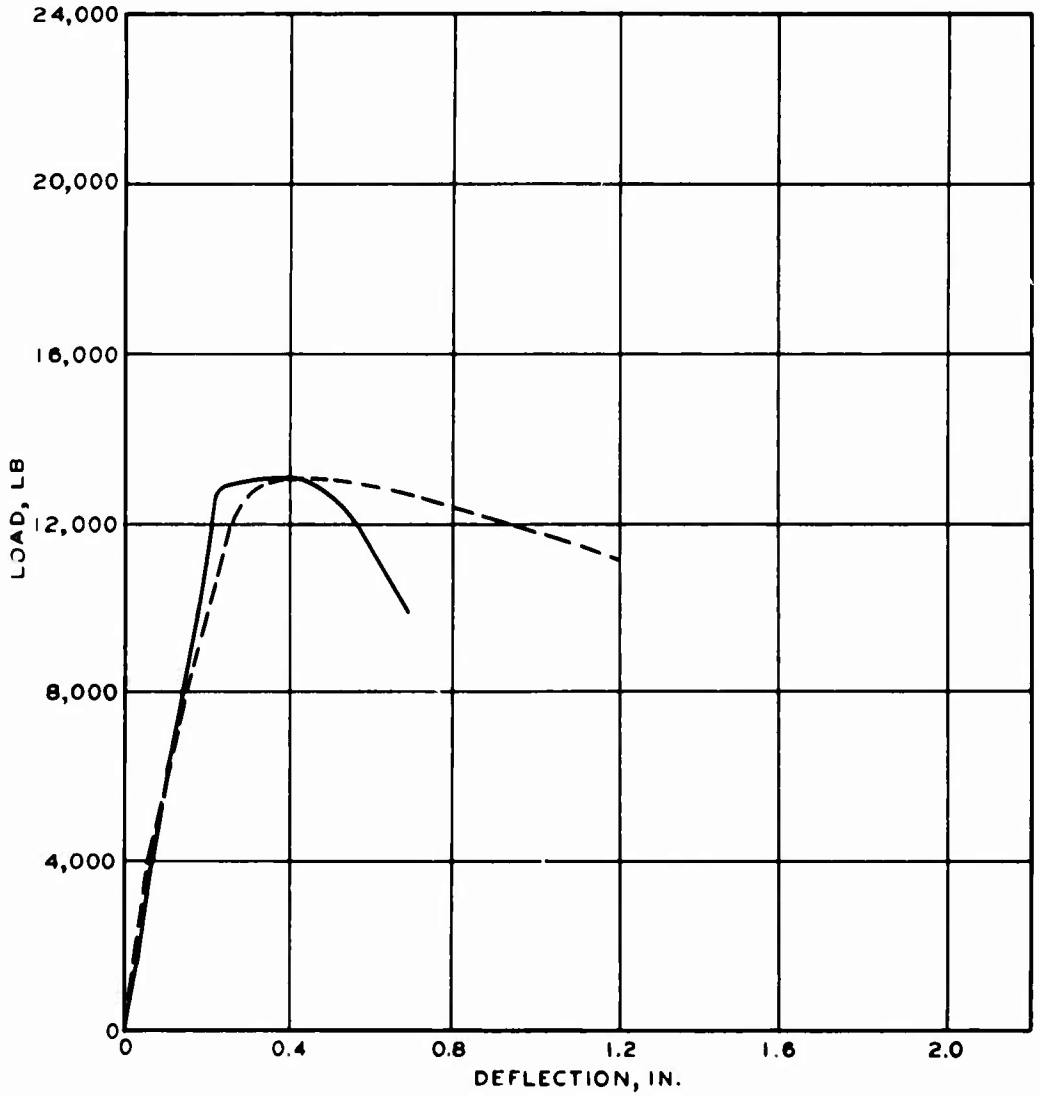

LEGEND

——— COMPUTED

– – – – MEASURED

THEORETICAL AND MEASURED MIDSPAN DEFLECTIONS

BEAM A-1

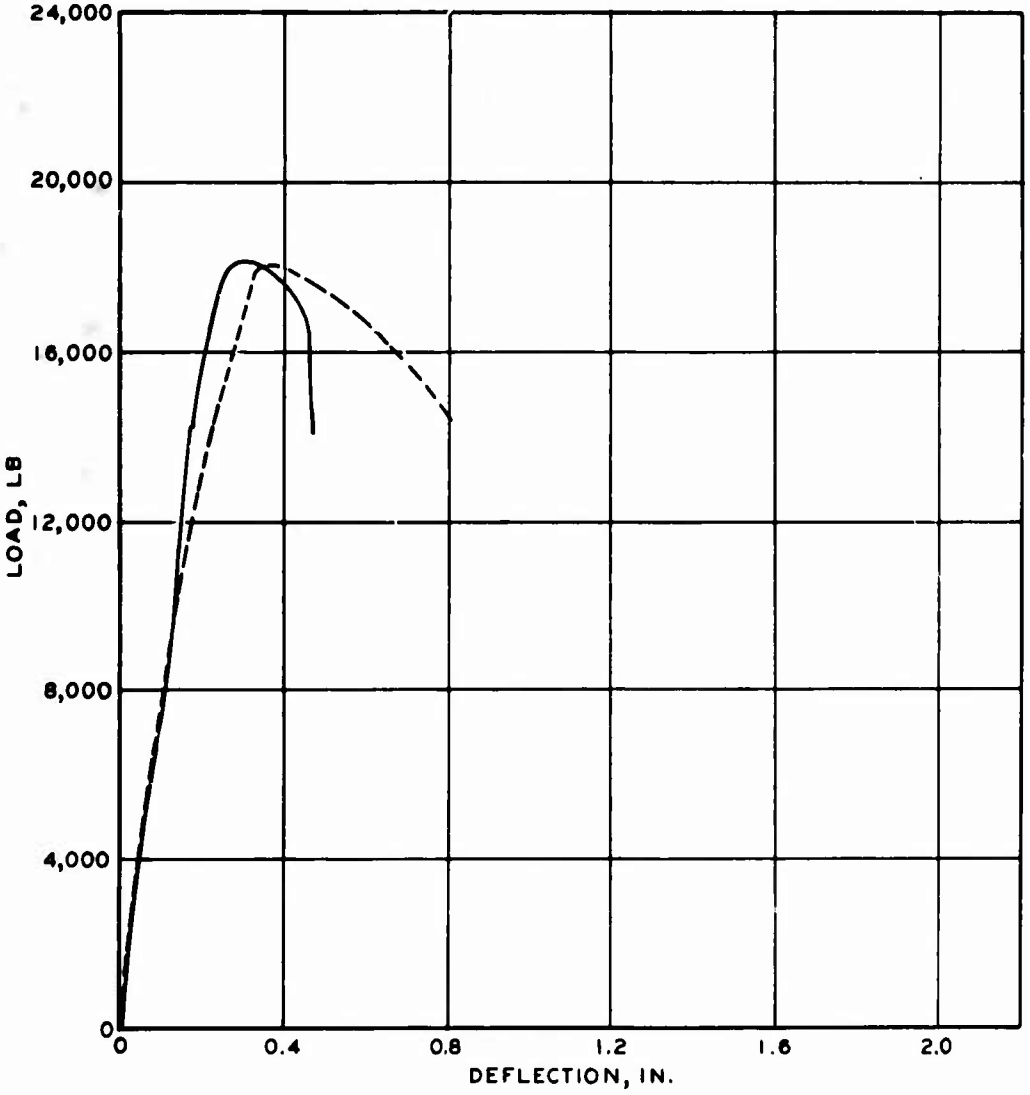

LEGEND

——— COMPUTED

– – – – MEASURED

THEORETICAL AND MEASURED MIDSPAN DEFLECTIONS

BEAM A-2

PLATE 32

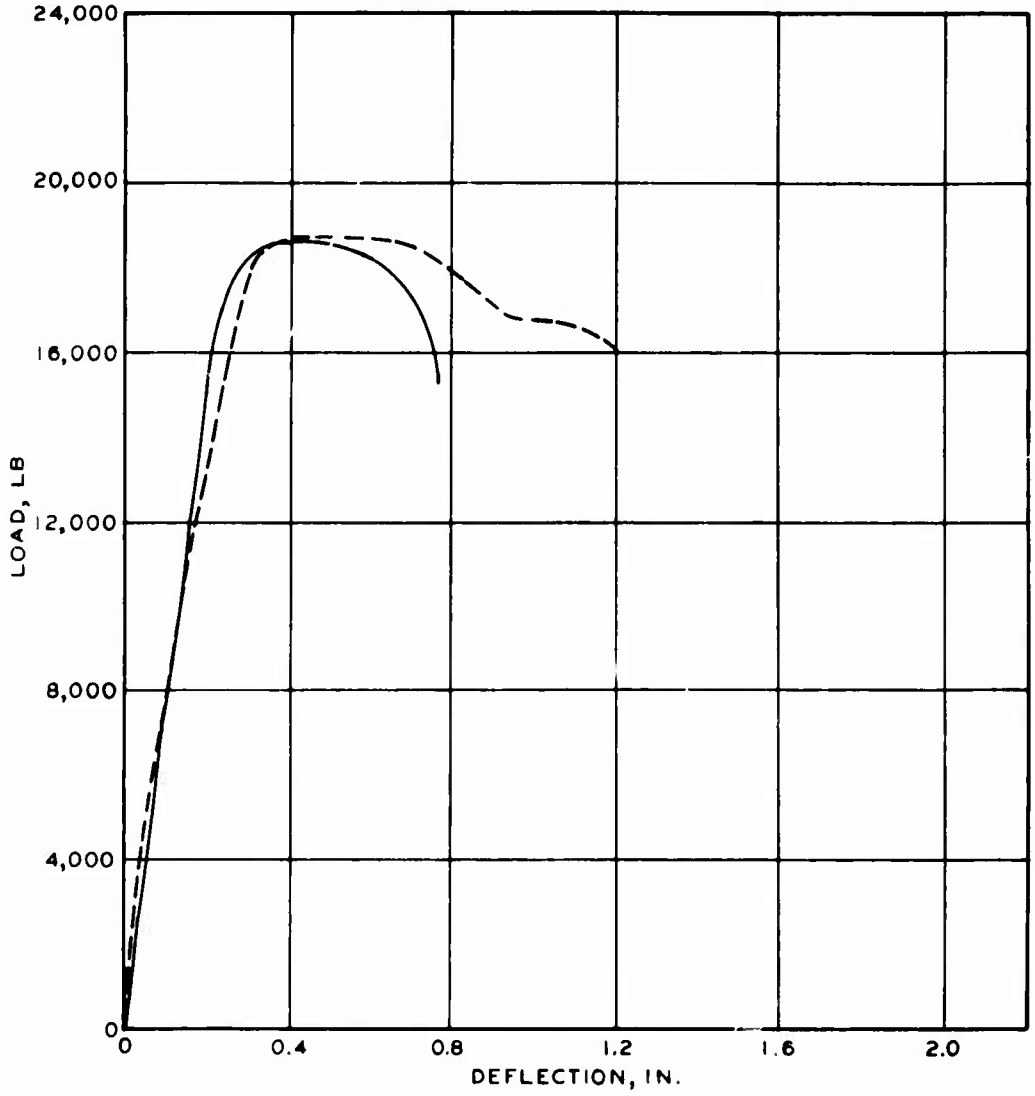

LEGEND

——— COMPUTED

– – – – MEASURED

THEORETICAL AND MEASURED MIDSPAN DEFLECTIONS

BEAM A-3A

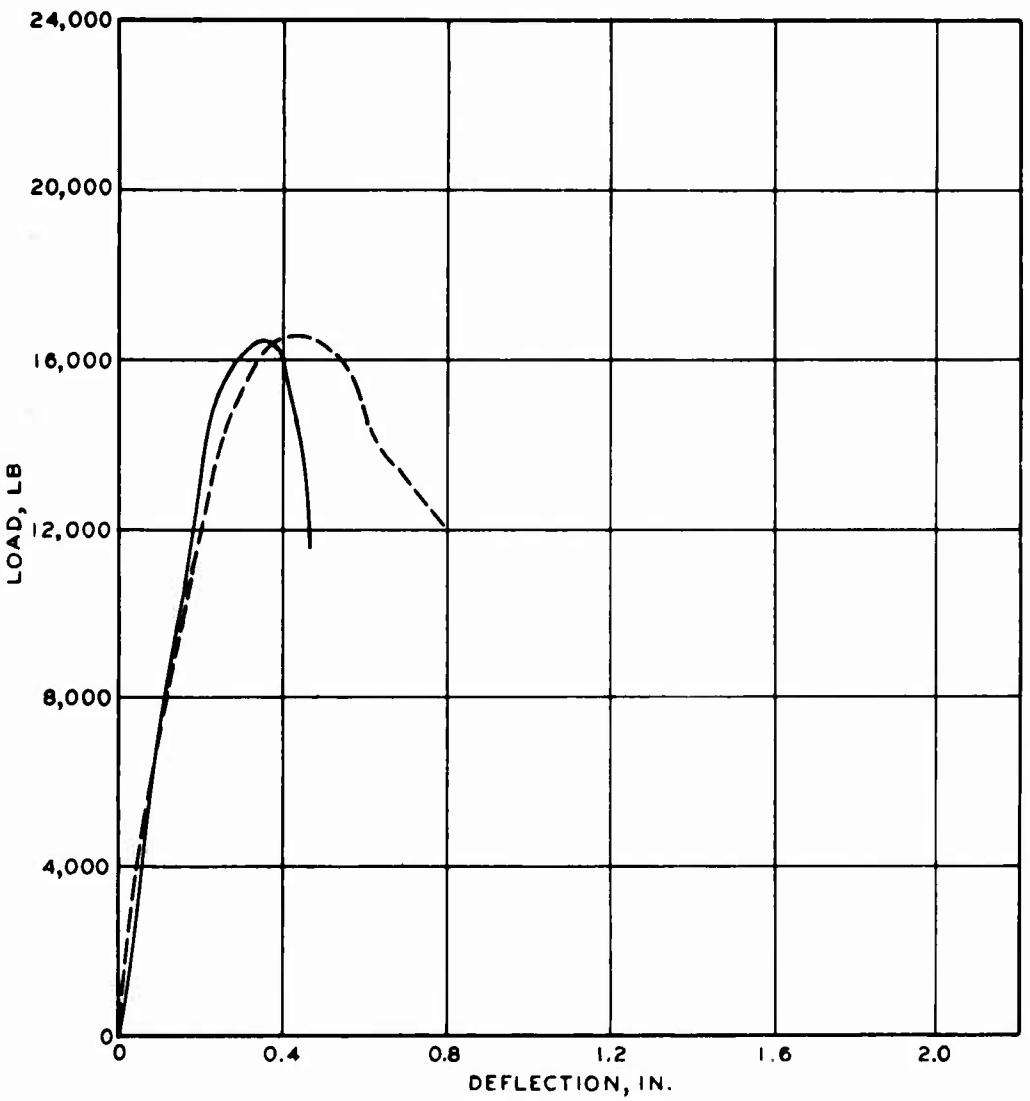

LEGEND

COMPUTED

MEASURED

THEORETICAL AND MEASURED MIDSPAN DEFLECTIONS

BEAM A-4

PLATE 34

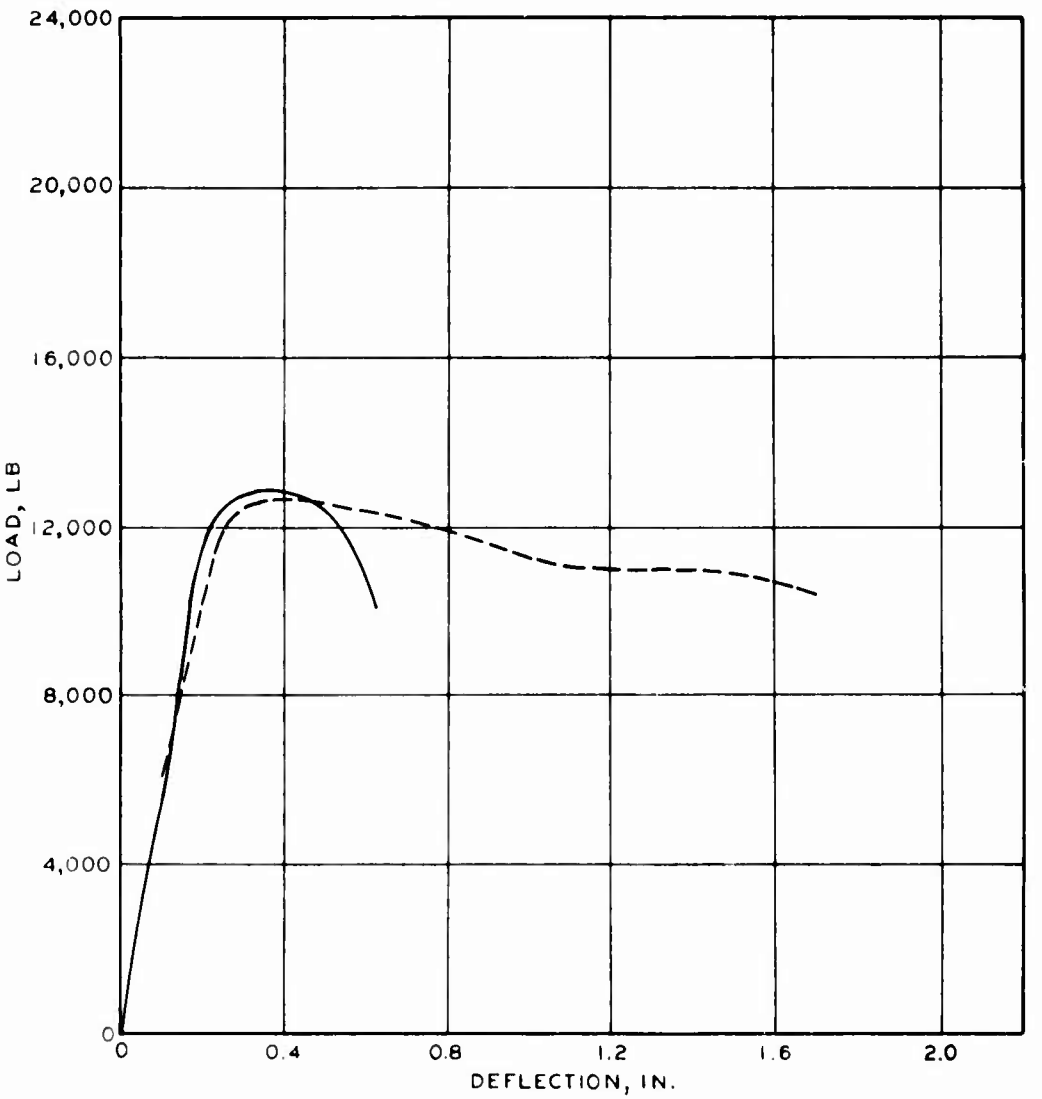

LEGEND

——— COMPUTED

– – – – MEASURED

THEORETICAL AND MEASURED MIDSPAN DEFLECTIONS

BEAM B-1

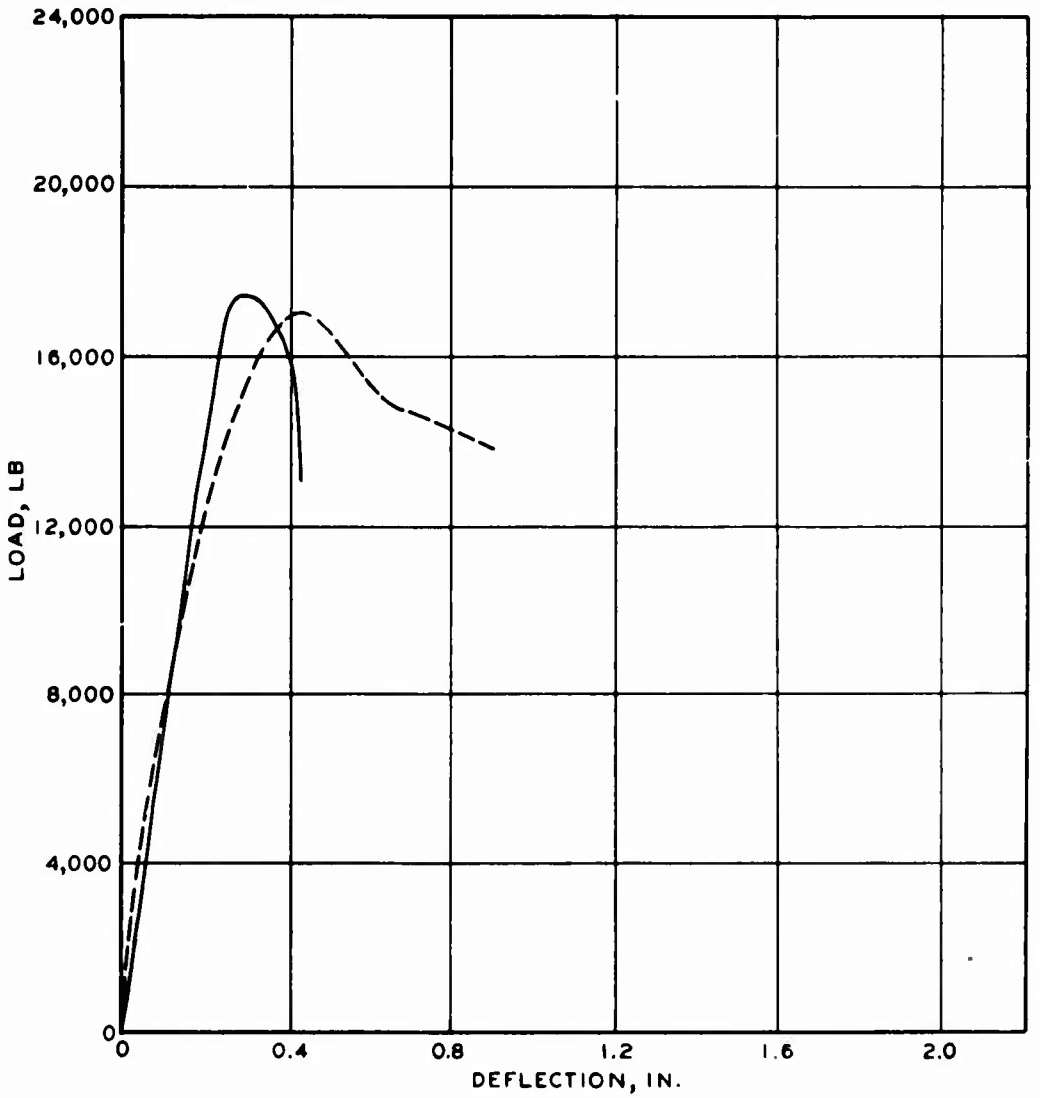

LEGEND

——— COMPUTED

– – – – MEASURED

THEORETICAL AND MEASURED MIDSPAN DEFLECTIONS

BEAM B-2

PLATE 36

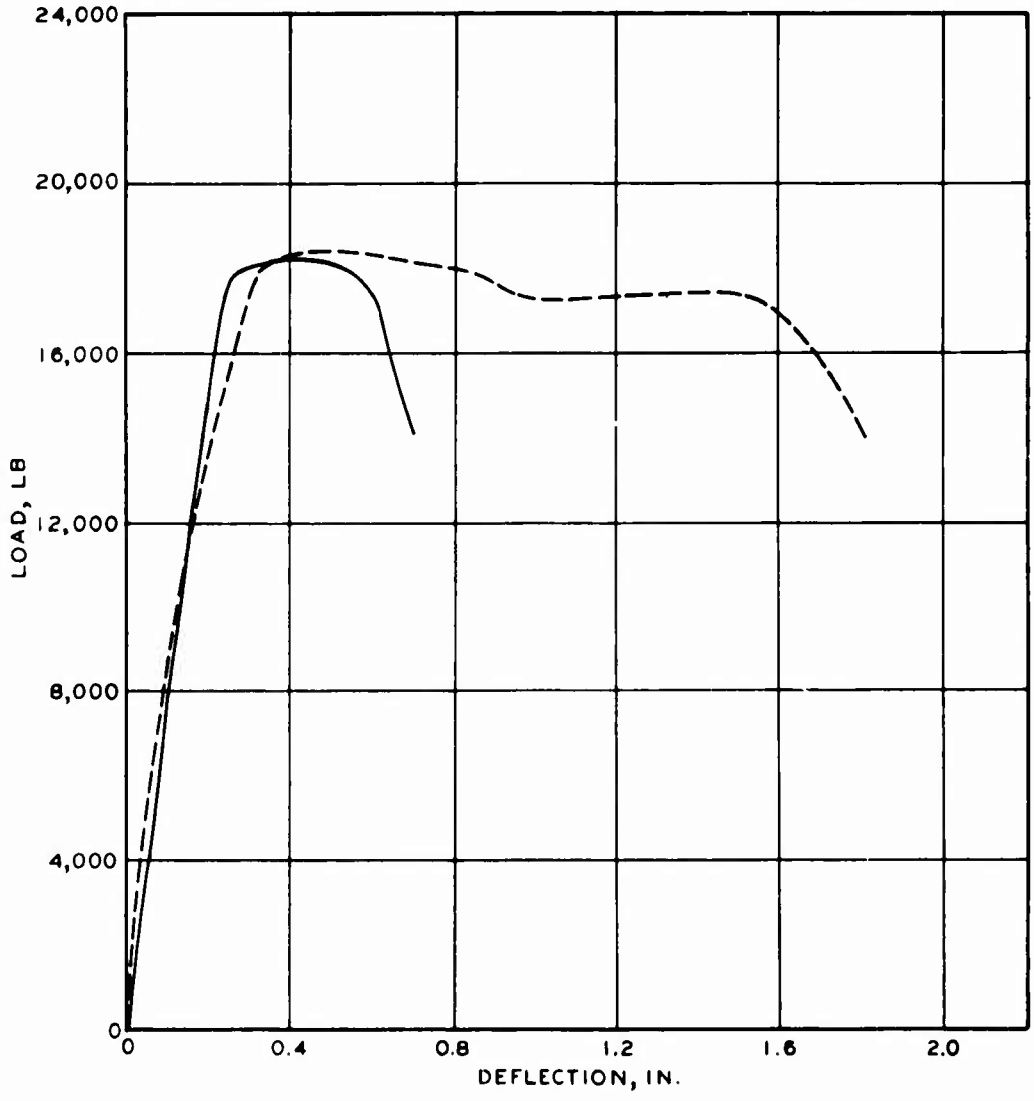

LEGEND

——— COMPUTED

– – – – MEASURED

THEORETICAL AND MEASURED MIDSPAN DEFLECTIONS

BEAM B-3

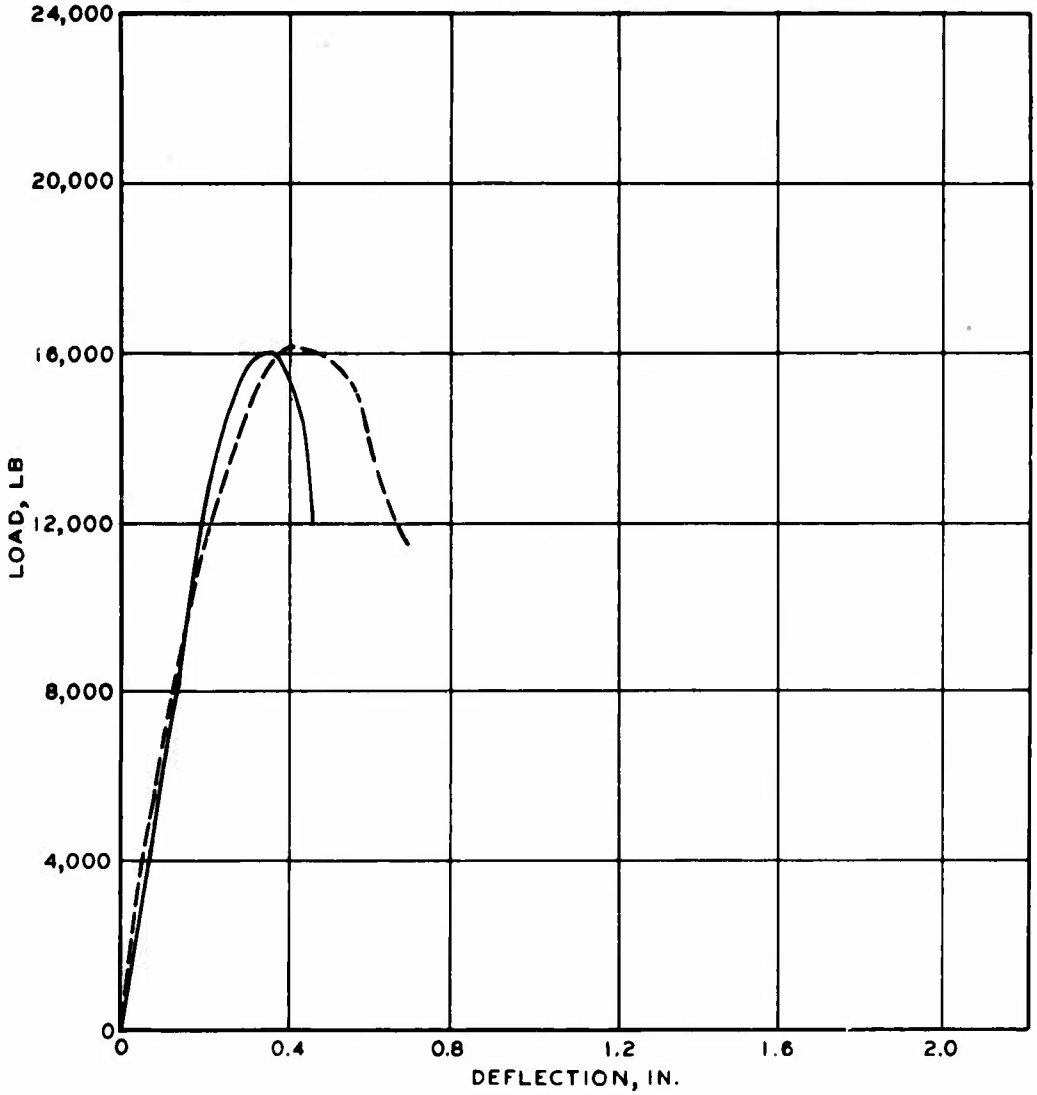

LEGEND

——— COMPUTED

– – – – MEASURED

THEORETICAL AND MEASURED MIDSPAN DEFLECTIONS

BEAM B-4

PLATE 38

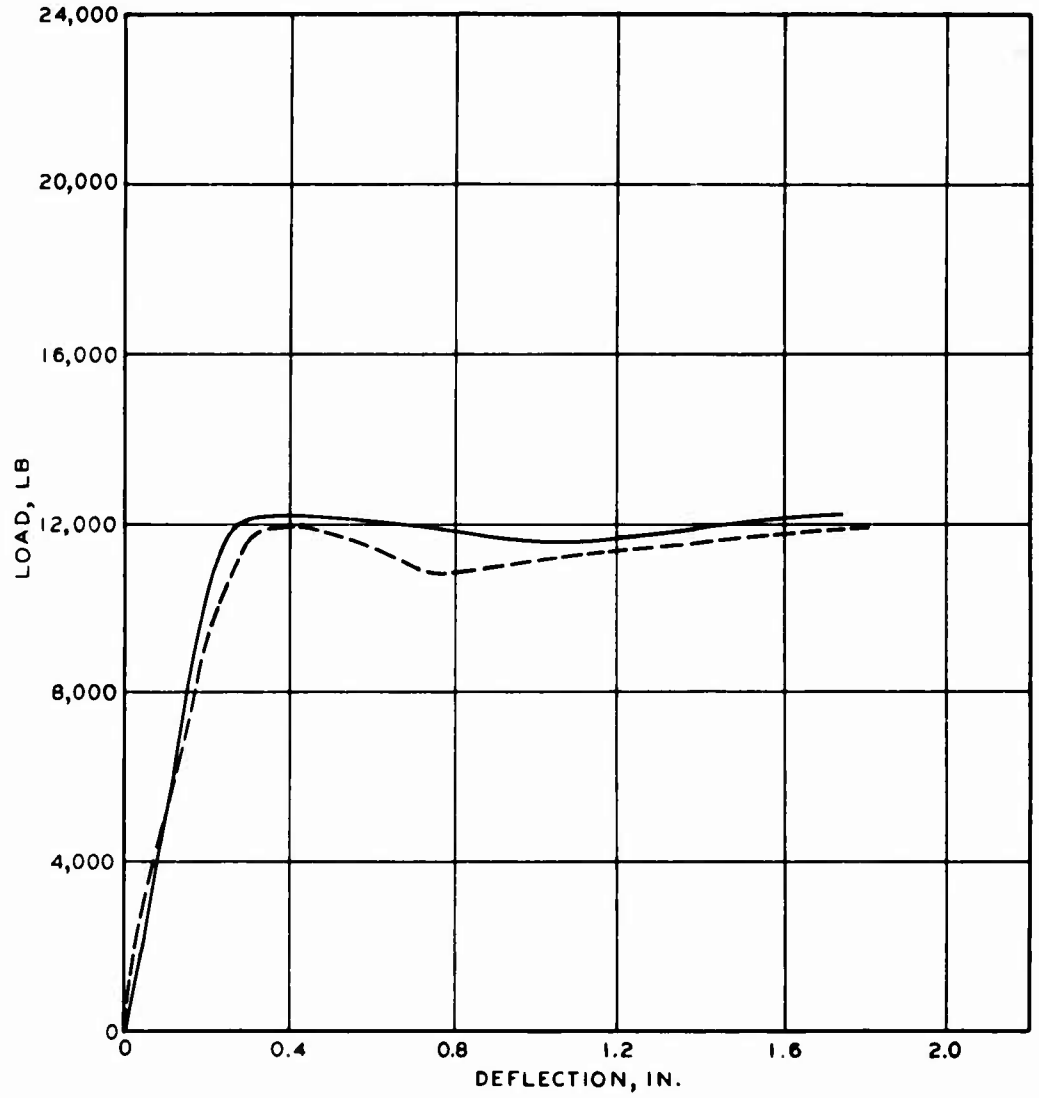

LEGEND

COMPUTED

MEASURED

THEORETICAL AND MEASURED MIDSPAN DEFLECTIONS

BEAM C-1

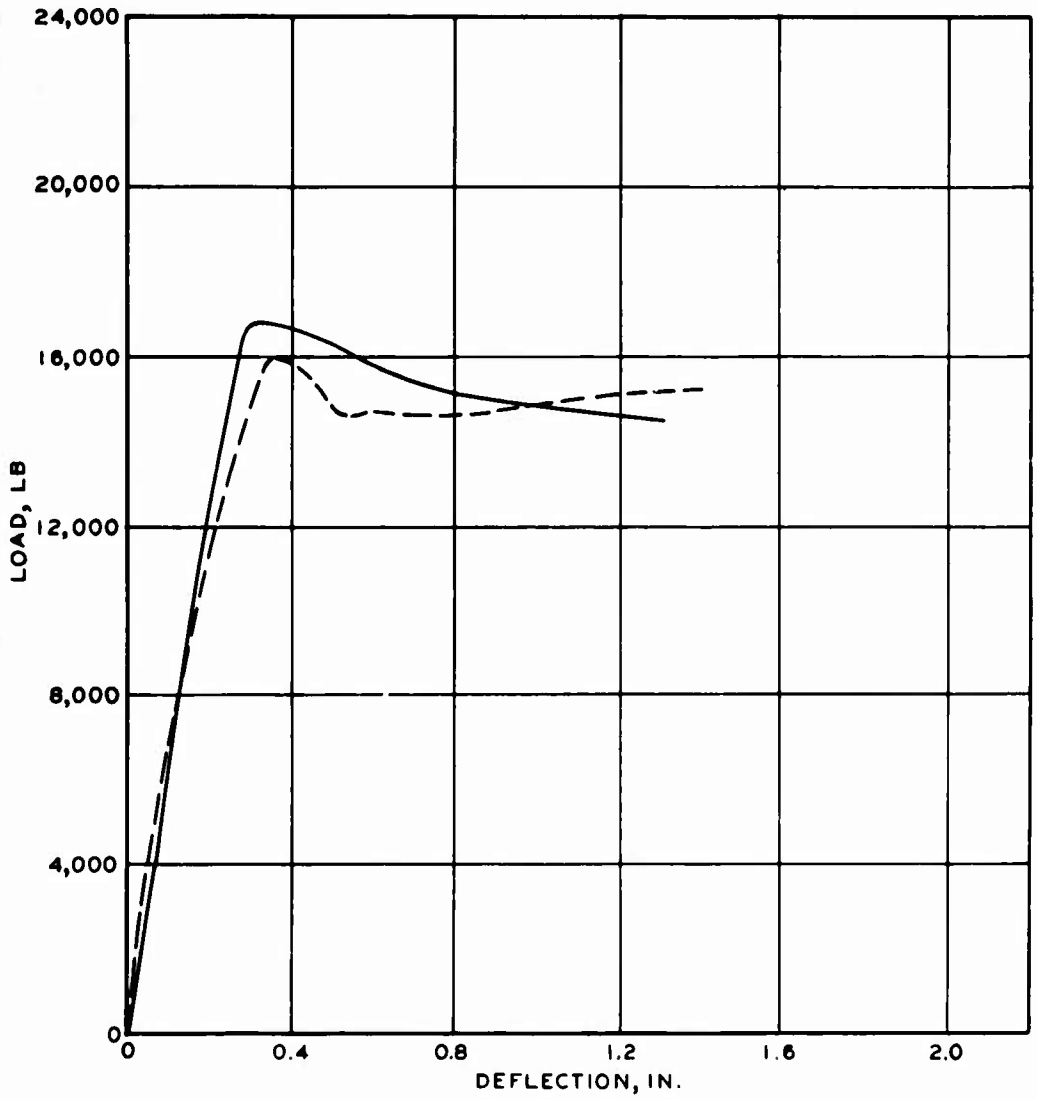

LEGEND

COMPUTED

MEASURED

THEORETICAL AND MEASURED MIDSPAN DEFLECTIONS

BEAM C-2

PLATE 40

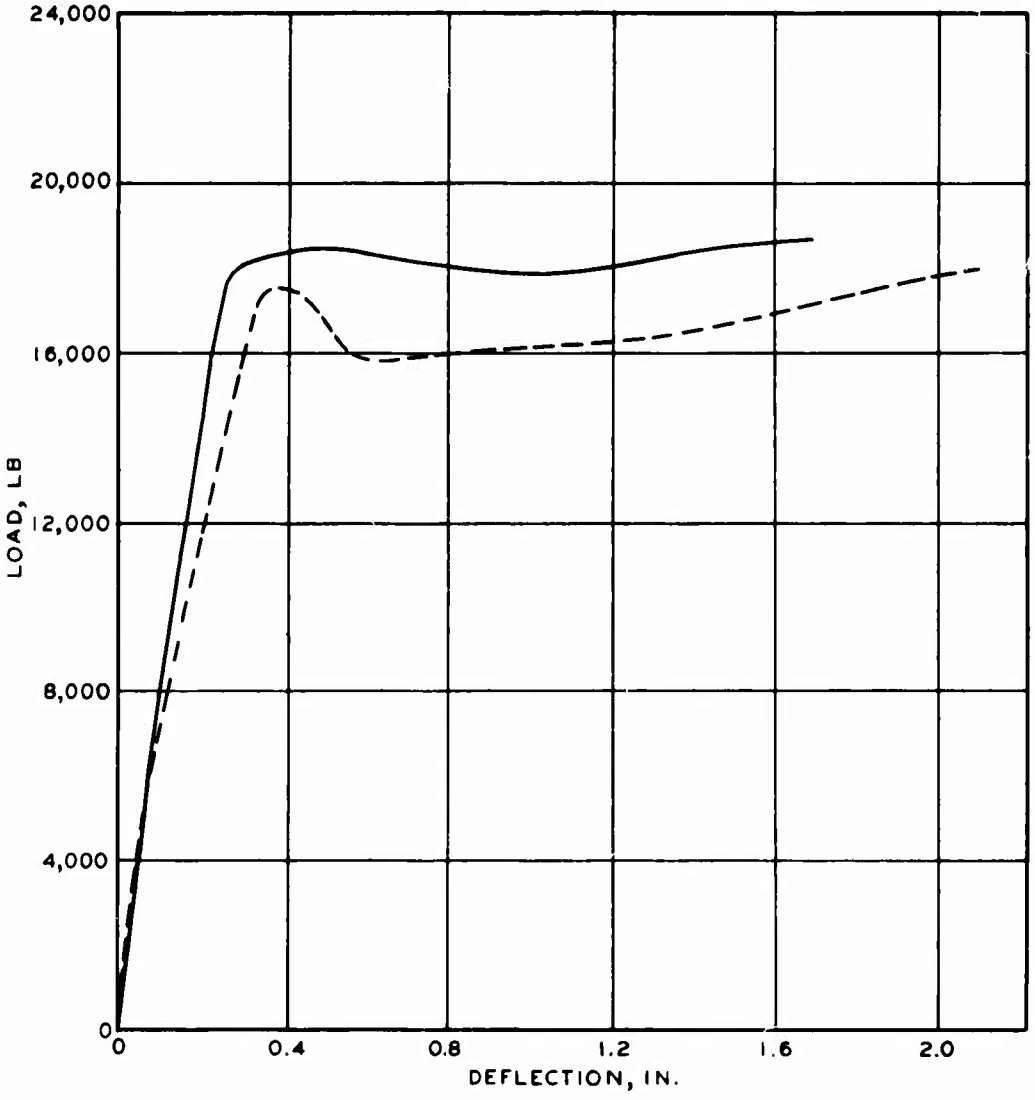

LEGEND

——— COMPUTED

– – – – MEASURED

THEORETICAL AND MEASURED MIDSPAN DEFLECTIONS

BEAM C-3

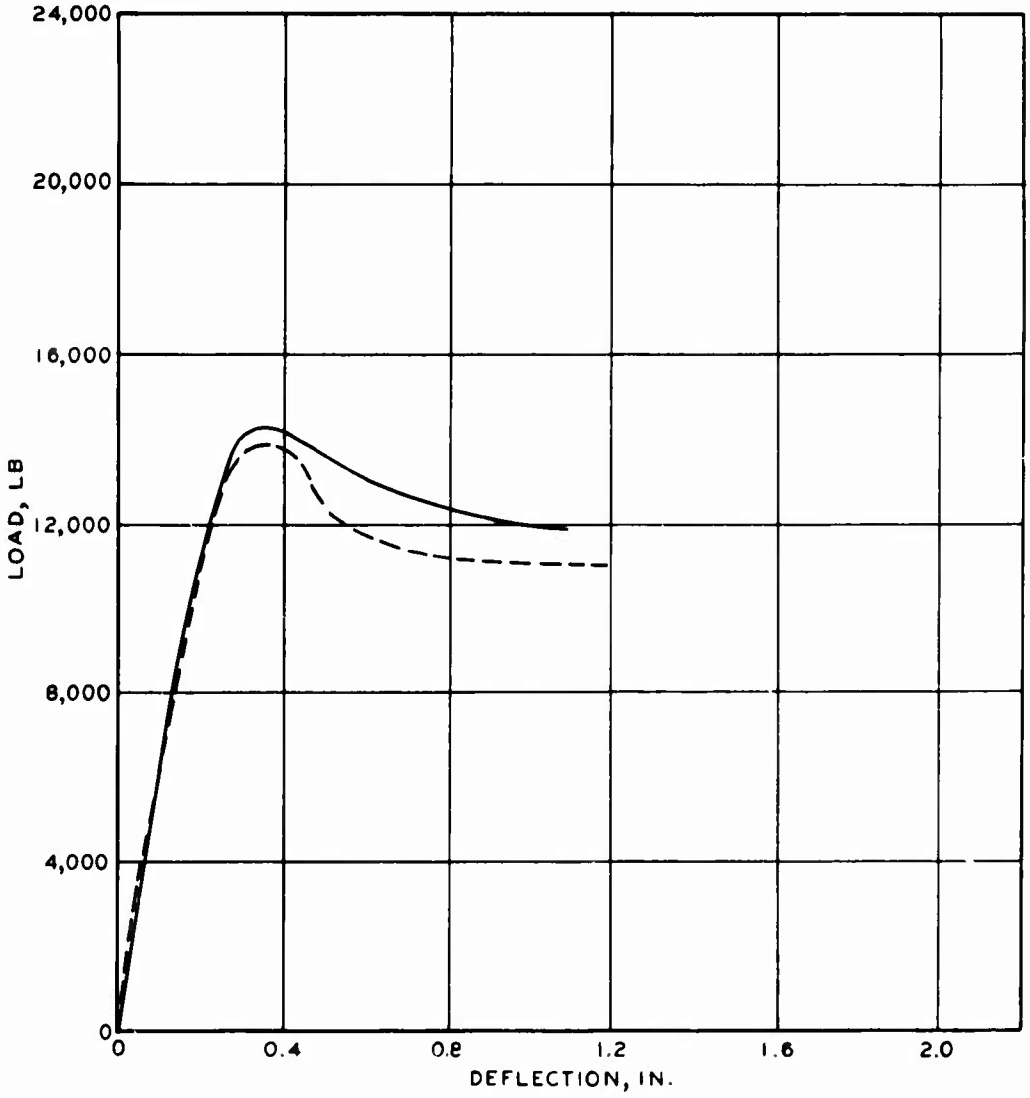

LEGEND

——— COMPUTED

– – – – MEASURED

THEORETICAL AND MEASURED MIDSPAN DEFLECTIONS

BEAM C-4

PLATE 42

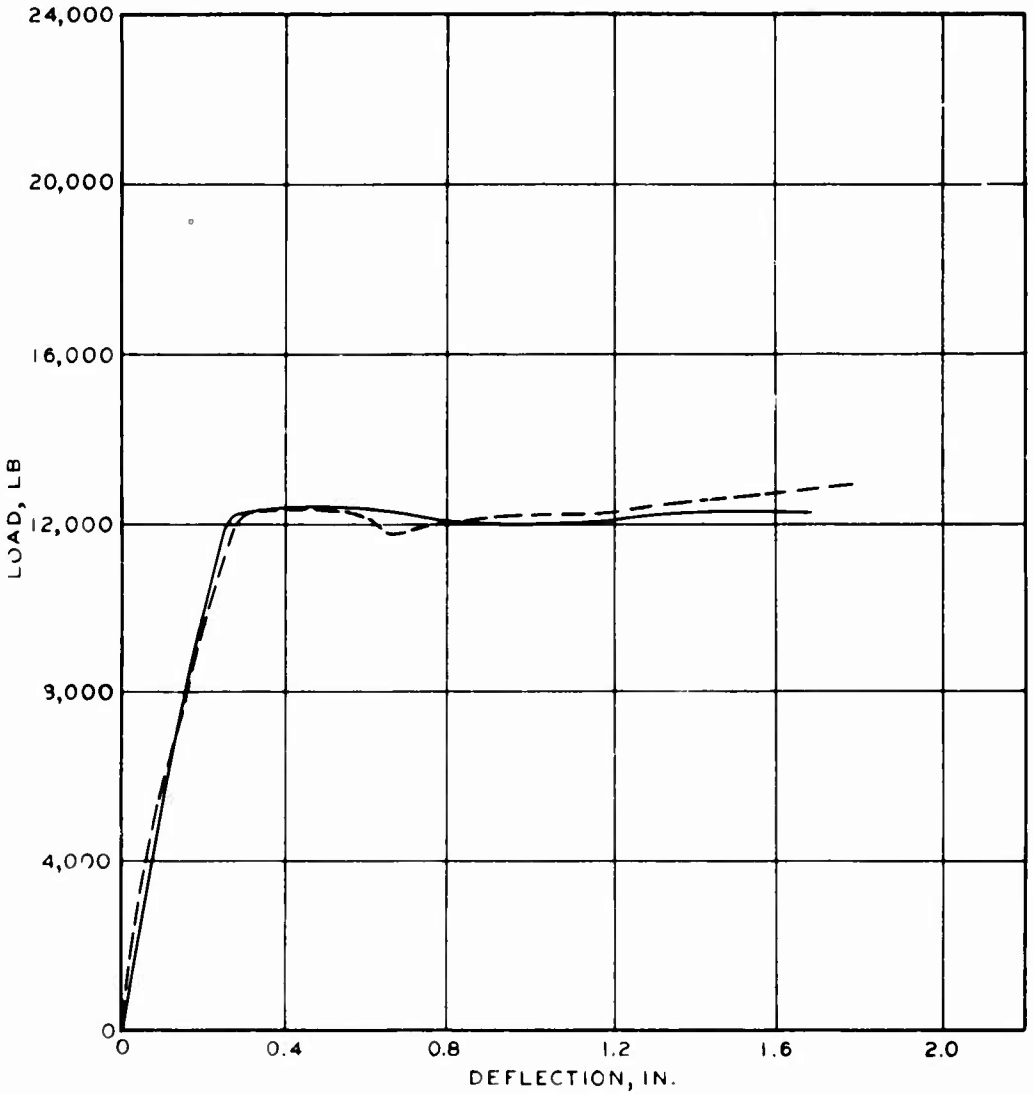

LEGEND

——— COMPUTED

– – – – MEASURED

THEORETICAL AND MEASURED MIDSPAN DEFLECTIONS

BEAM D-1

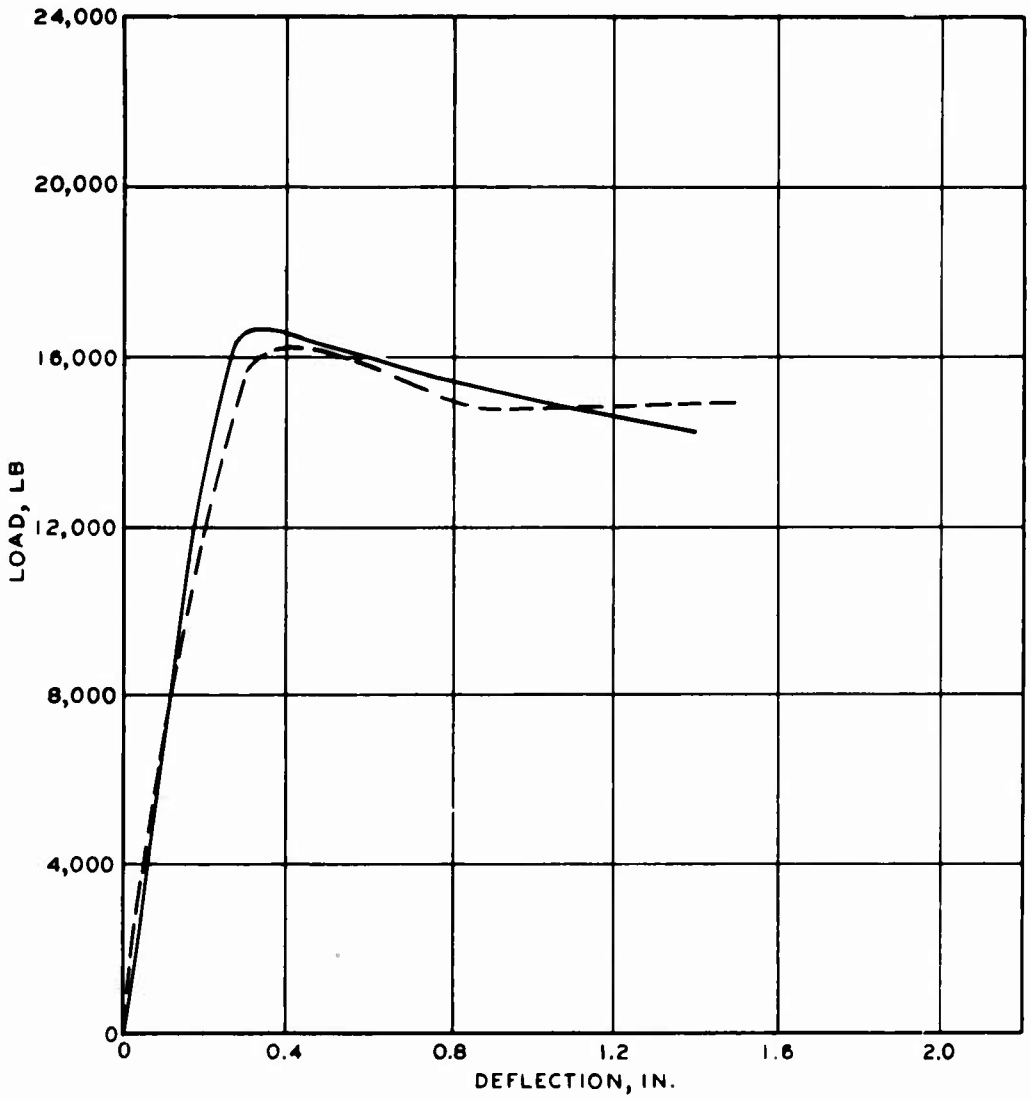

LEGEND

——— COMPUTED

– – – – MEASURED

THEORETICAL AND MEASURED MIDSPAN DEFLECTIONS

BEAM D-2A

PLATE 44

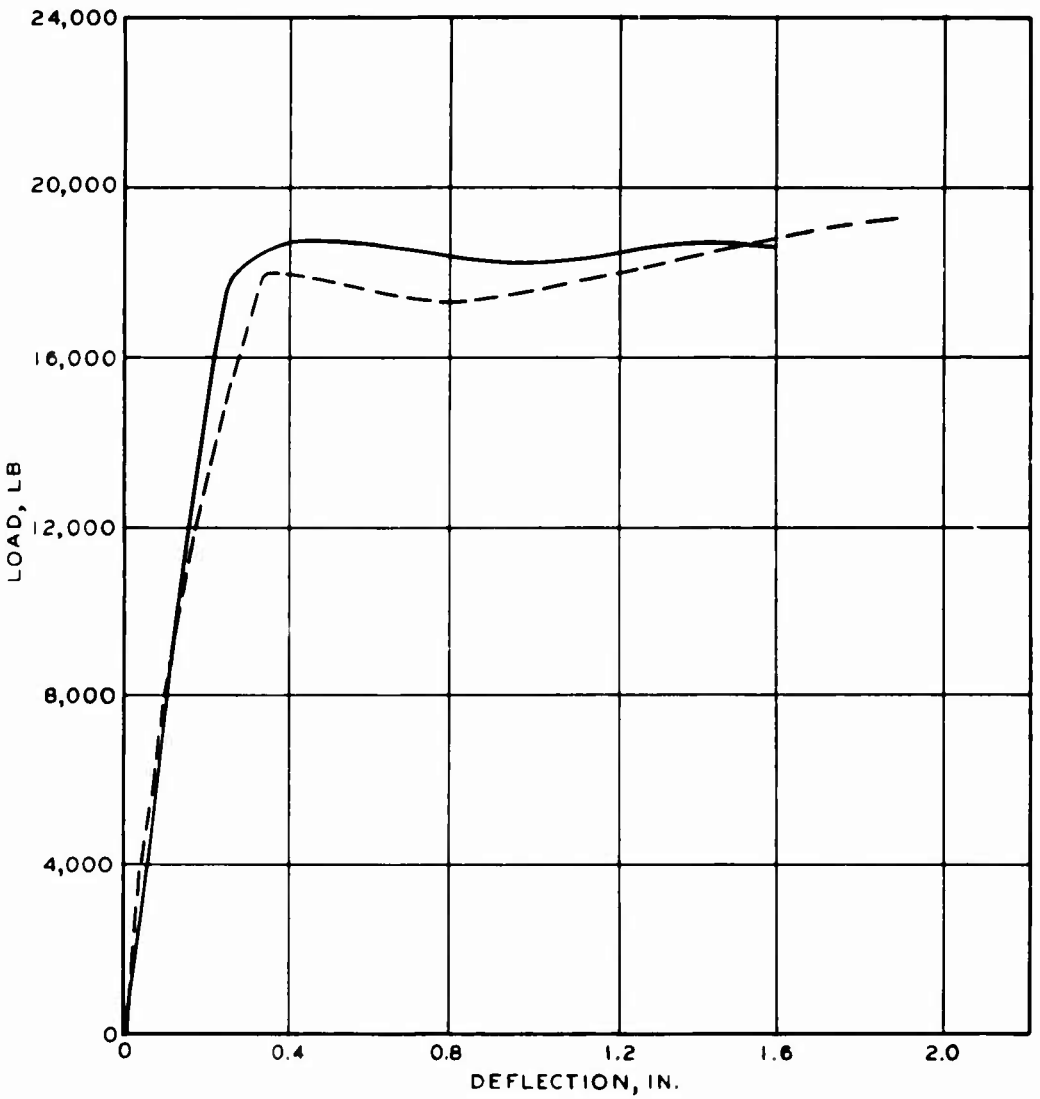

LEGEND

——— COMPUTED

– – – – MEASURED

THEORETICAL AND MEASURED MIDSPAN DEFLECTIONS

BEAM D-3

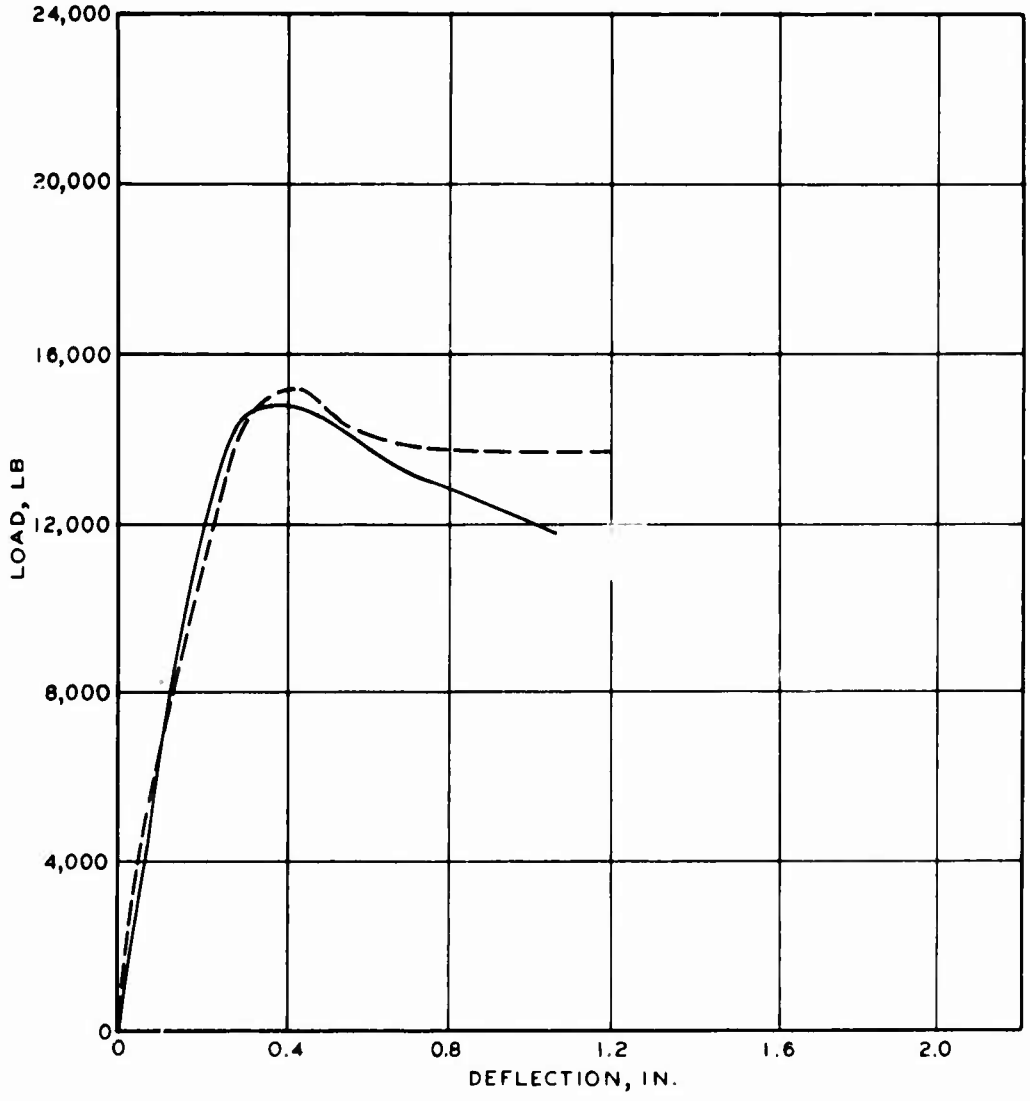

LEGEND

——— COMPUTED

– – – – MEASURED

THEORETICAL AND MEASURED MIDSPAN DEFLECTIONS

BEAM D-4

PLATE 46

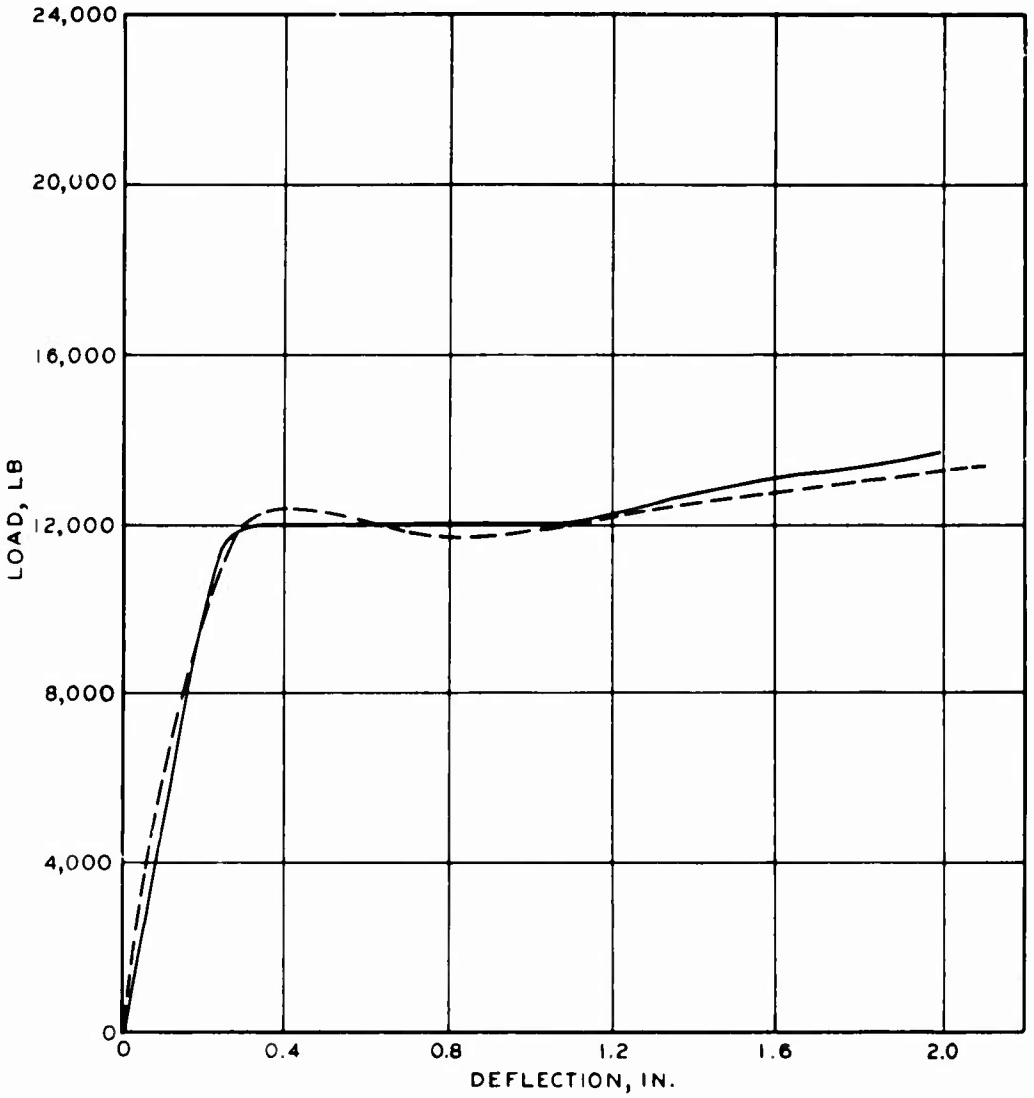

LEGEND

——— COMPUTED

– – – – MEASURED

THEORETICAL AND MEASURED MIDSPAN DEFLECTIONS

BEAM E-1

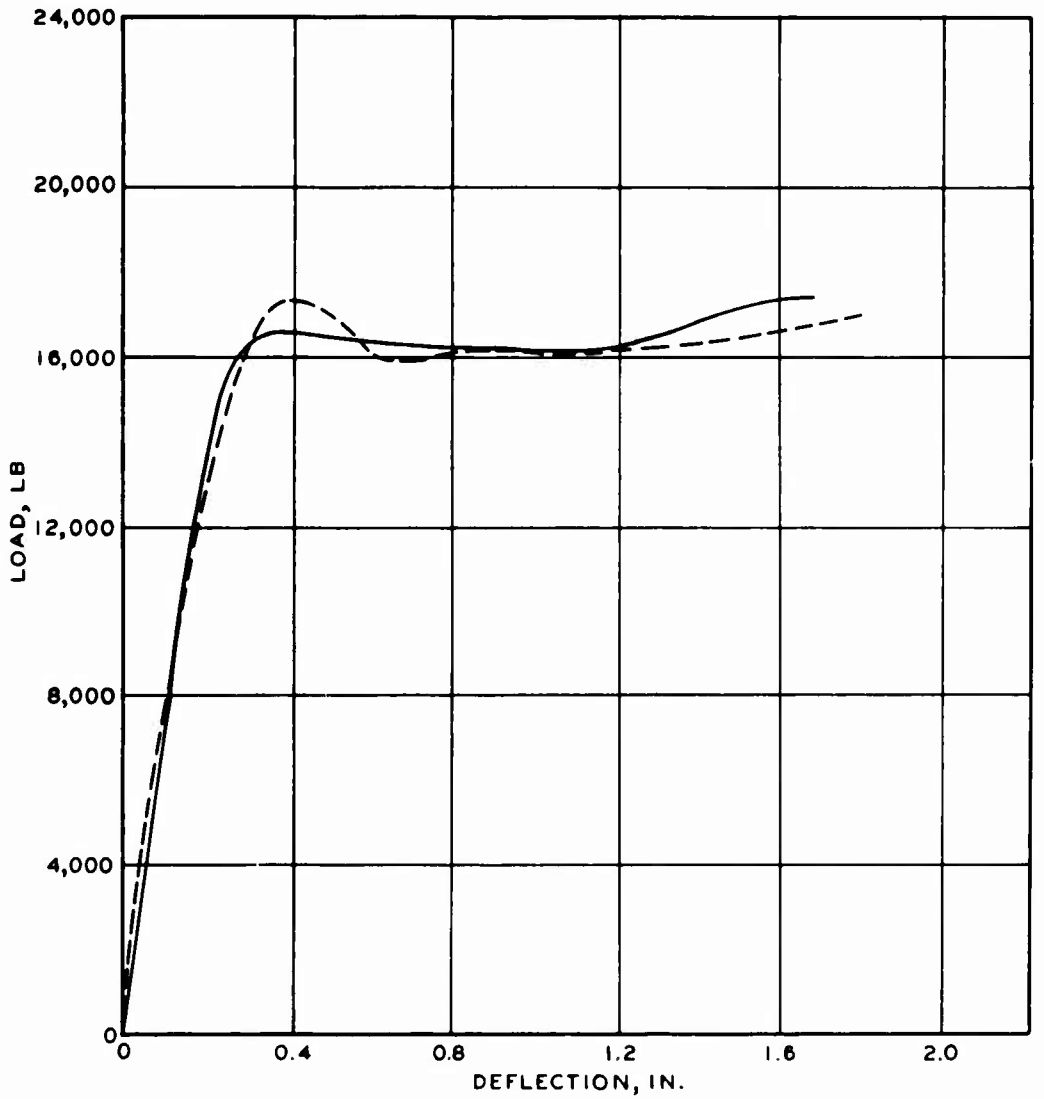

LEGEND

——— COMPUTED

– – – – MEASURED

THEORETICAL AND MEASURED MIDSPAN DEFLECTIONS

BEAM E-2A

PLATE 48

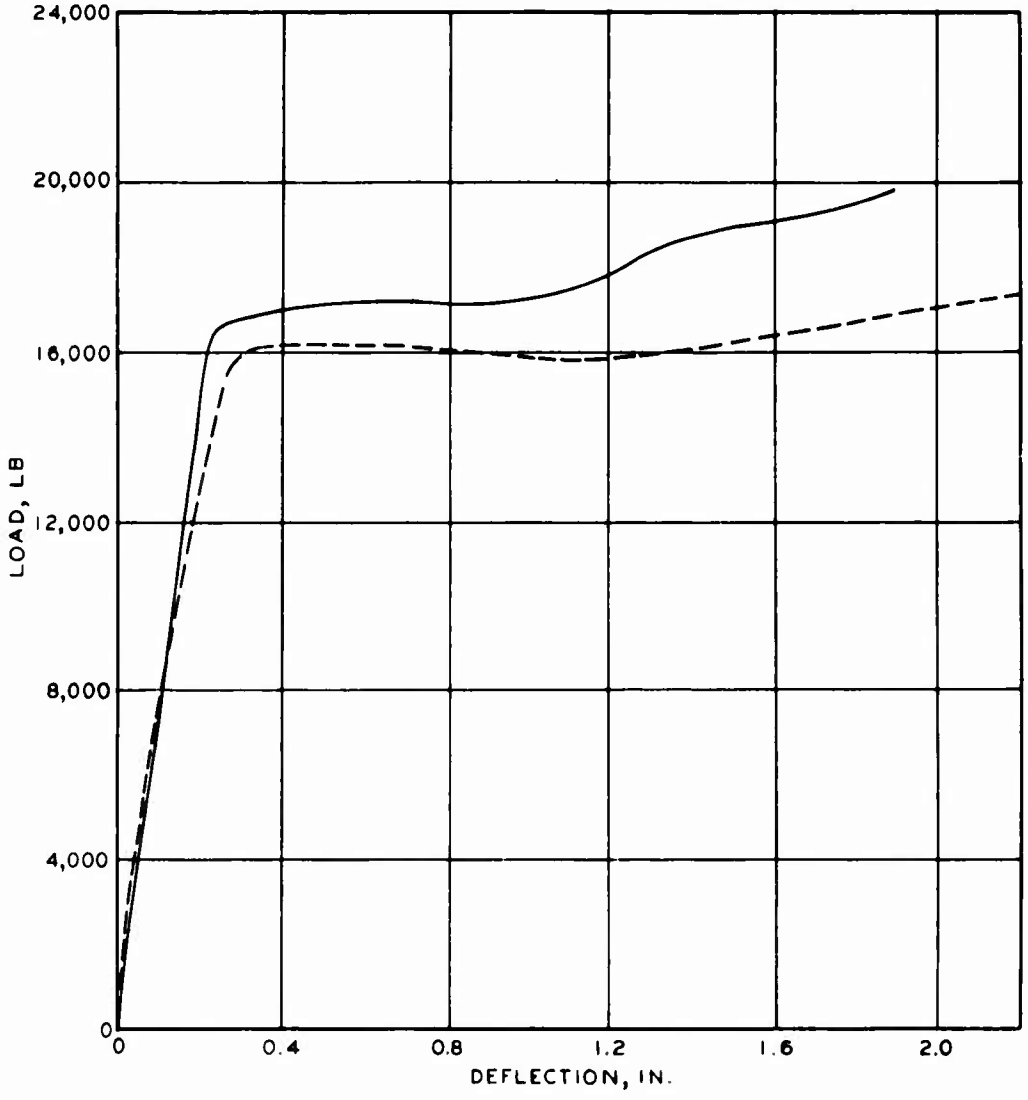

LEGEND

——— COMPUTED

– – – – MEASURED

THEORETICAL AND MEASURED MIDSPAN DEFLECTIONS

BEAM E-3

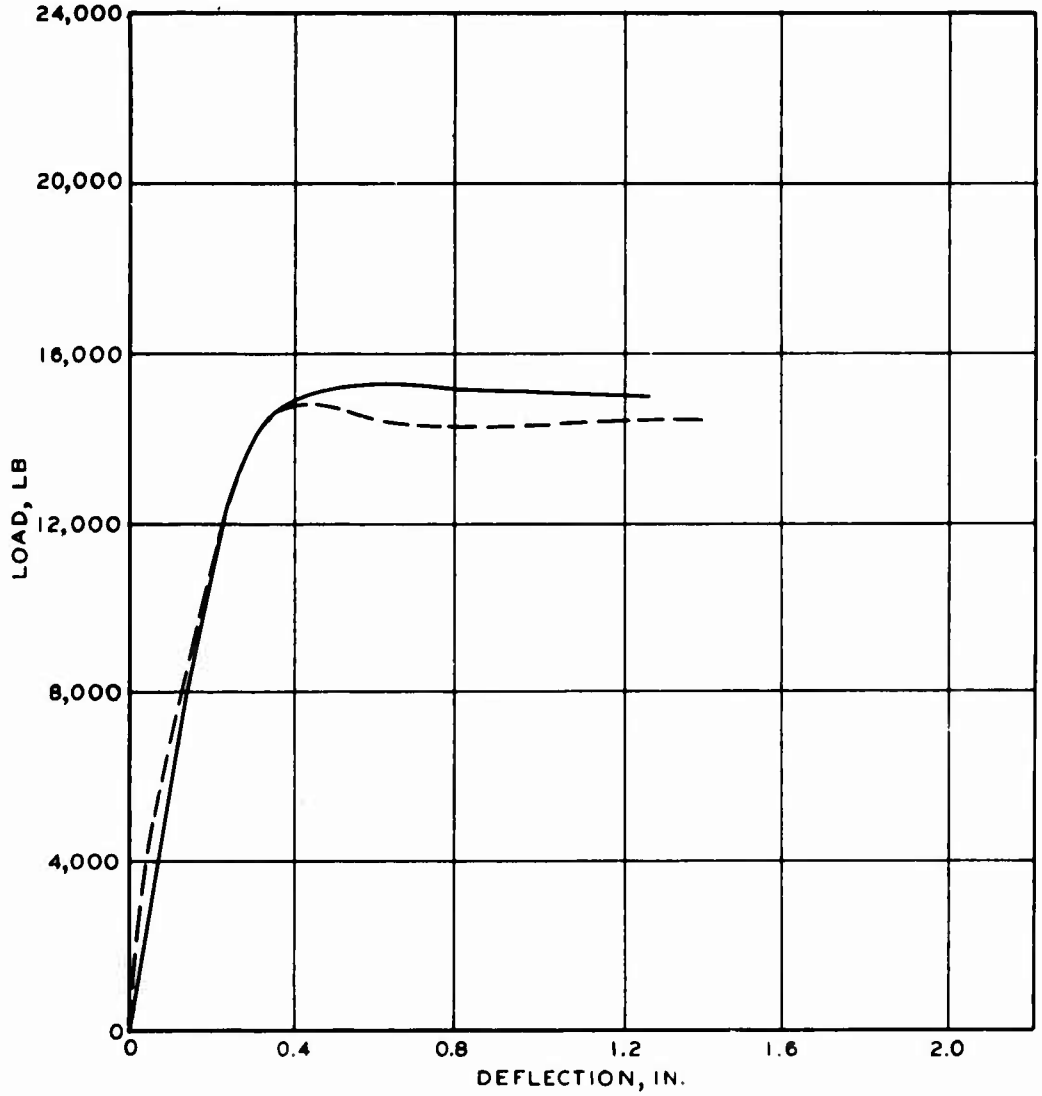

LEGEND

COMPUTED

MEASURED

THEORETICAL AND MEASURED MIDSPAN DEFLECTIONS

BEAM E-4

PLATE 50

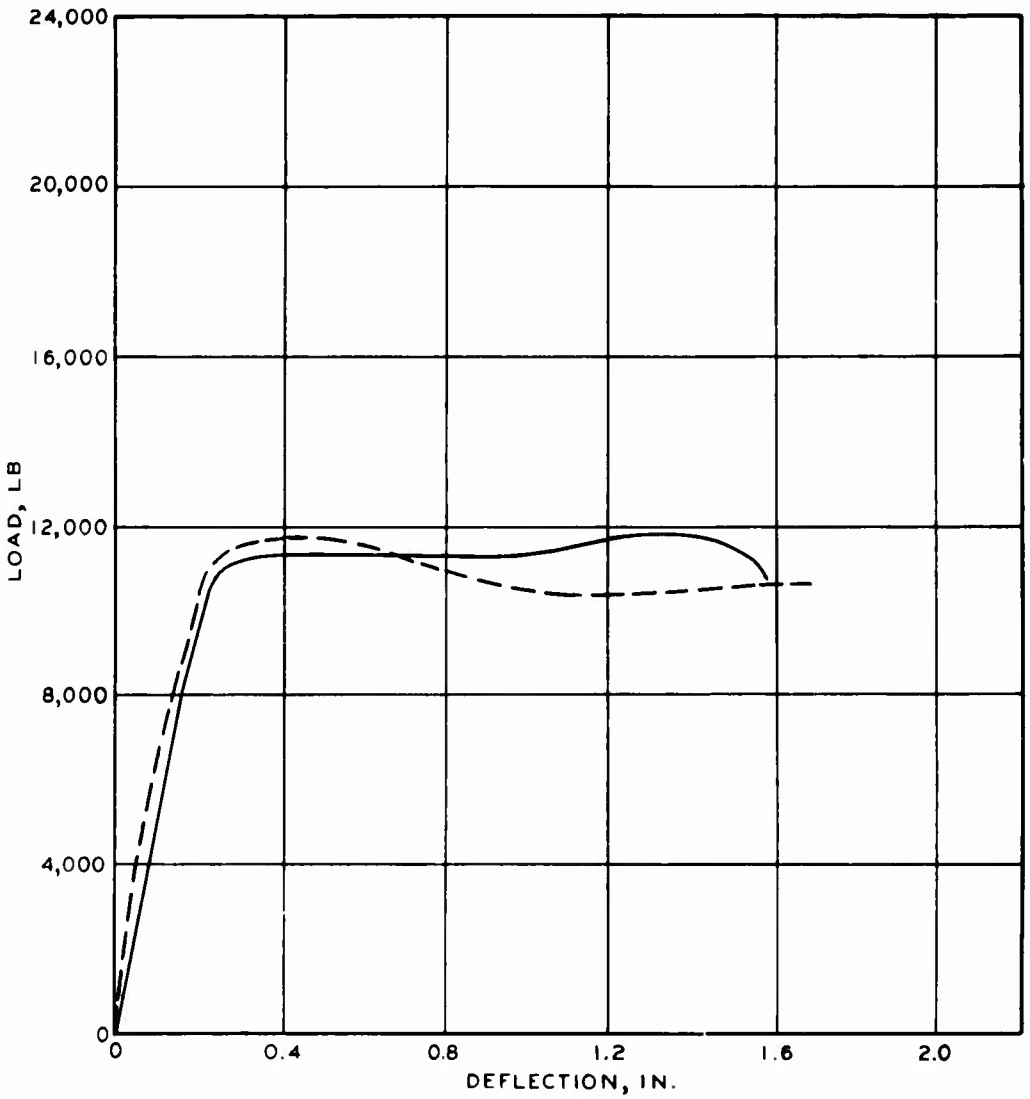

LEGEND

——— COMPUTED

– – – – MEASURED

THEORETICAL AND MEASURED MIDSPAN DEFLECTIONS

BEAM F-1

PLATE 51

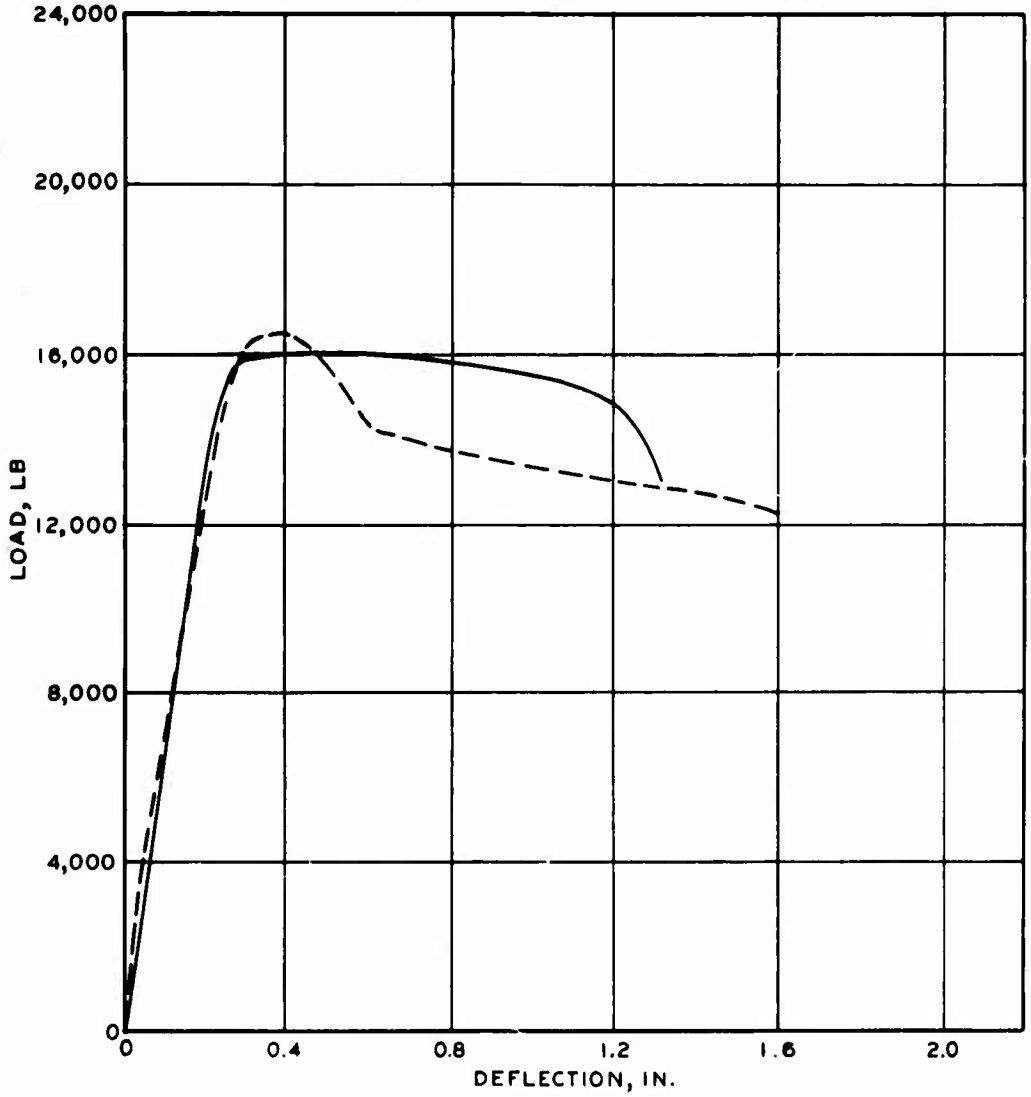

LEGEND

COMPUTED

MEASURED

THEORETICAL AND MEASURED MIDSPAN DEFLECTIONS

BEAM F-2

PLATE 52

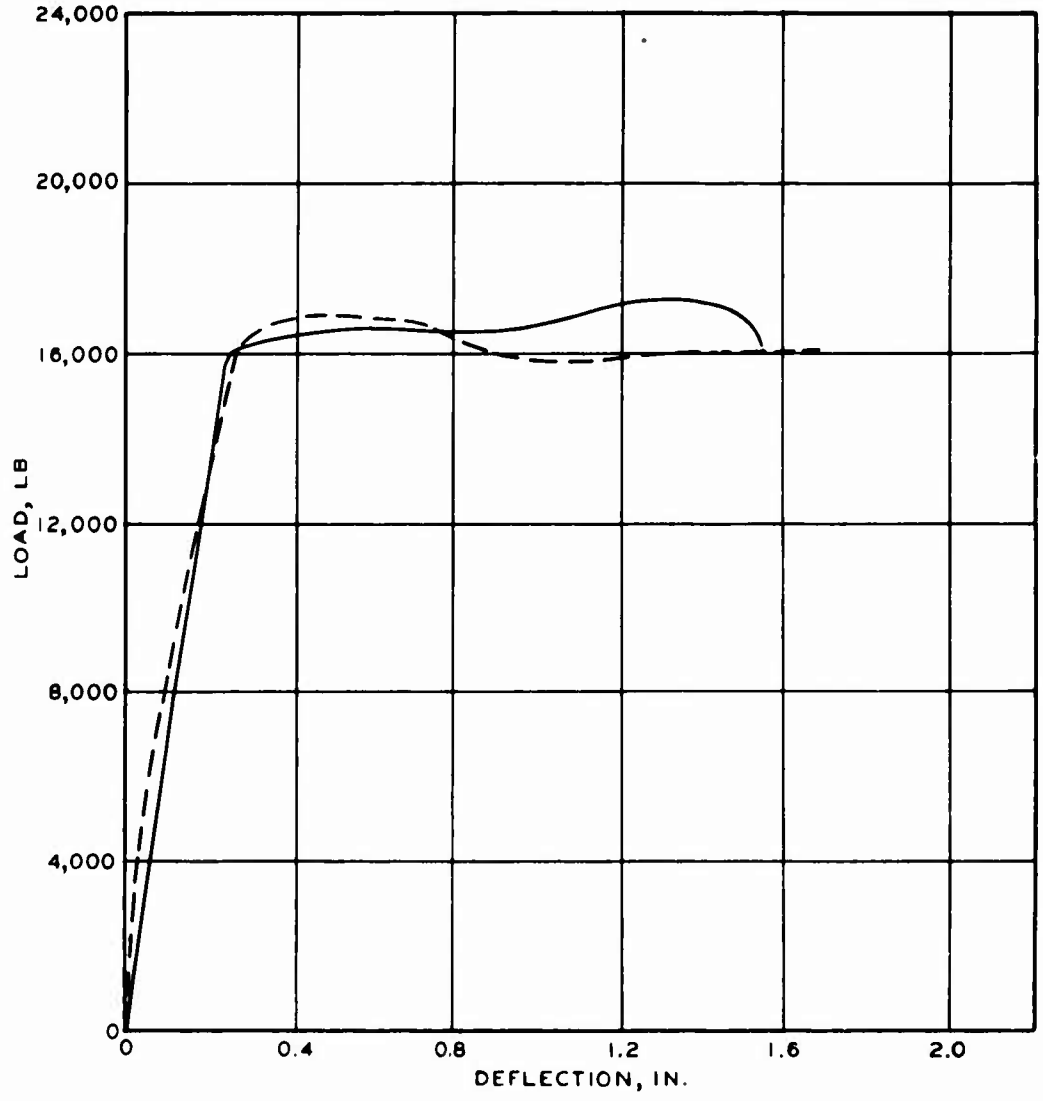

LEGEND

——— COMPUTED

– – – – MEASURED

THEORETICAL AND MEASURED MIDSPAN DEFLECTIONS

BEAM F-3

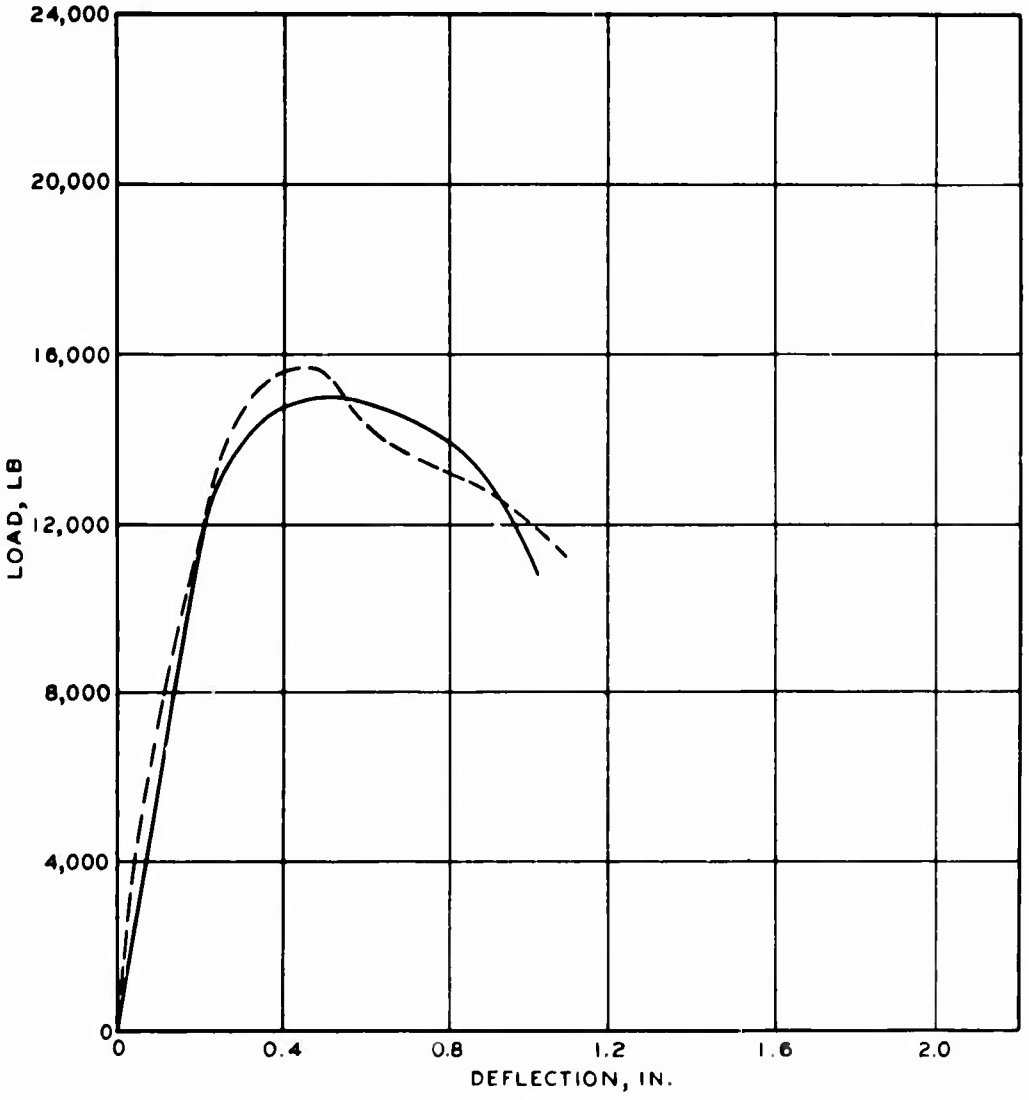

LEGEND

——— COMPUTED

– – – – MEASURED

THEORETICAL AND MEASURED MIDSPAN DEFLECTIONS

BEAM F-4

PLATE 54

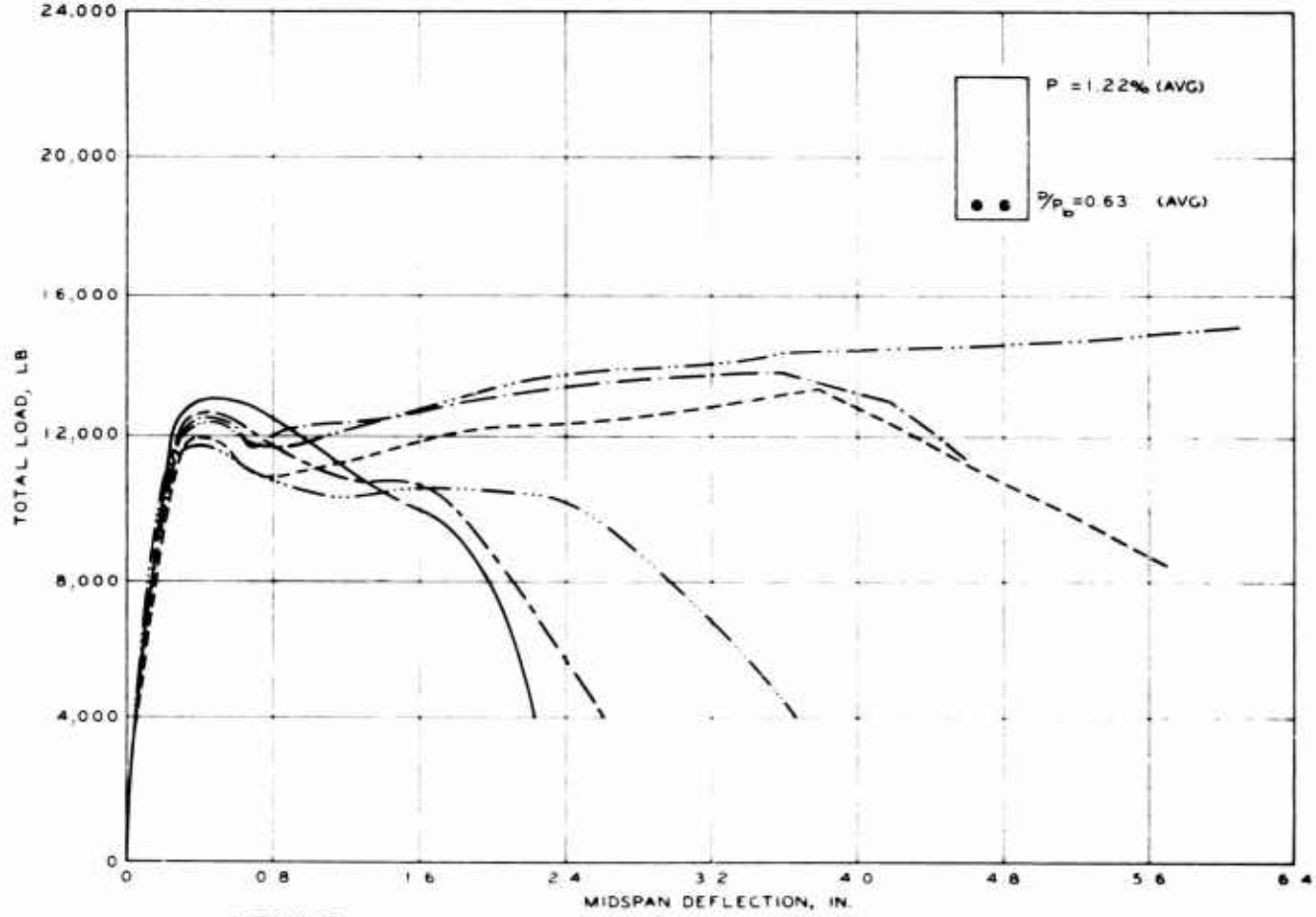

MEASURED MIDSPAN DEFLECTIONS
DESIGN 1

PLATE 55

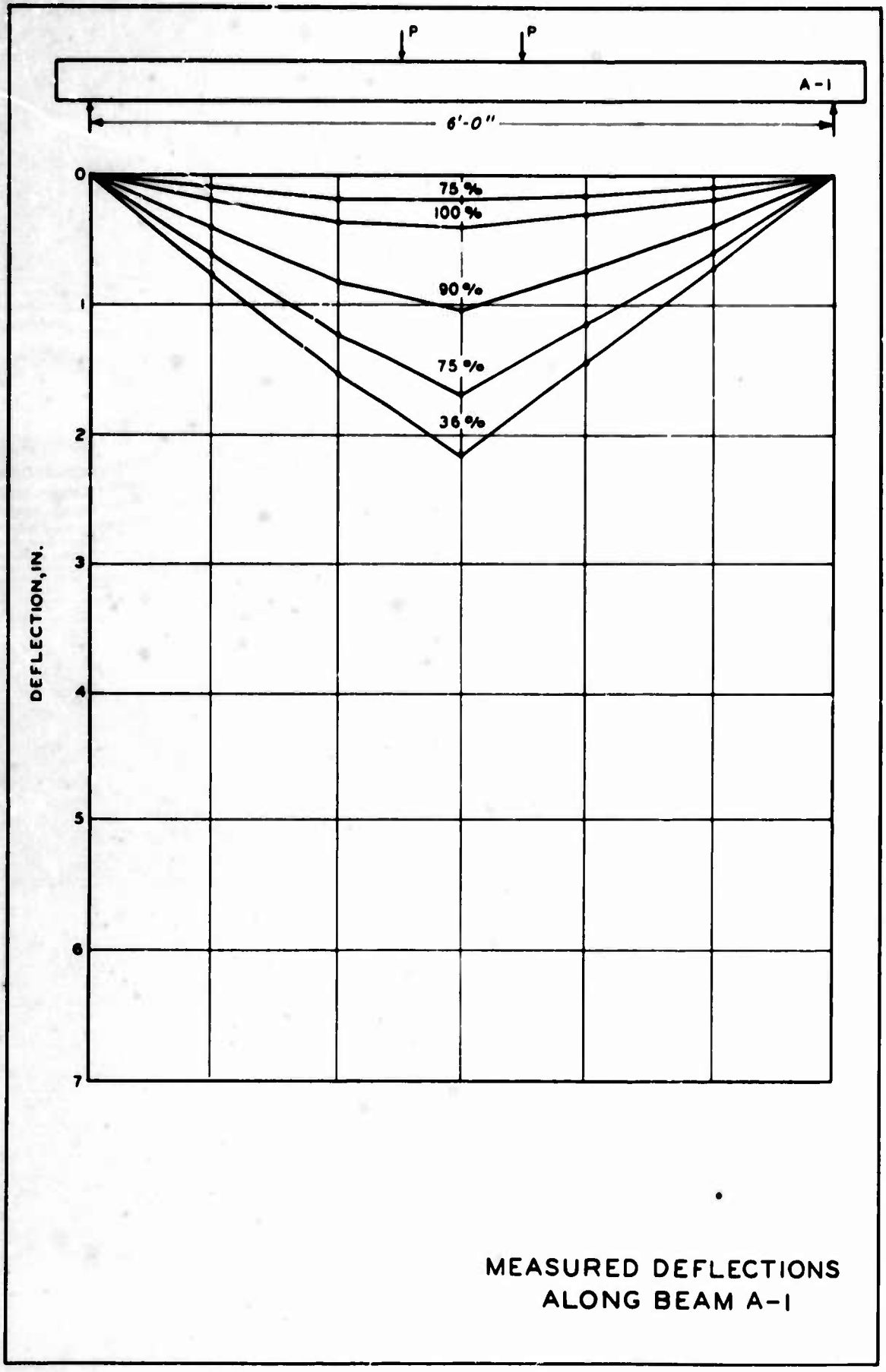

MEASURED DEFLECTIONS
ALONG BEAM A-1

PLATE 56

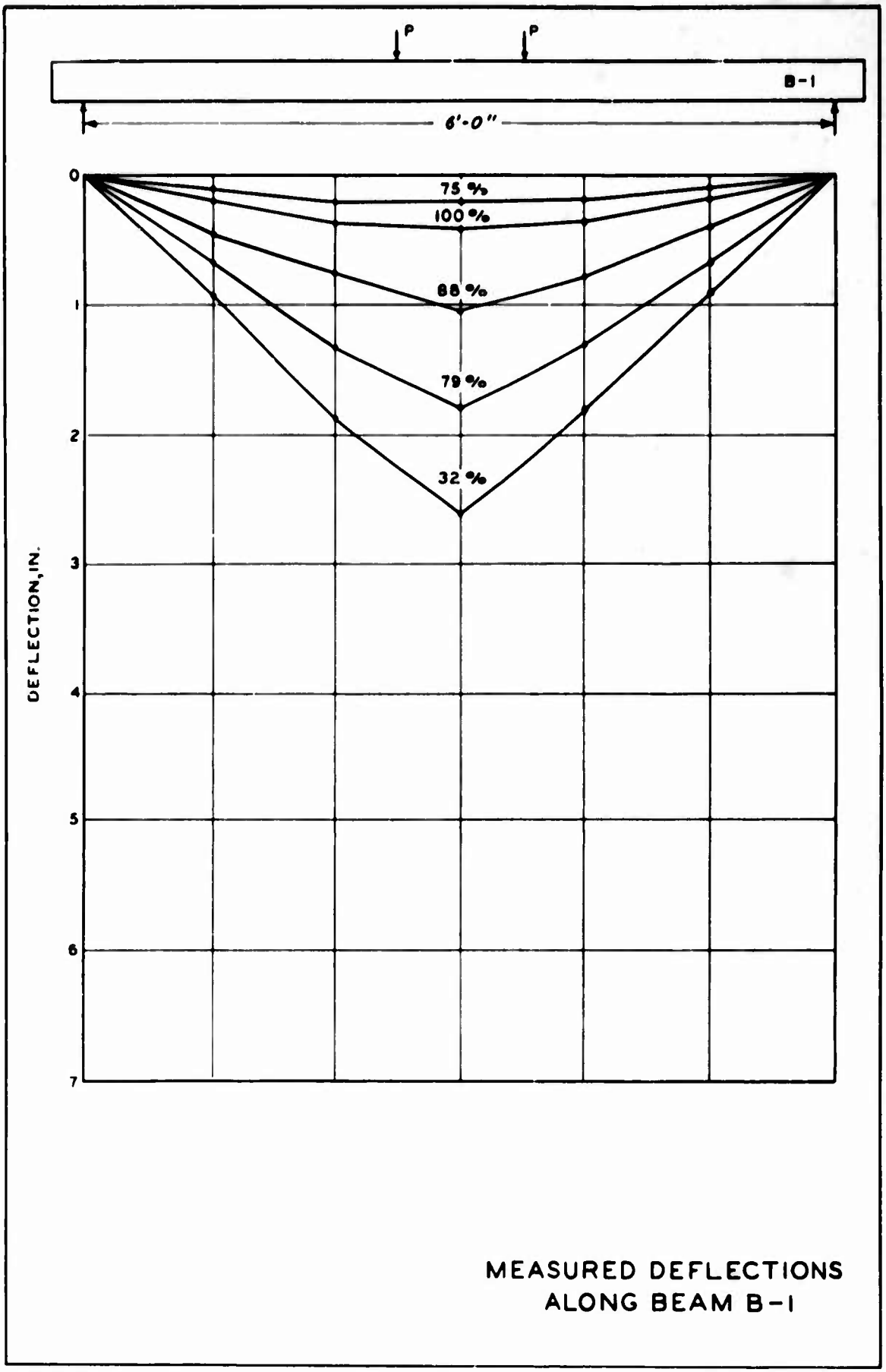

MEASURED DEFLECTIONS
ALONG BEAM B-1

PLATE 57

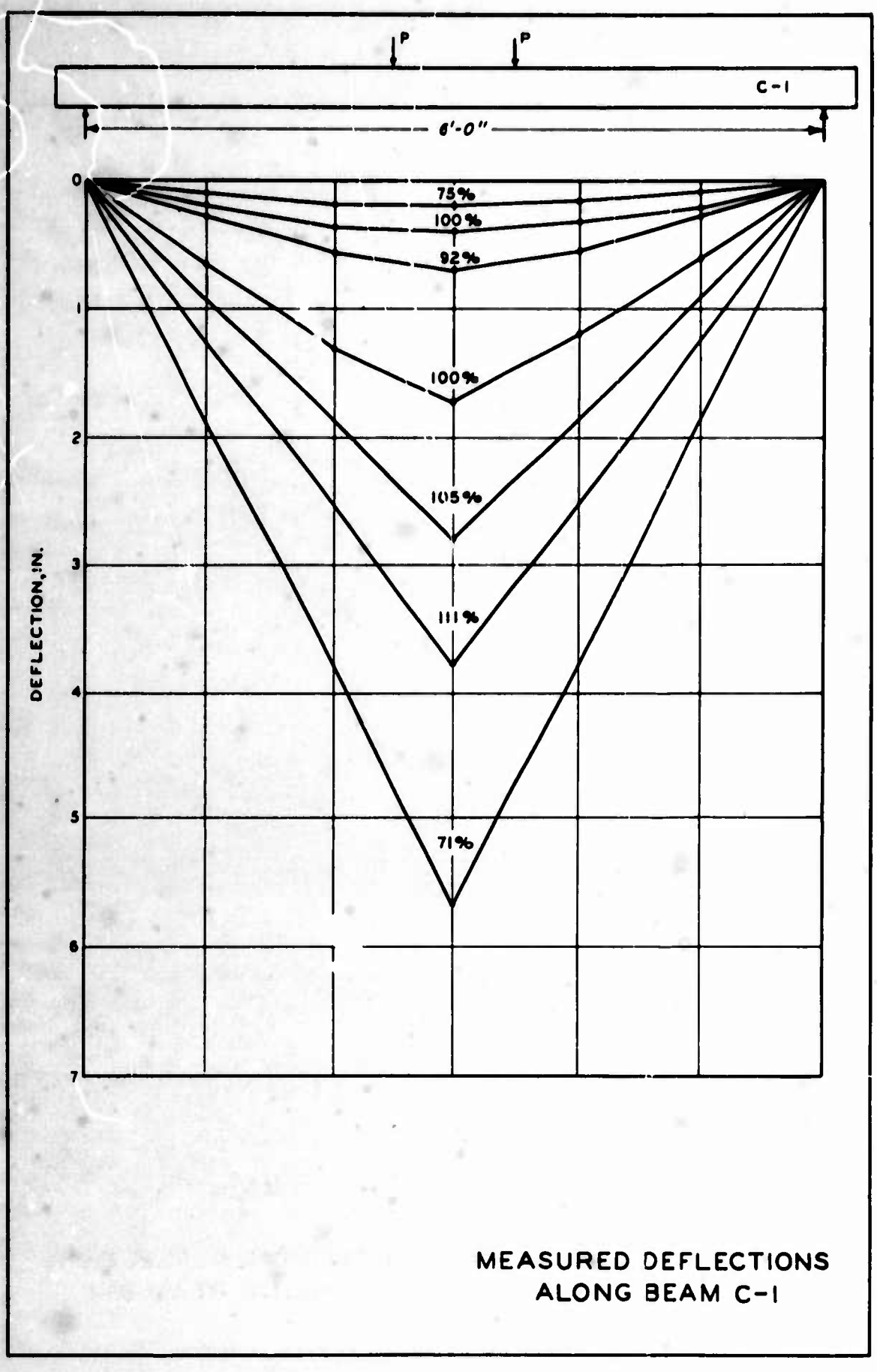

MEASURED DEFLECTIONS
ALONG BEAM C-1

PLATE 58

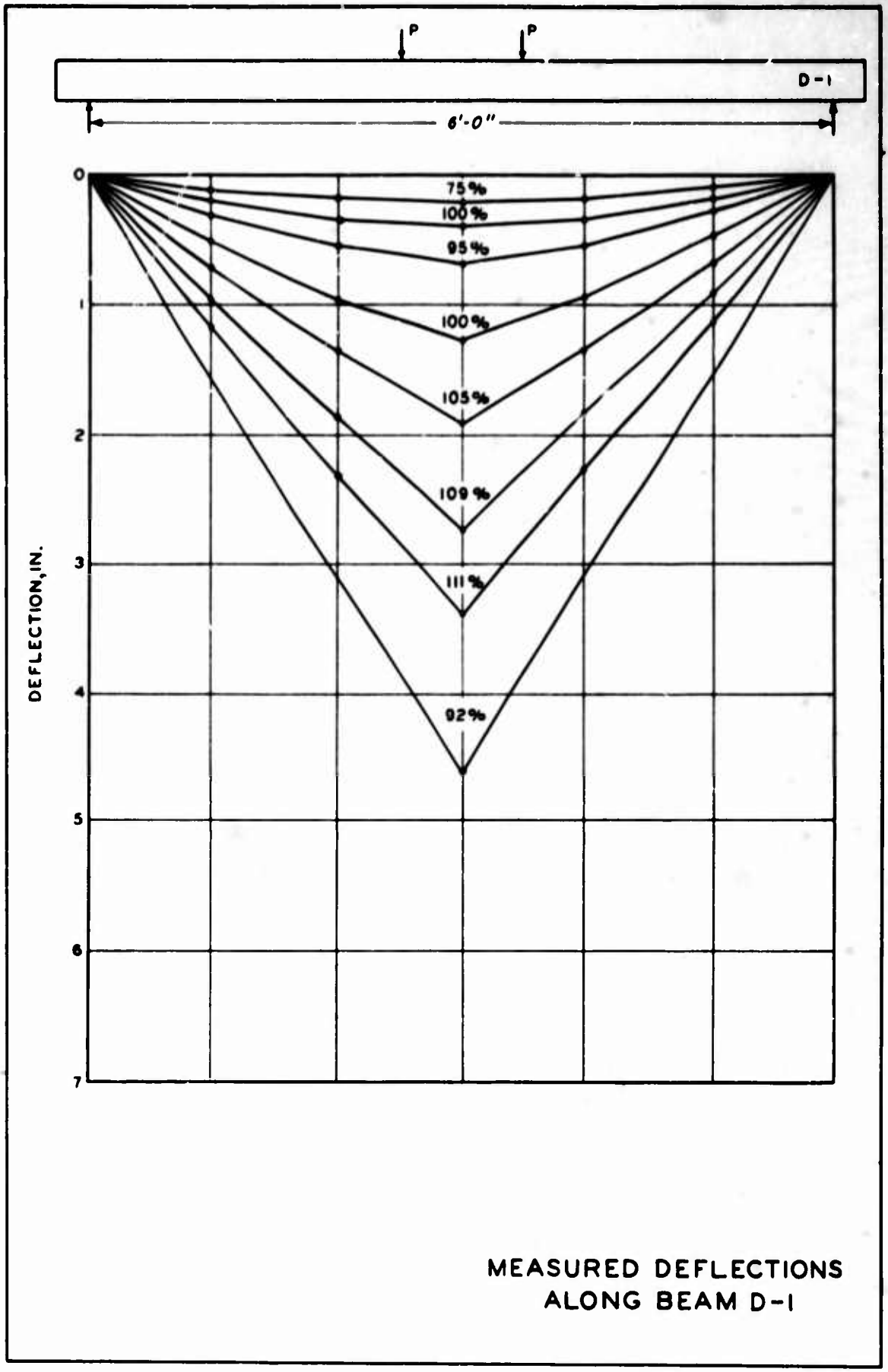

MEASURED DEFLECTIONS
ALONG BEAM D-1

PLATE 59

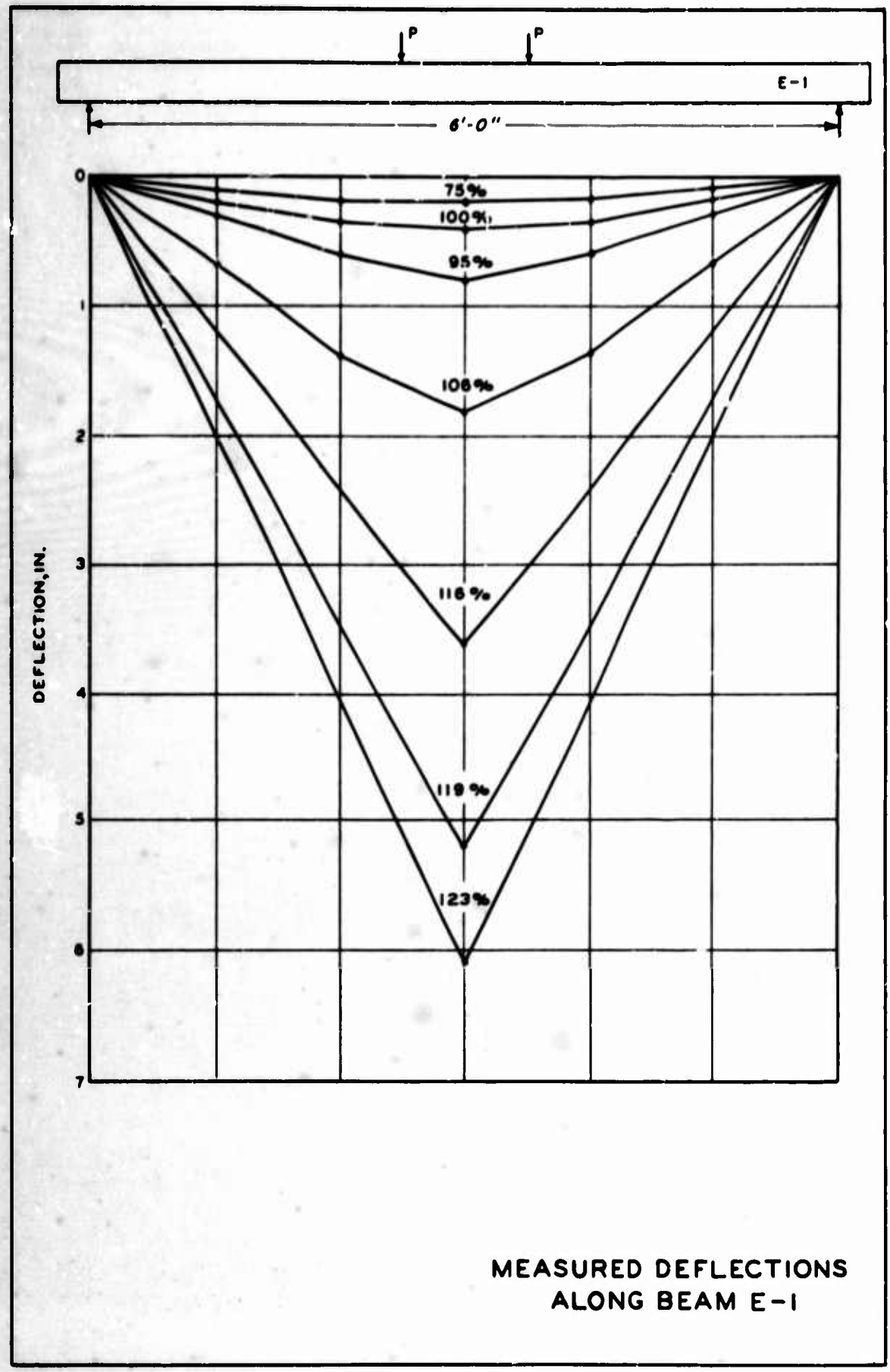

MEASURED DEFLECTIONS
ALONG BEAM E-1

PLATE 60

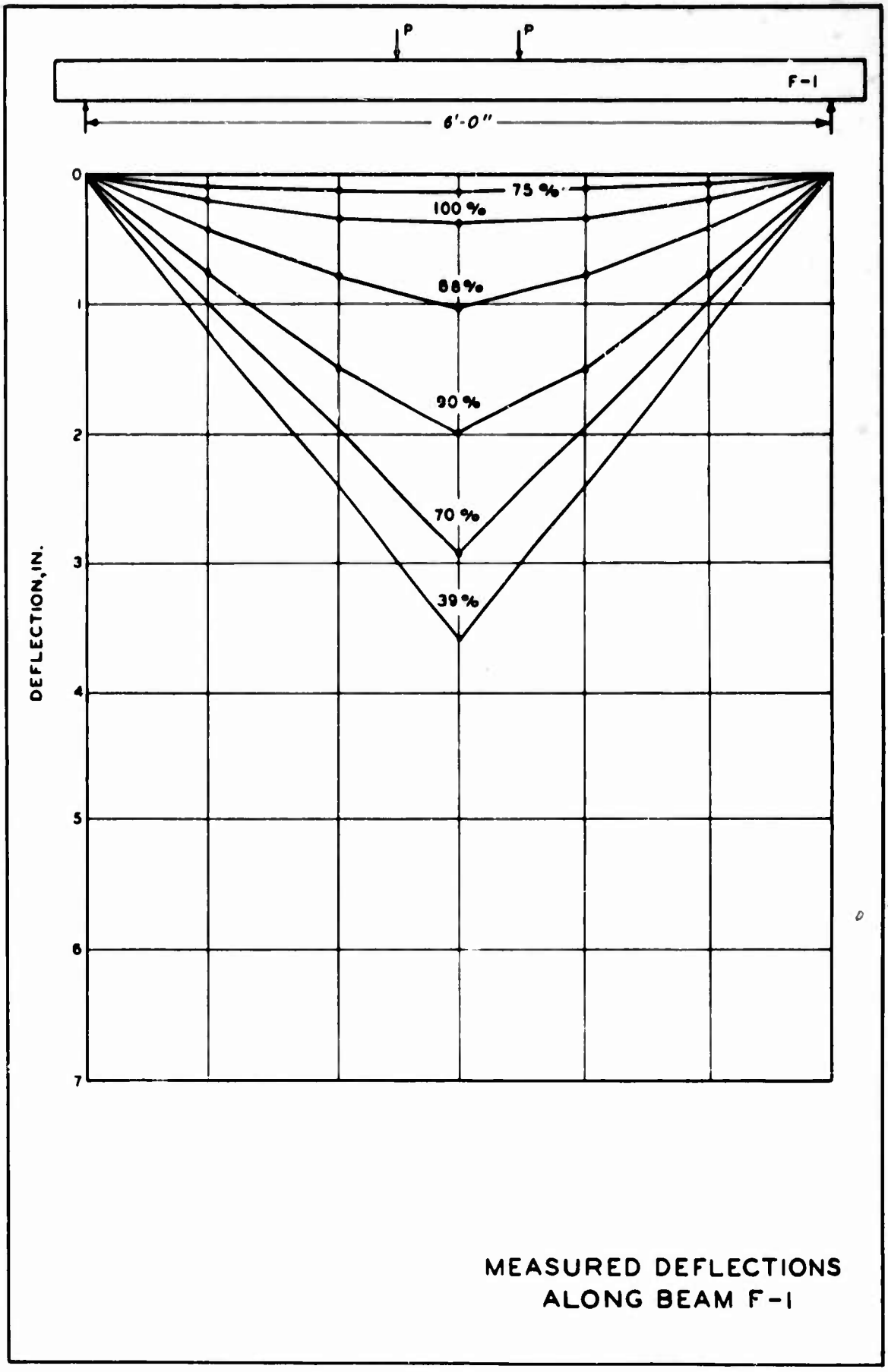

MEASURED DEFLECTIONS
ALONG BEAM F-1

PLATE 61

PLATE 62

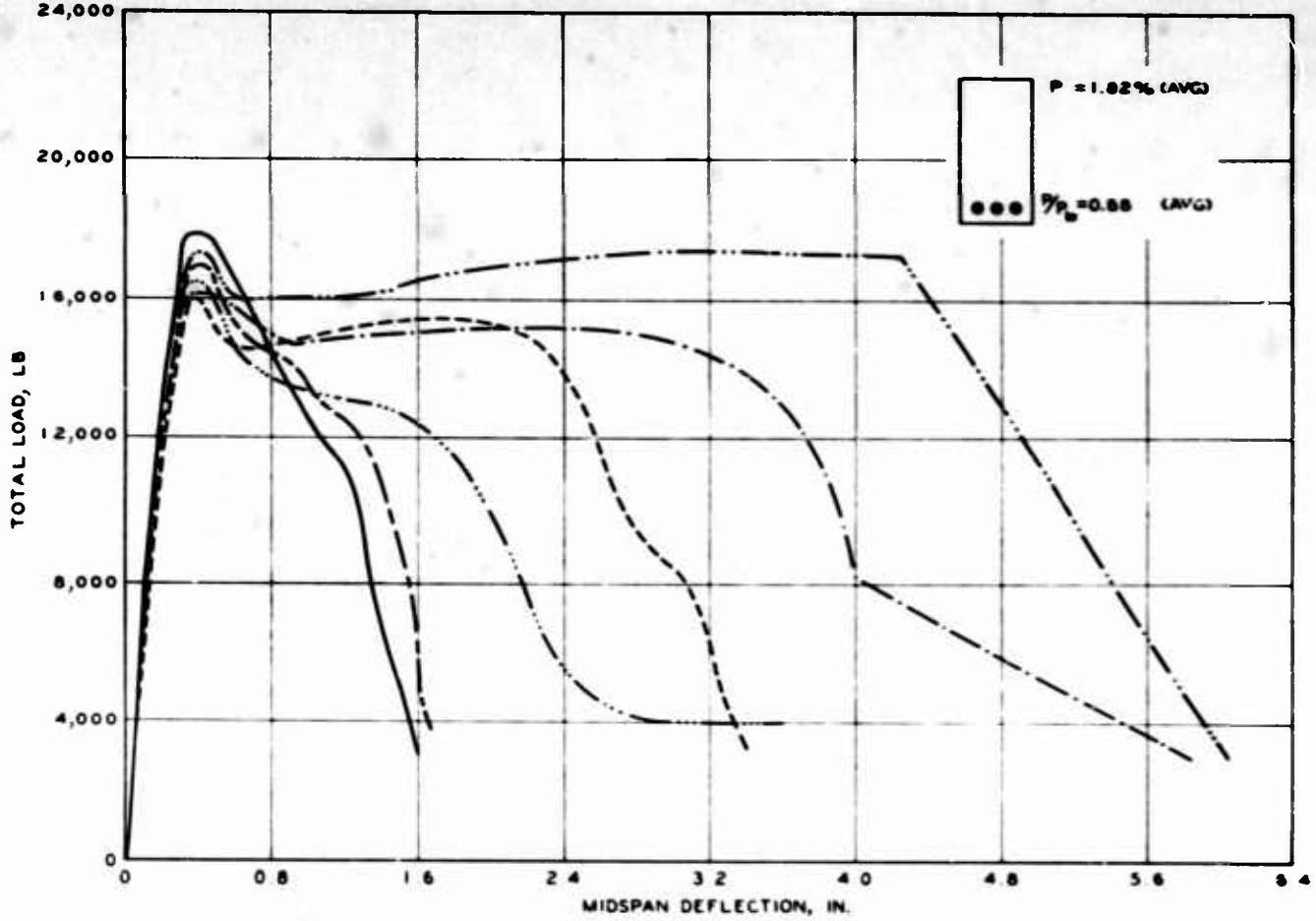

MEASURED
MIDSPAN DEFLECTIONS
DESIGN 2

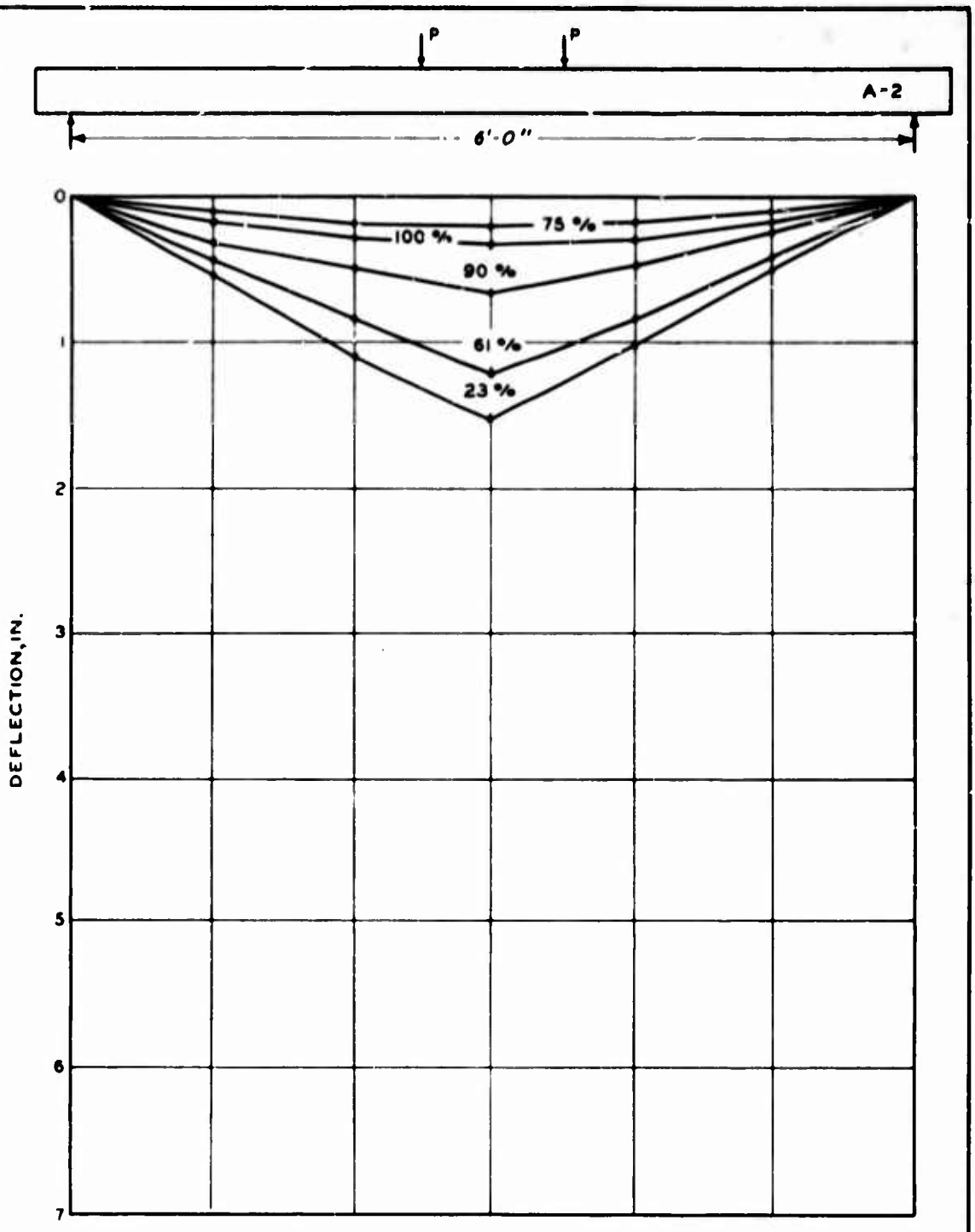

MEASURED DEFLECTIONS
ALONG BEAM A-2

PLATE 63

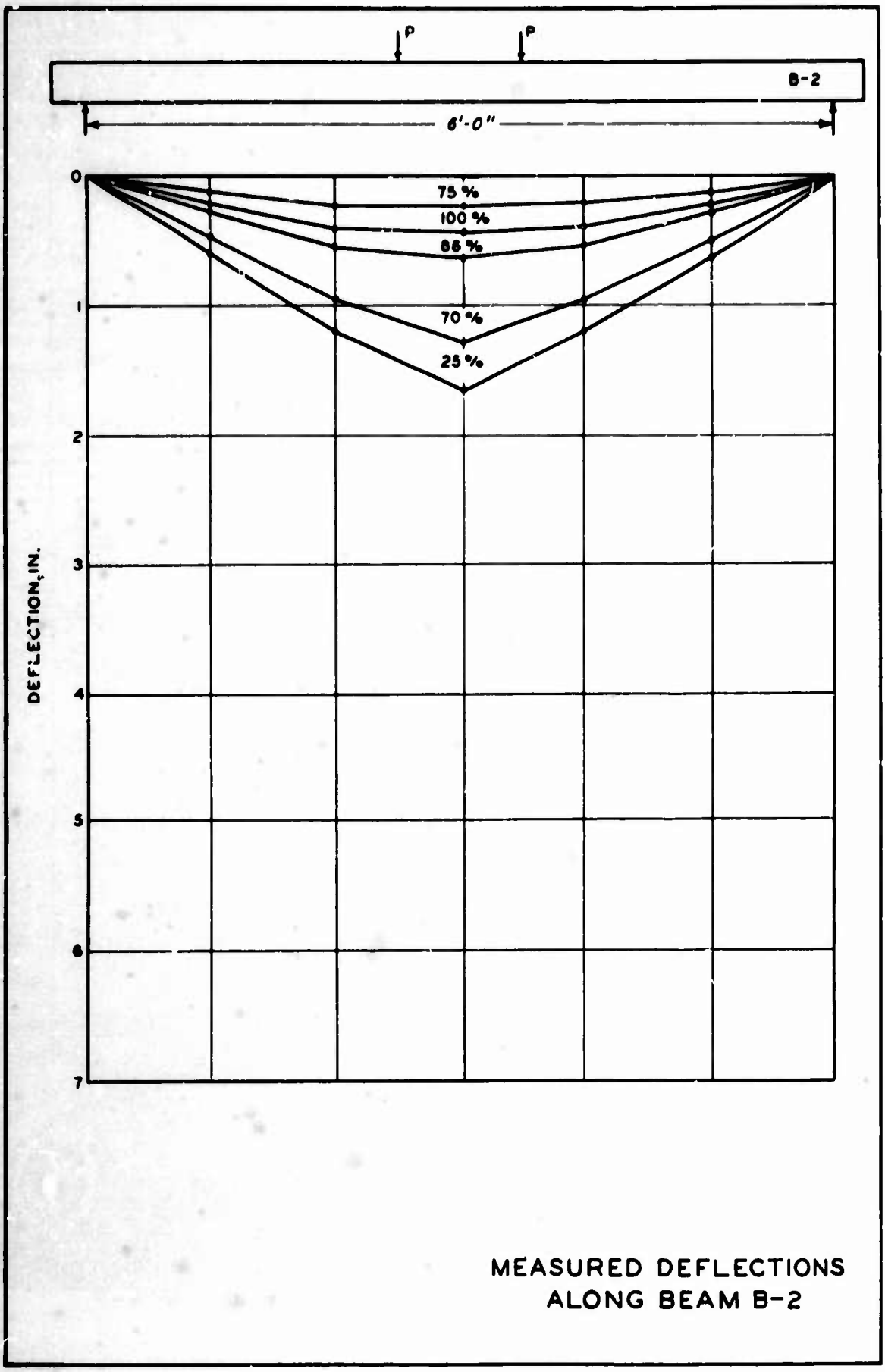

MEASURED DEFLECTIONS
ALONG BEAM B-2

PLATE 64

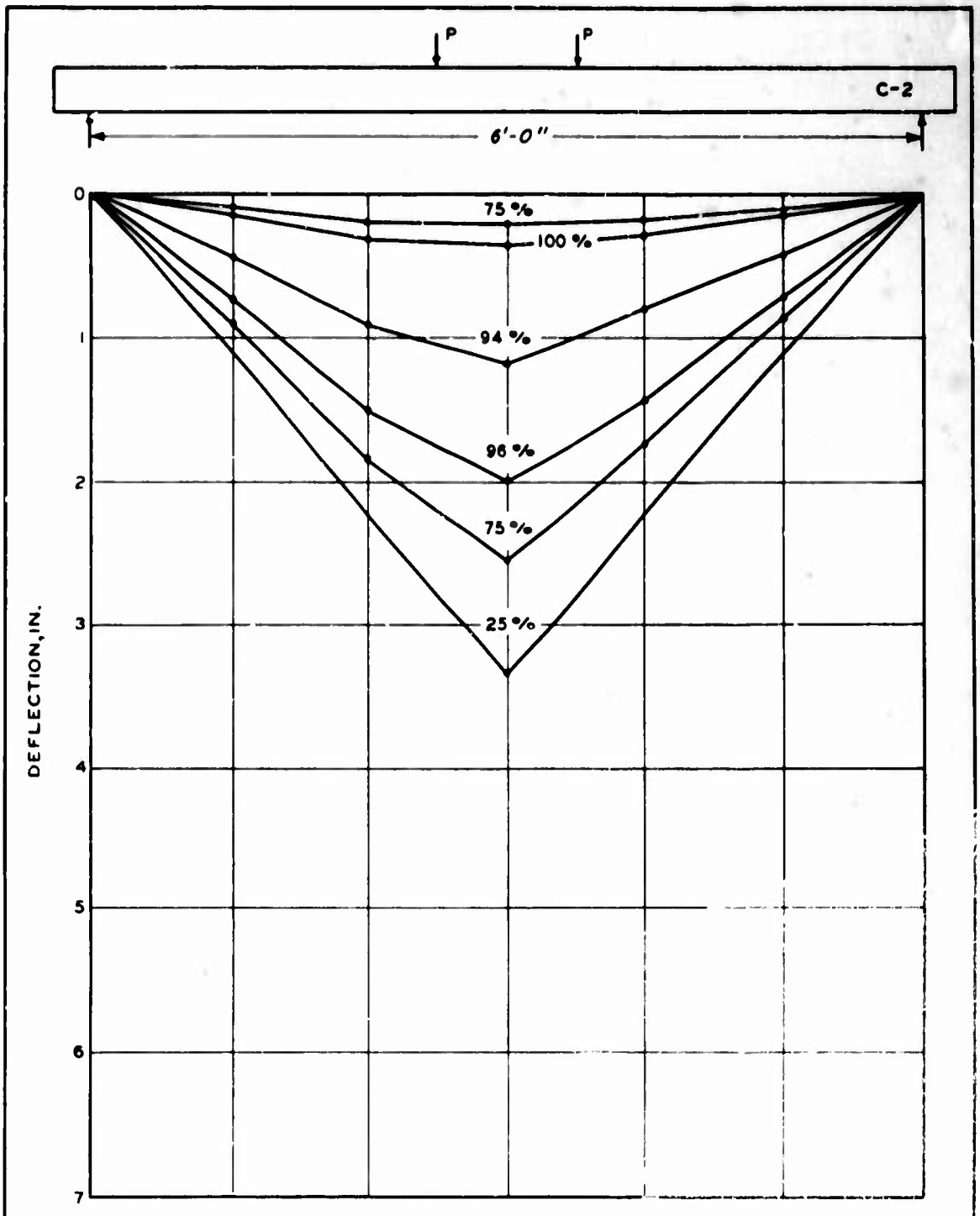

MEASURED DEFLECTIONS
ALONG BEAM C-2

PLATE 65

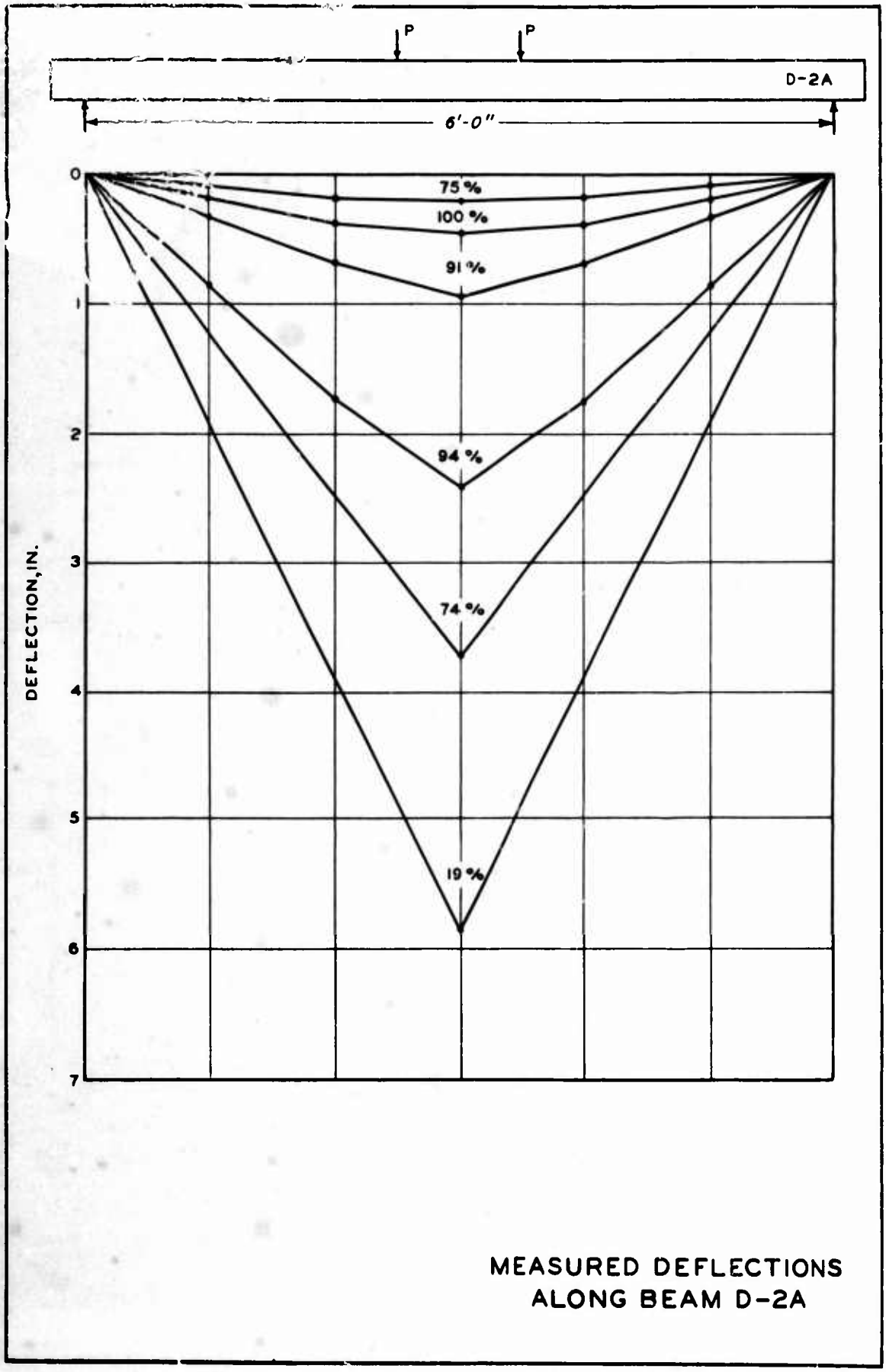

MEASURED DEFLECTIONS
ALONG BEAM D-2A

PLATE 66

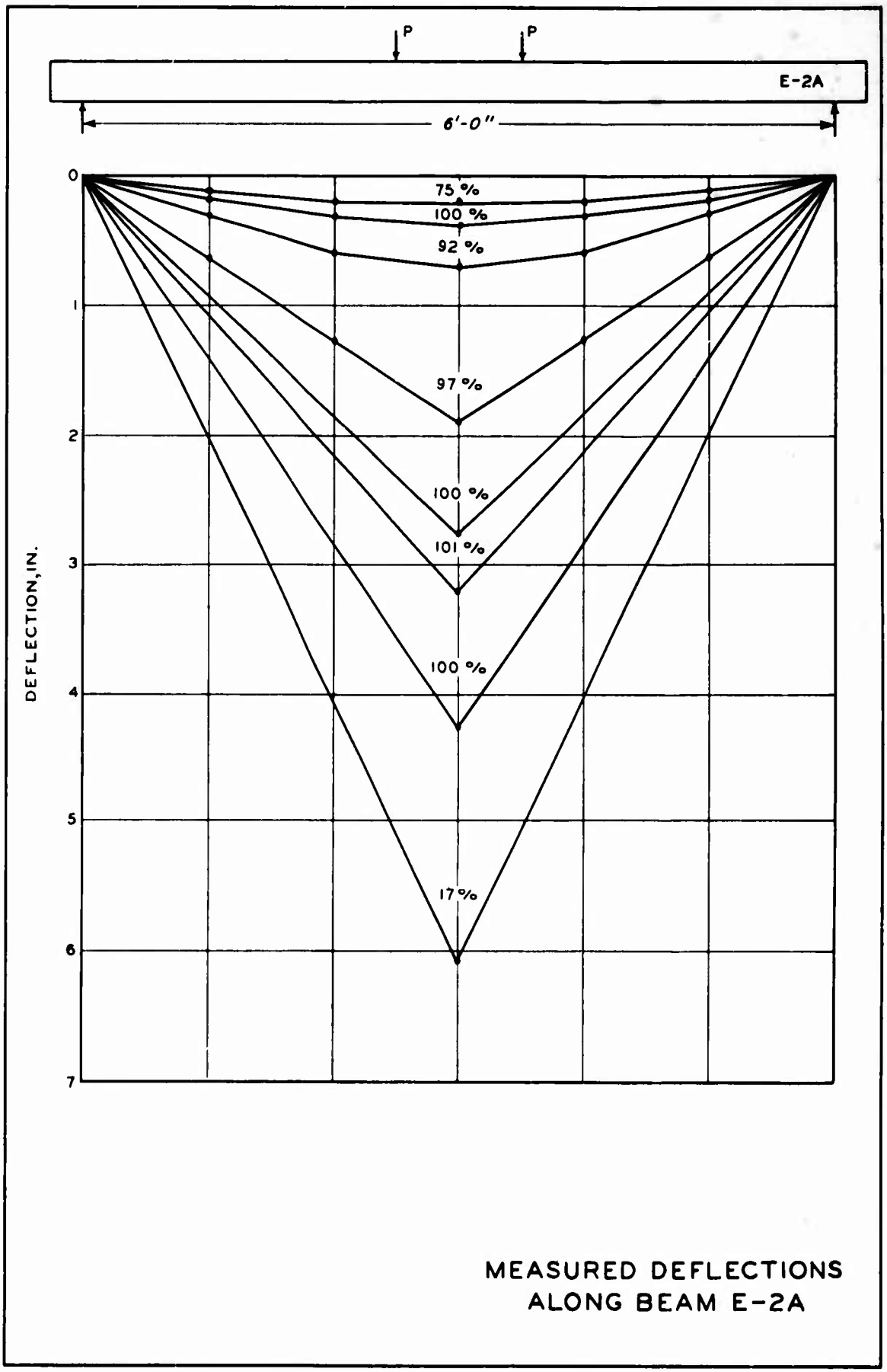

MEASURED DEFLECTIONS
ALONG BEAM E-2A

PLATE 67

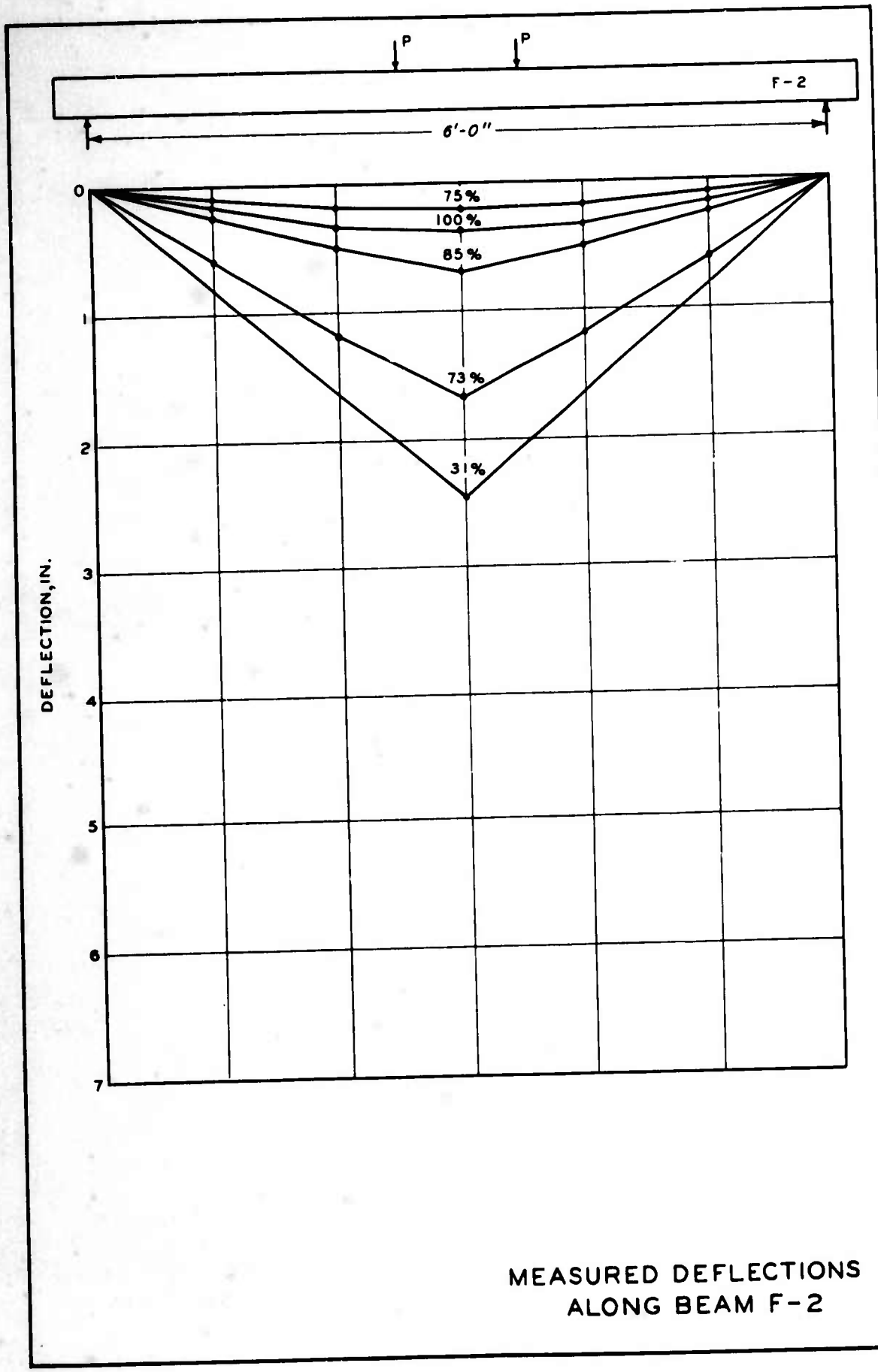

MEASURED DEFLECTIONS
ALONG BEAM F-2

PLATE 68

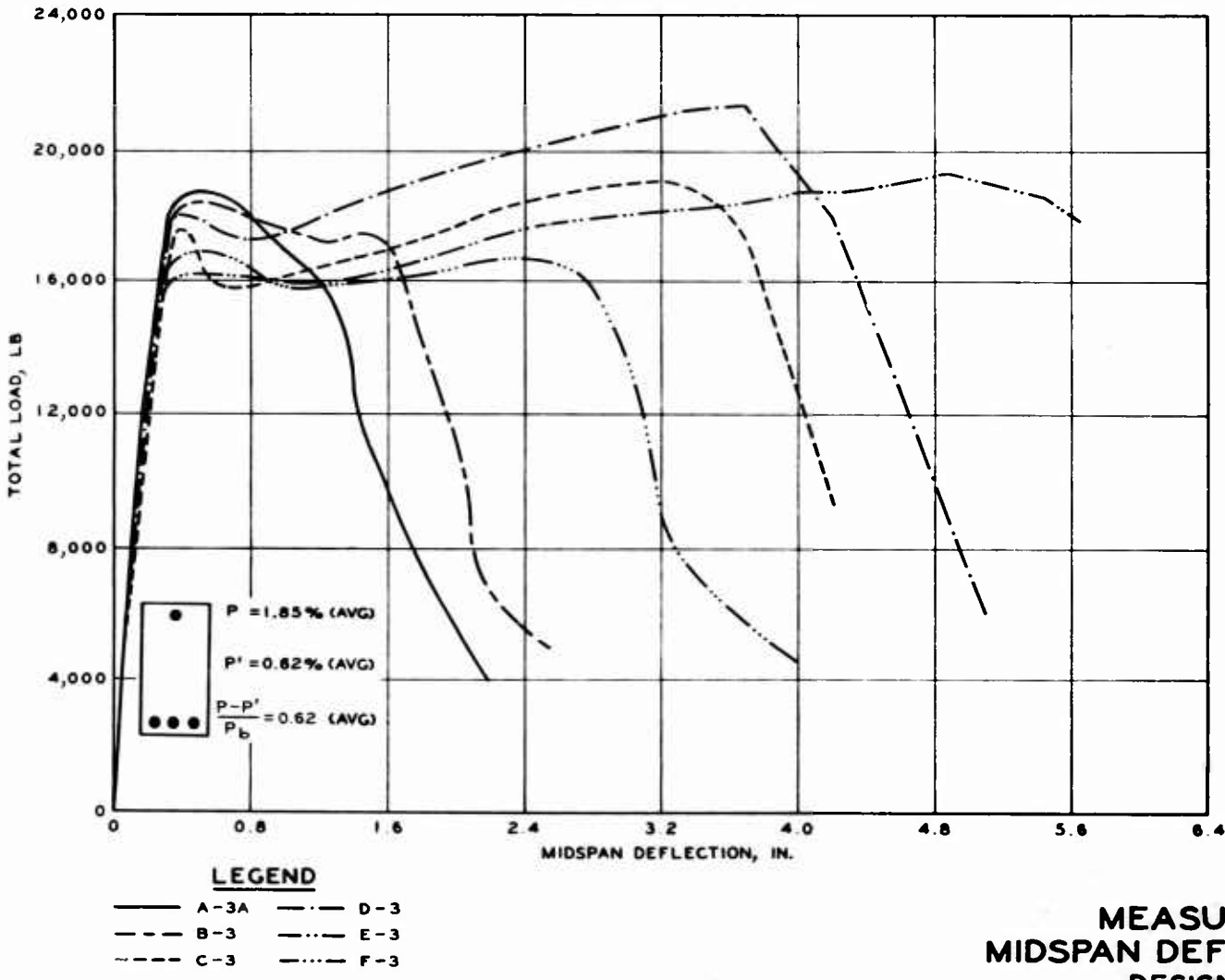

MEASURED MIDSPAN DEFLECTIONS
DESIGN 3

PLATE 69

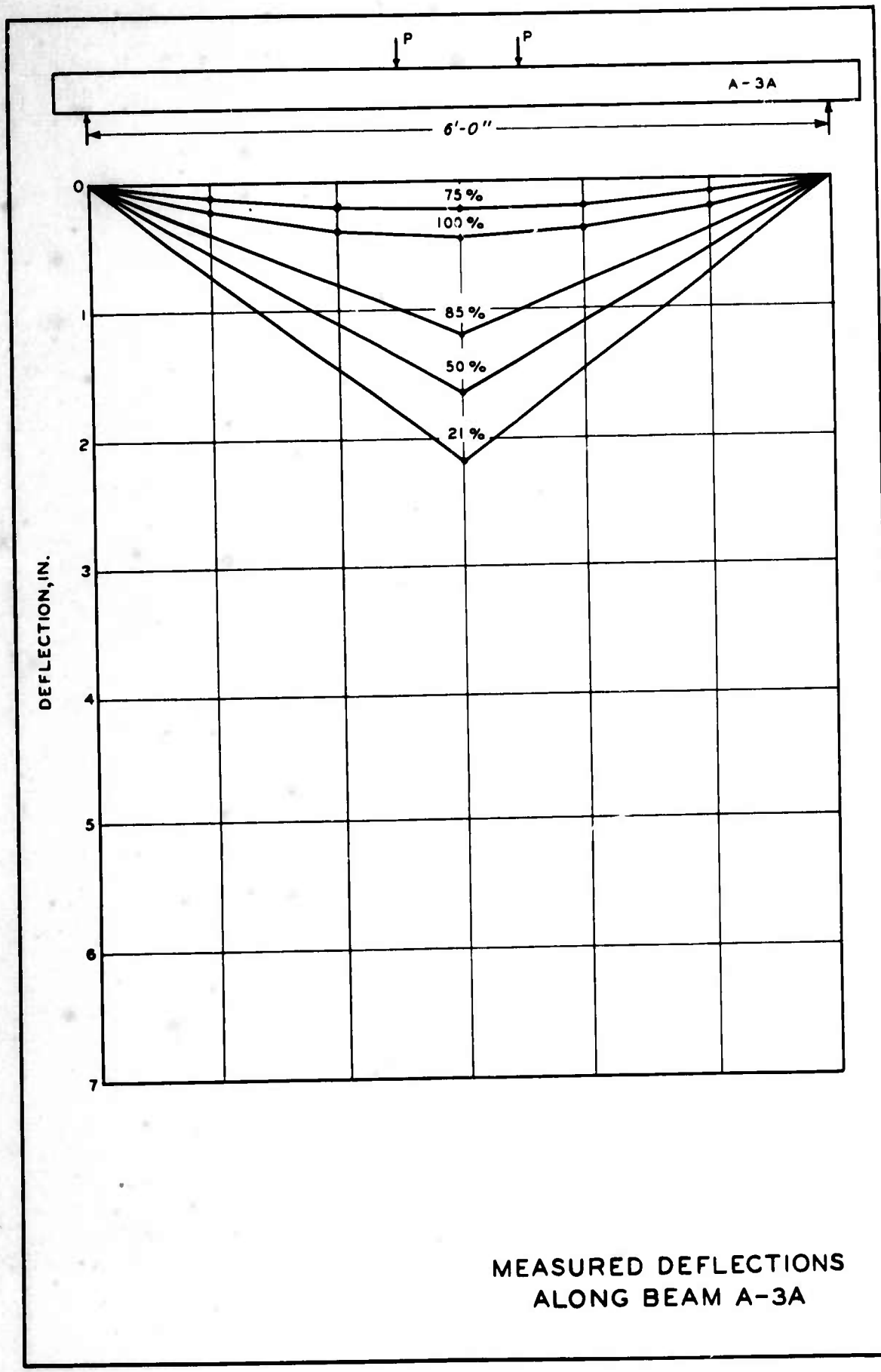

MEASURED DEFLECTIONS
ALONG BEAM A-3A

PLATE 70

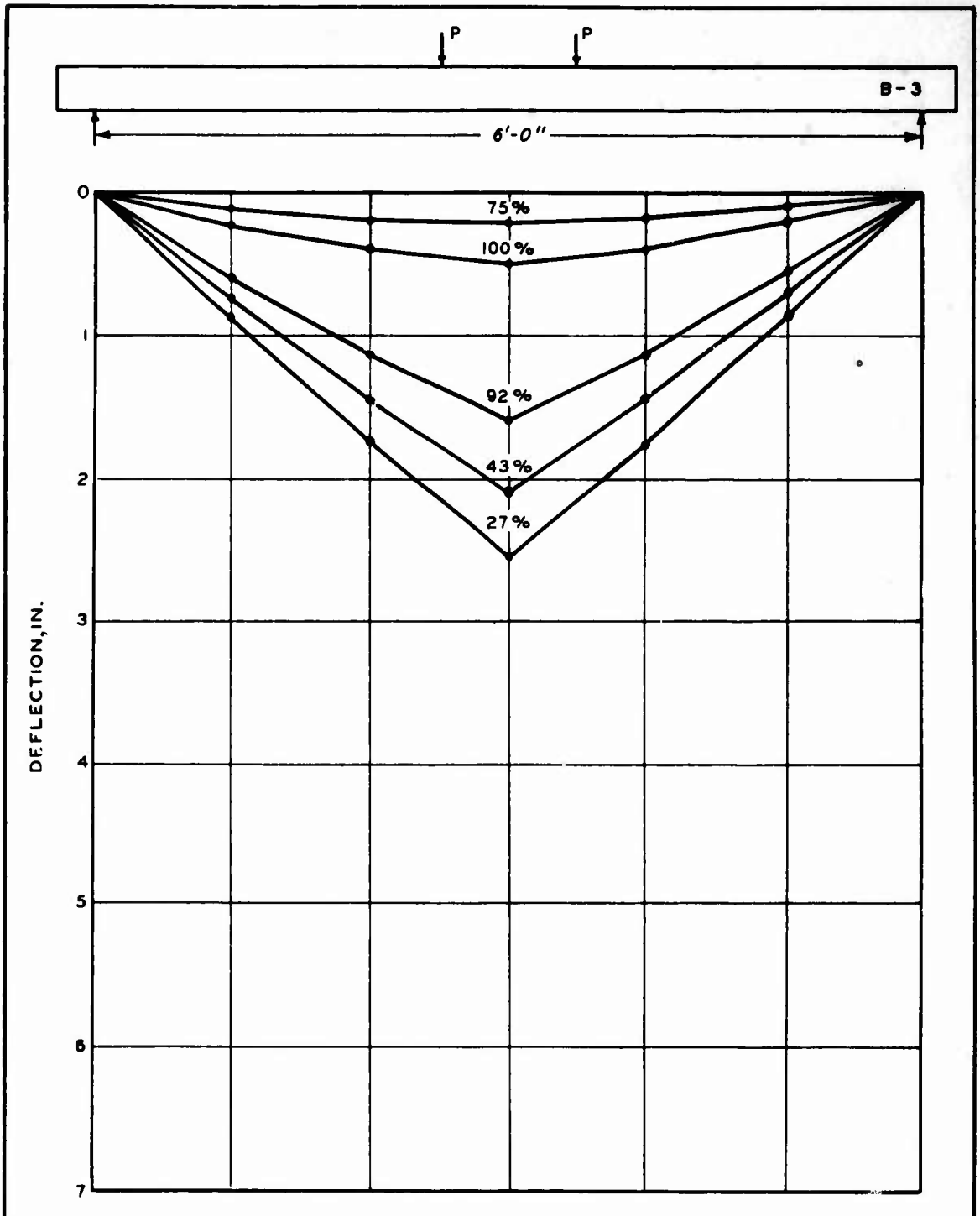

MEASURED DEFLECTIONS
ALONG BEAM B-3

PLATE 71

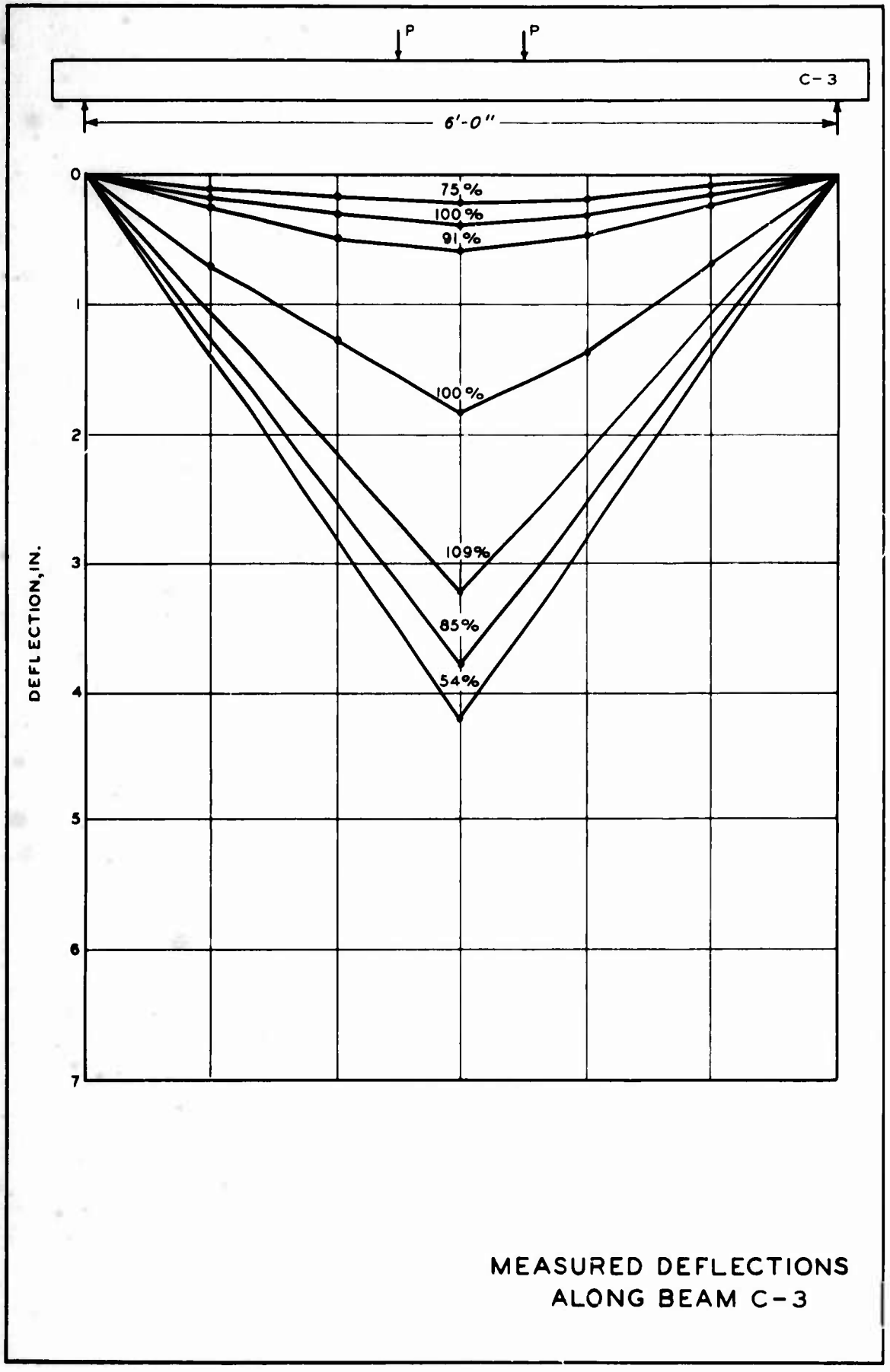

MEASURED DEFLECTIONS
ALONG BEAM C-3

PLATE 72

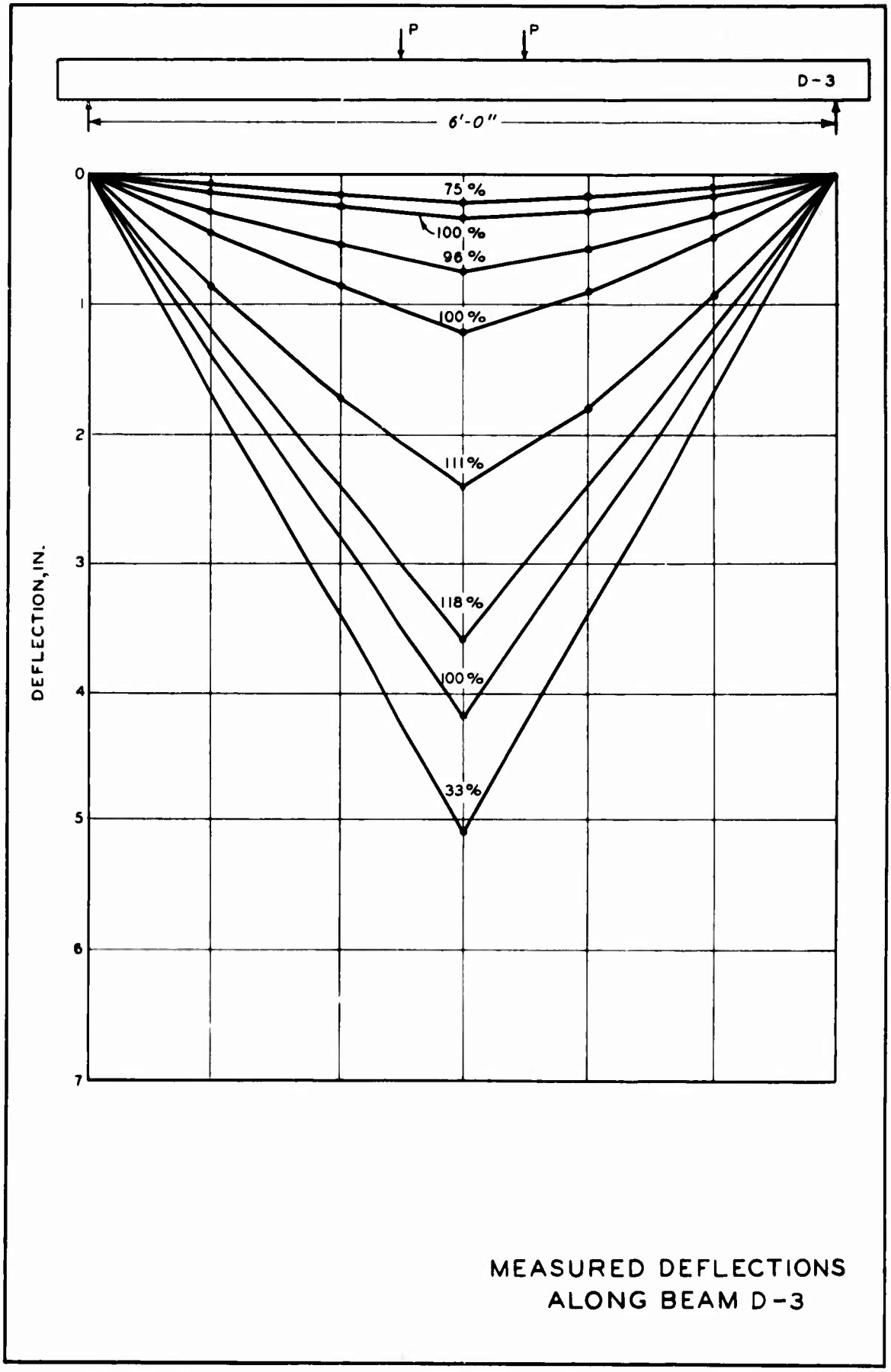

MEASURED DEFLECTIONS
ALONG BEAM D-3

PLATE 73

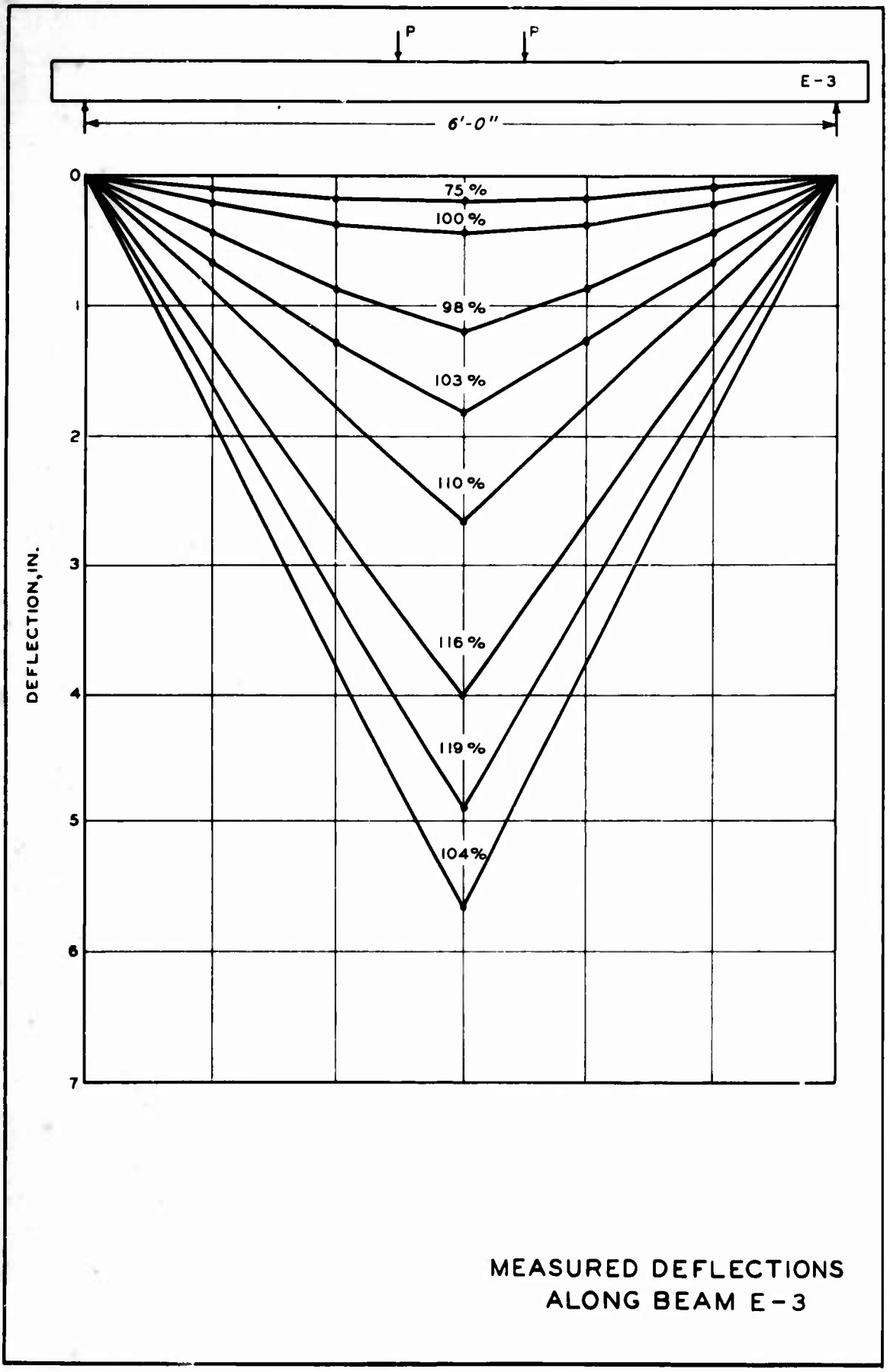

MEASURED DEFLECTIONS
ALONG BEAM E-3

PLATE 74

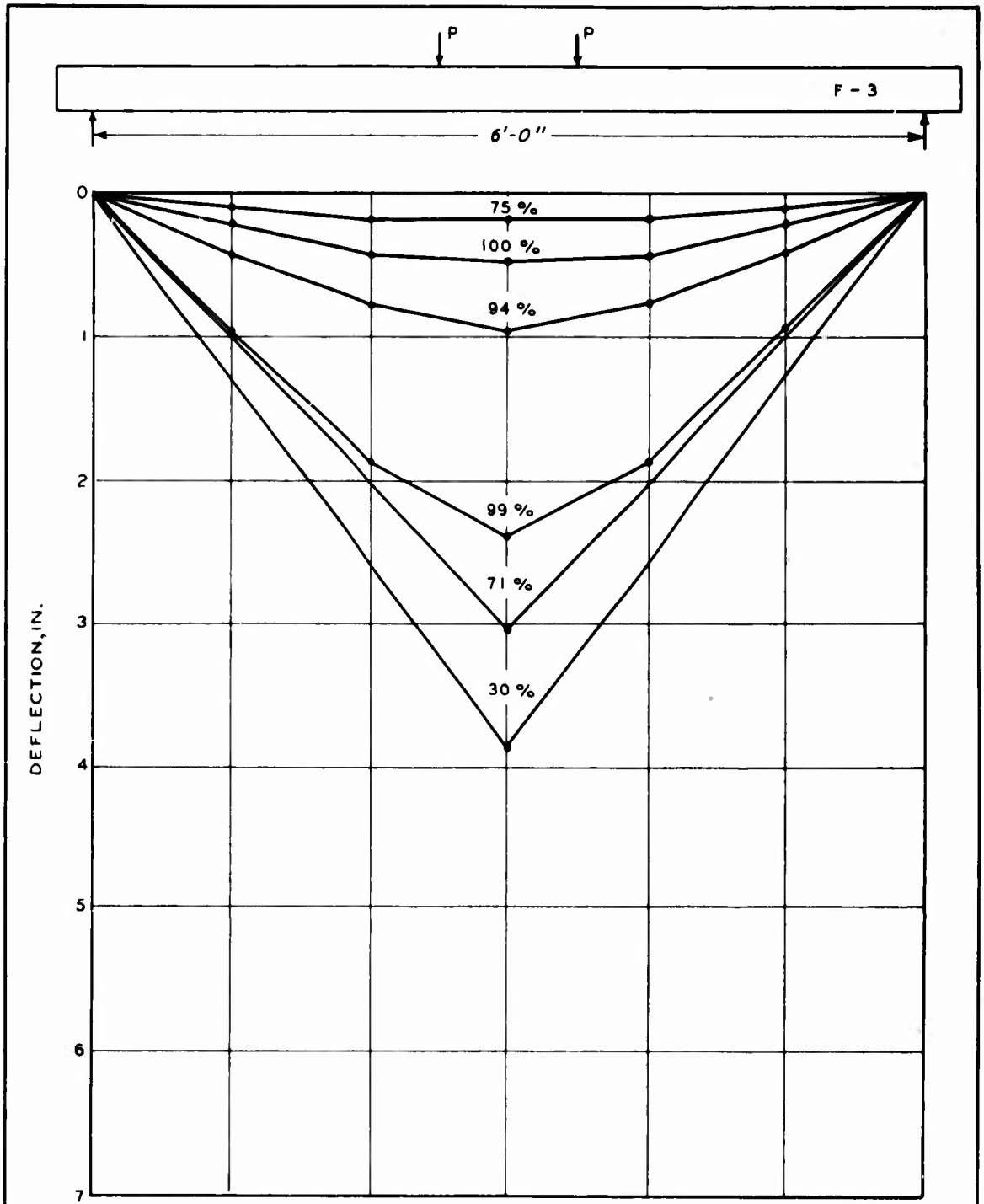

MEASURED DEFLECTIONS
ALONG BEAM F-3

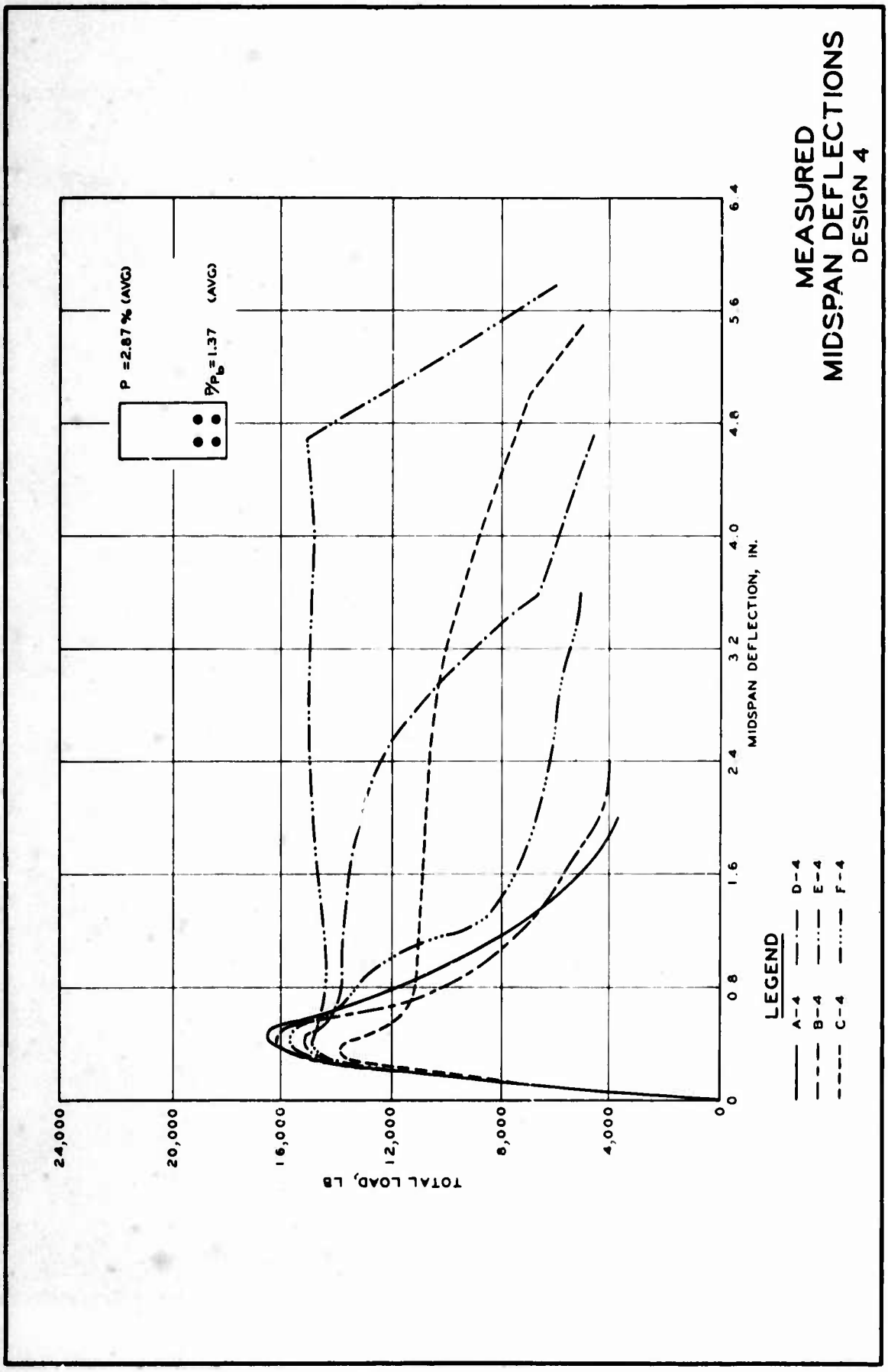
MEASURED
MIDSPAN DEFLECTIONS
DESIGN 4
P =2.87 % (AVG)
P/Pb=1.37 (AVG)
TOTAL LOAD, LB
24,000
20,000
16,000
12,000
8,000
4,000
0
0.8
1.6
2.4
3.2
4.0
4.8
5.6
6.4
MIDSPAN DEFLECTION, IN.
LEGEND
A-4
B-4
C-4
D-4
E-4
F-4

PLATE 76

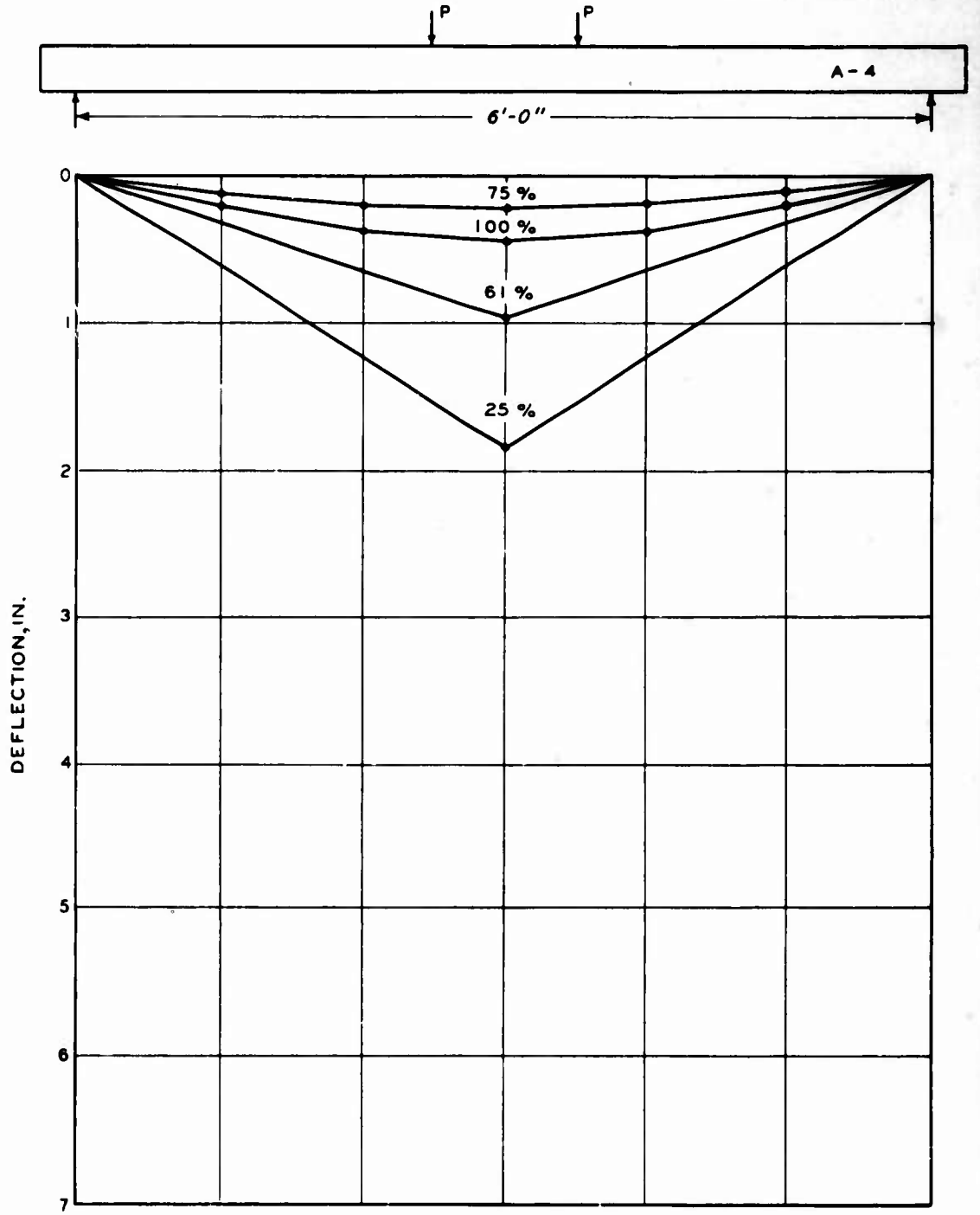

MEASURED DEFLECTIONS
ALONG BEAM A-4

PLATE 77

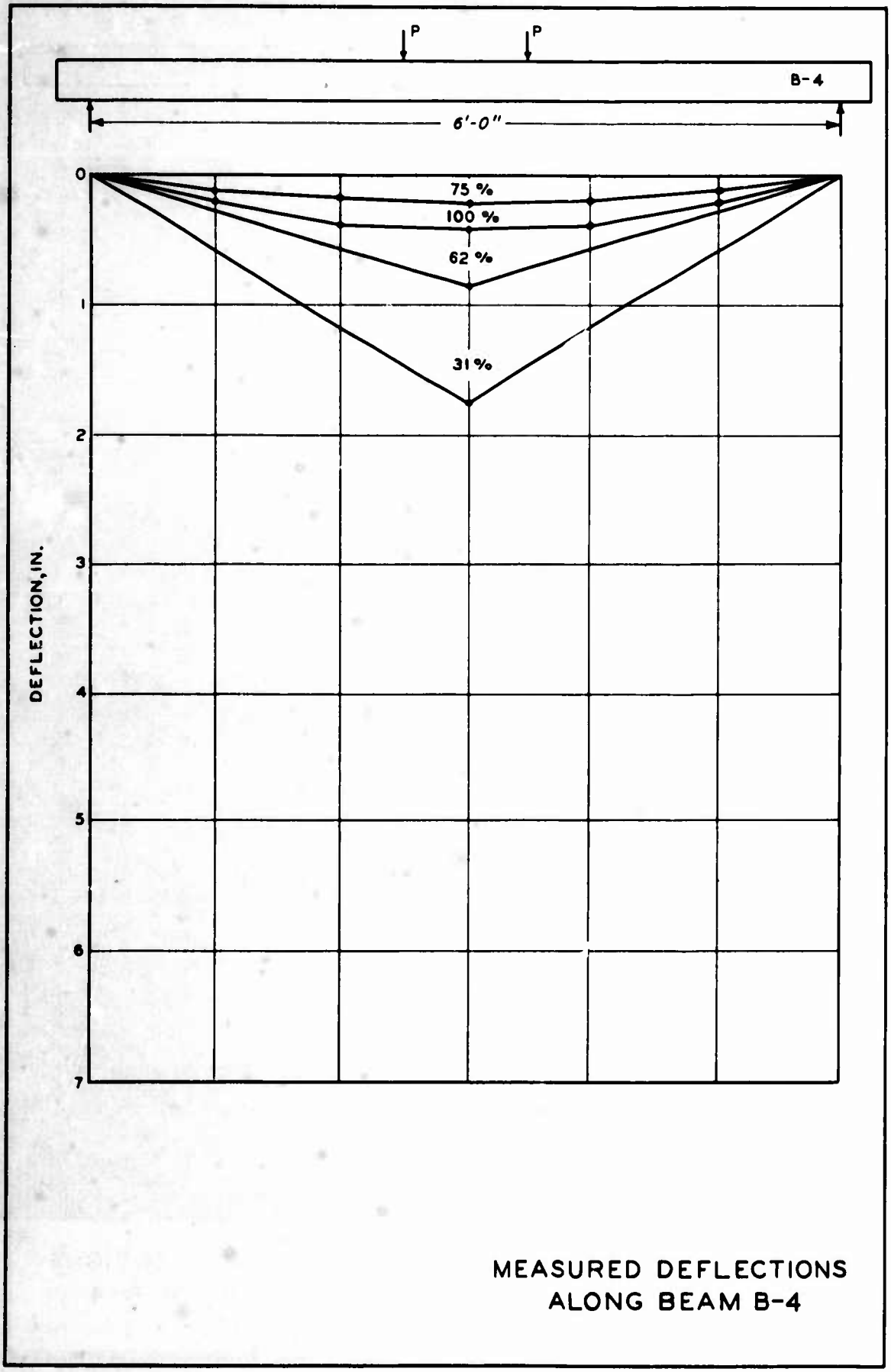

MEASURED DEFLECTIONS
ALONG BEAM B-4

PLATE 78

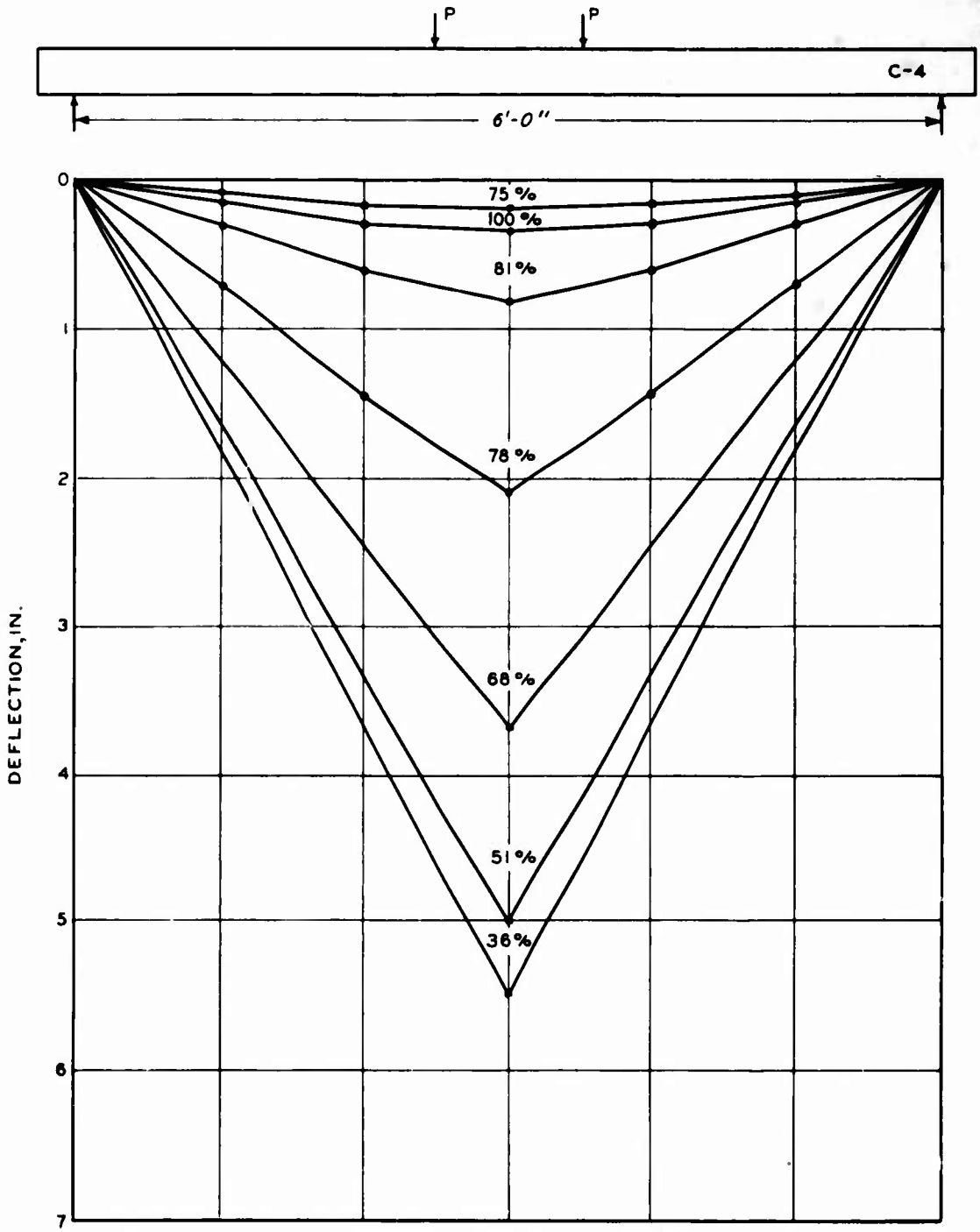

MEASURED DEFLECTIONS
ALONG BEAM C-4

PLATE 79

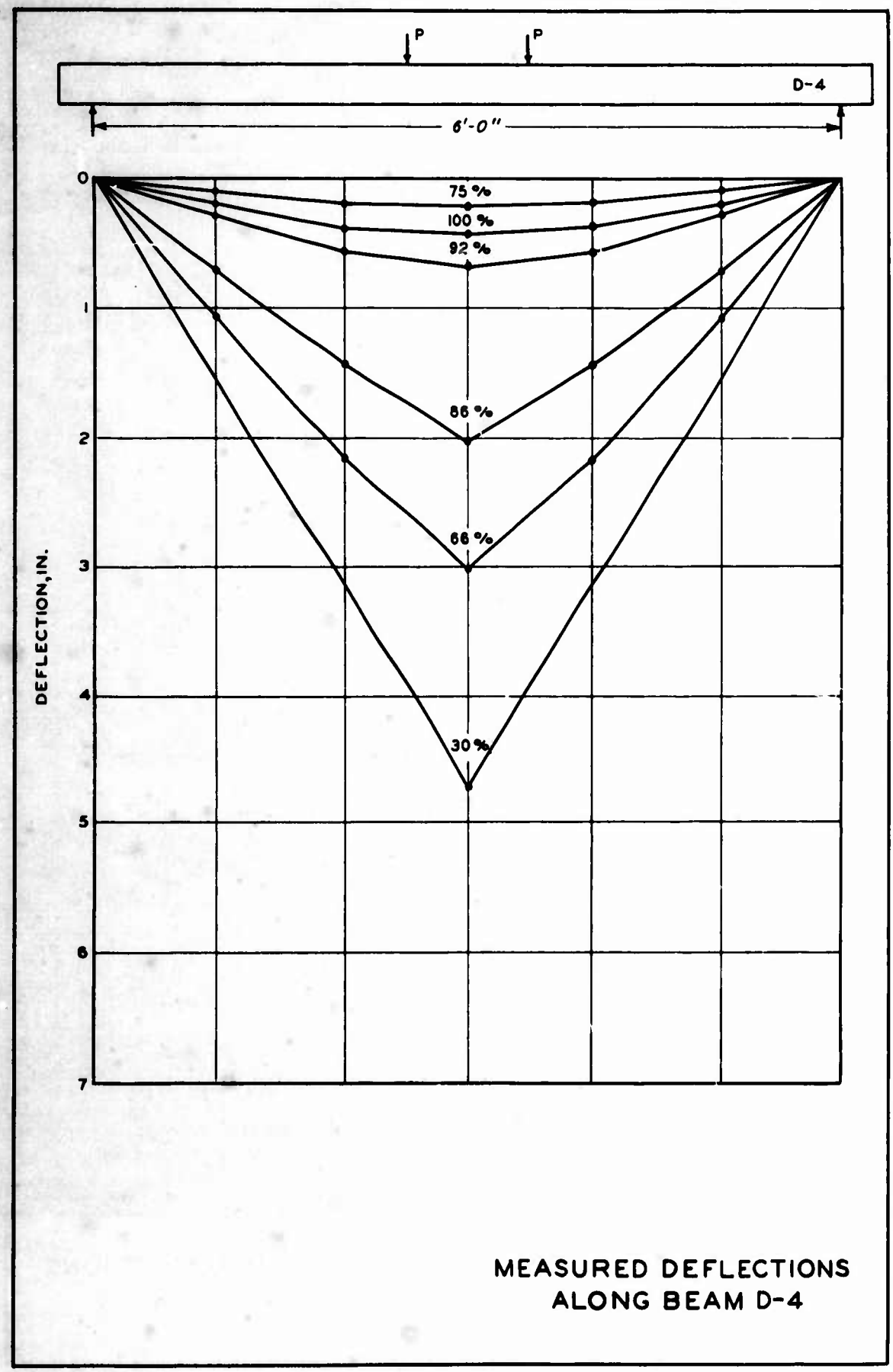

MEASURED DEFLECTIONS
ALONG BEAM D-4

PLATE 80

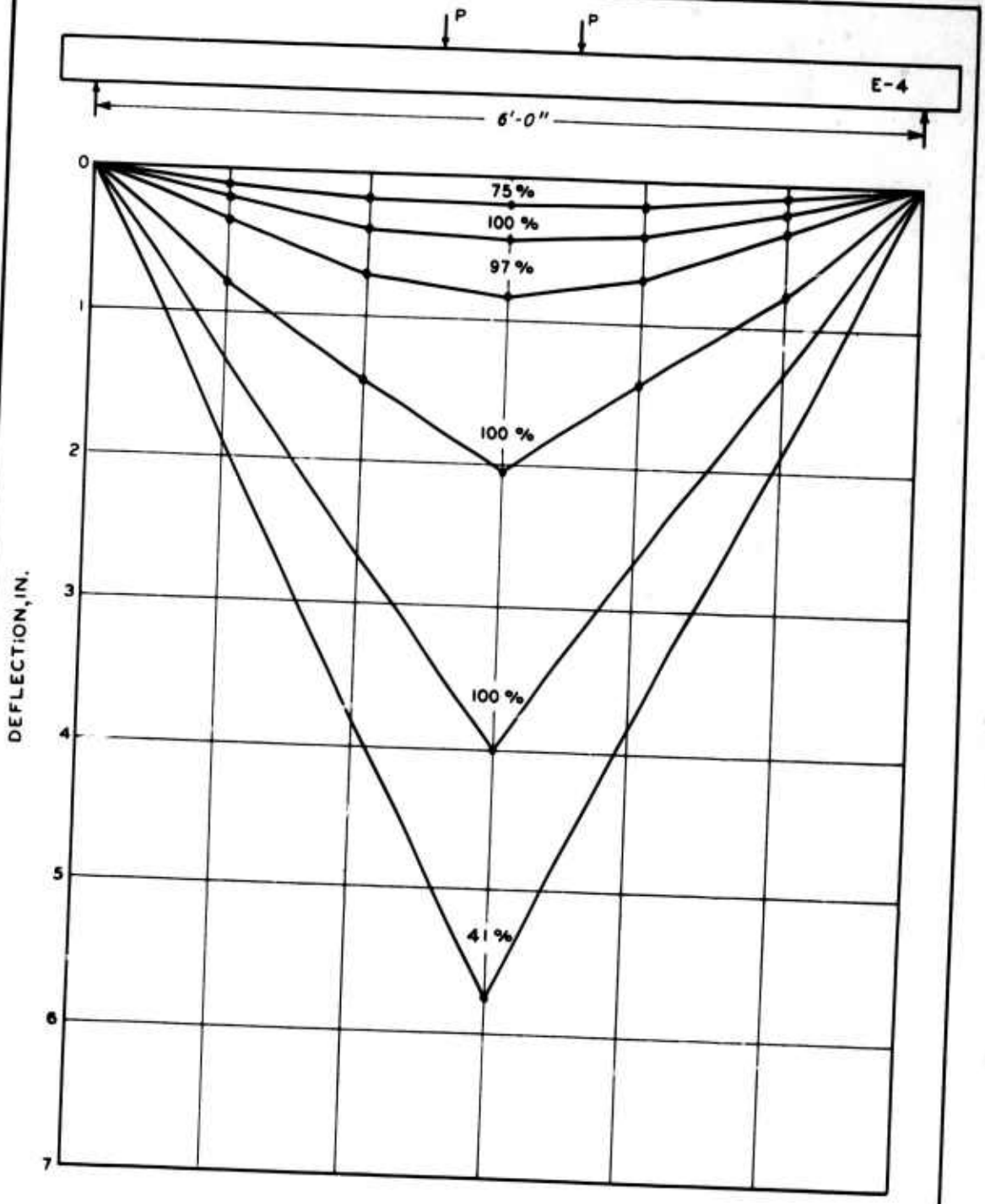

MEASURED DEFLECTIONS
ALONG BEAM E-4

PLATE 81

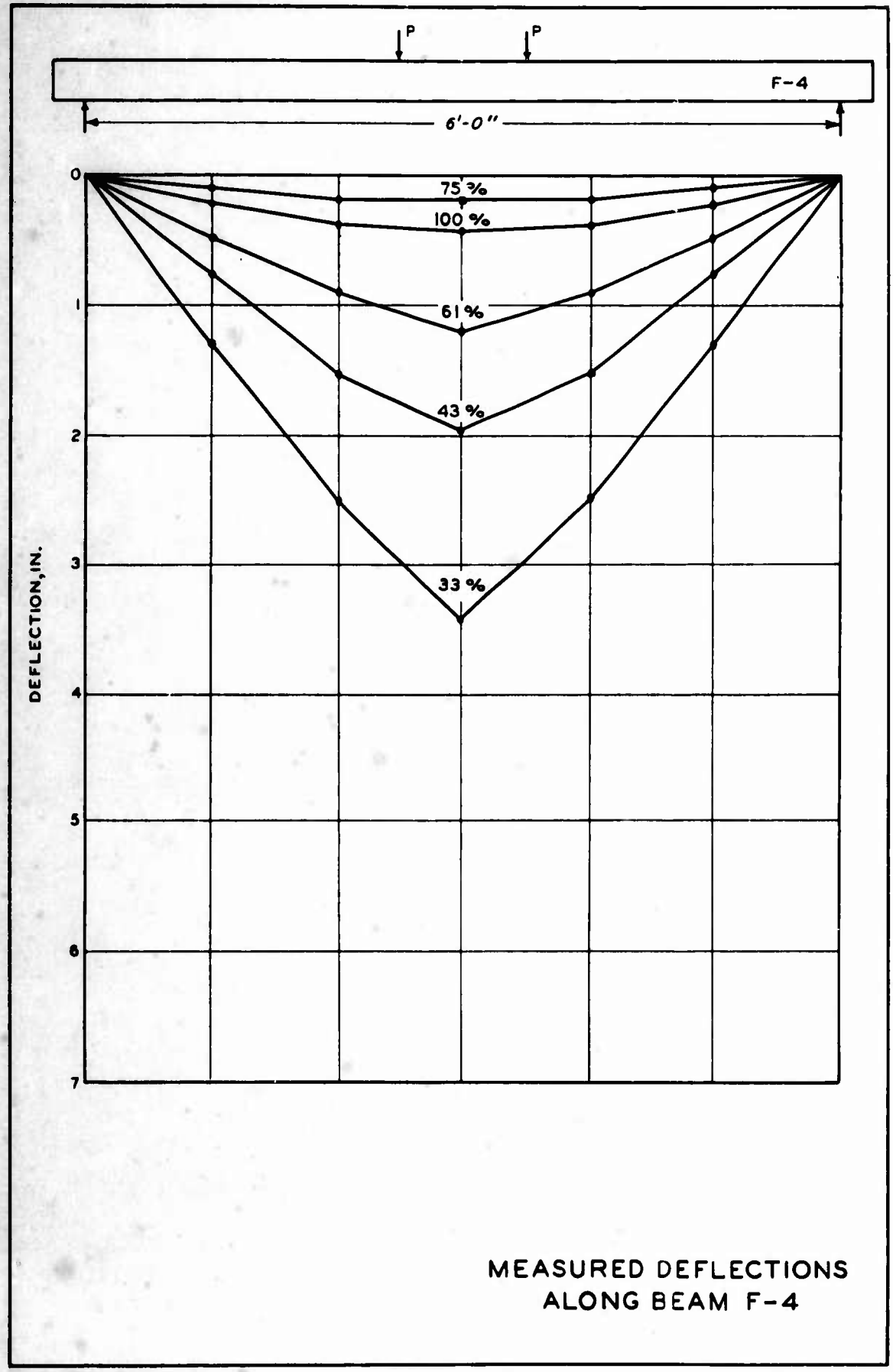

MEASURED DEFLECTIONS
ALONG BEAM F-4

PLATE 82

DISTRIBUTION LIST

Address	No. of Copies
Army	
Chief of Research and Development, Headquarters, Department of the Army ATTN: Director of Army Technical Information Washington, D. C. 20310	3 copies of Form 1473
Chief of Research and Development, Department of the Army	
ATTN: Atomic Office	1
CRDES	1
Washington, D. C. 20310	
Chief of Engineers, Department of the Army	
ATTN: ENGME-S	1
ENGME	1
ENGCW-E	1
ENGMC-E	1
ENGMC-EM	1
ENGMC-DE	1
ENGMC-M	1
ENGMC-EA	1
ENGMC-DS	1
ENGCW-EC	1
ENGCW-ED	1
Washington, D. C. 20315	
Department of the Army CE Ballistic Missile Construction Office P. O. Box 4187 Norton AFB, Calif. 92409	1
Director U. S. Army Terrestrial Sciences Research Center ATTN: Mr. K. Boyd P. O. Box 282 Hanover, N. H. 03755	1
Director, Technical Documents Center Evans Signal Laboratory Belmar, N. J. 07719	1

Unclassified

Security Classification

DOCUMENT CONTROL DATA - R & D

(Security classification of title, body of abstract and indexing annotation must be entered when the overall report is classified)

1. ORIGINATING ACTIVITY (Corporate author)	2a. REPORT SECURITY CLASSIFICATION
U. S. Army Engineer Waterways Experiment Station Vicksburg, Miss.	Unclassified
	2b. GROUP

3. REPORT TITLE

THE EFFECT OF CONFINING REINFORCEMENT ON THE DUCTILITY OF REINFORCED CONCRETE BEAMS

4. DESCRIPTIVE NOTES (Type of report and inclusive dates)

Final report

5. AUTHOR(S) (First name, middle initial, last name)

James E. McDonald

6. REPORT DATE	7a. TOTAL NO. OF PAGES	7b. NO. OF REFS
March 1969	152	17

8a. CONTRACT OR GRANT NO.	9a. ORIGINATOR'S REPORT NUMBER(S)
b. PROJECT NO. 4A013001A91D	Technical Report C-69-5
c.	9b. OTHER REPORT NO(S) (Any other numbers that may be assigned this report)
d.	

10. DISTRIBUTION STATEMENT

This document has been approved for public release and sale; its distribution is unlimited.

11. SUPPLEMENTARY NOTES	12. SPONSORING MILITARY ACTIVITY
The report [illegible]	Assistant Secretary of the Army (R&D) Department of the Army

13. ABSTRACT Some means of improving the compressive strain capacity of concrete is necessary to provide the ductile members or connections which will safely allow for formation of the plastic hinges assumed in designs based on collapse and energy-absorption concepts. The primary objectives of this investigation were to evaluate the effects of various types of confining reinforcement (helices, plane and tubular meshes, and rectangular ties) on the static stress-strain characteristics of rectangular concrete prisms tested in uniaxial compression, and, based on the results of these tests, determine the effectiveness of using selected confining reinforcement in the compressive zone of reinforced concrete flexural members to increase their ultimate strength and ductility. One hundred and eighteen 4- by 4- by 12-in. concrete prisms (one hundred and twelve with and six without confining reinforcement) were cast and tested. The ability of confining reinforcement to increase the ultimate strain capacity and ductility of rectangular concrete prisms in uniaxial compression was clearly demonstrated by the results of these tests. Concrete properly confined by lateral reinforcement had a considerable load-carrying capacity up to strains in excess of two percent, or more than six times the amount of strain usually considered as ultimate for concrete. The data indicate that the horizontal plane mesh (14-gage wire; 1- by 1-in. openings) was the most efficient confining reinforcement of those investigated. Within the range of spacings, sizes, and mesh openings studied, it appears that the primary factor affecting ductility is the amount or weight of the confining reinforcement used. Twenty-four 4- by 9- by 78-in. concrete beams (6-ft span) reinforced with various amounts of high-strength steel, with and without confining compressive reinforcement (plane meshes,

(Continued)

DD FORM 1 NOV 65 1473 REPLACES DD FORM 1473, 1 JAN 64, WHICH IS OBSOLETE FOR ARMY USE.

Unclassified

Security Classification

Unclassified

Security Classification

14. KEY WORDS	LINK A		LINK B		LINK C	
	ROLE	WT	ROLE	WT	ROLE	WT
Concrete beams						
Confining reinforcement						
Ductility						
Reinforced concrete						

13. ABSTRACT (Continued)

helices, and closed stirrups), were cast. The beams were tested to failure under two symmetrical line loads applied 6 in. from the beam center line. Results of these tests clearly demonstrated the ability of confining compressive reinforcement, particularly plane mesh, to significantly increase the ductility of reinforced concrete beams using high-strength steel. Plane mesh confining compressive reinforcement transformed the brittle failure mode normally associated with an overreinforced section into a plastic failure mode which gave ample warning of imminent collapse. This increased ductility can and should be used to advantage in structural designs based on collapse and energy-absorption concepts.

Unclassified

Security Classification